The University of Adelaide

Faculty of Engineering, Computer and Mathematical Sciences

School of Civil, Environment and Mining Engineering

A dissertation submitted to the School of Civil, Environment and Mining Engineering and Adelaide Graduate Centre of the University of Adelaide in partial fulfilment of the requirements for the degree of Doctor of Philosophy

Rock Strength and Deformability Characterisation and Assessment for Drilling Performance Estimation

By

Henry Munoz

MEng Geotechnical Engineering, BS Civil Engineering

Adelaide, 2017

STATEMENT OF ORIGINALITY

I certify that this work contains no material which has been accepted for the award of any other degree or diploma in my name, in any university or other tertiary institution and, to the best of my knowledge and belief, contains no material previously published or written by another person, except where due reference has been made in the text. In addition, I certify that no part of this work will, in the future, be used in a submission in my name, for any other degree or diploma in any university or other tertiary institution without the prior approval of the University of Adelaide and where applicable, any partner institution responsible for the joint-award of this degree.

I give consent to this copy of my thesis when deposited in the University Library, being made available for loan and photocopying, subject to the provisions of the Copyright Act 1968.

The author acknowledges that copyright of published works contained within this thesis resides with the copyright holder(s) of those works.

I also give permission for the digital version of my thesis to be made available on the web, via the University's digital research repository, the Library Search and also through web search engines, unless permission has been granted by the University to restrict access for a period of time.

H Munoz

SUMMARY

Rock Strength and Deformability Characterisation and Assessment for Drilling Performance Estimation

Rock drilling and cutting is essential in the mining industry. Rock characterisation and classification methods have been proposed to assess drilling or cutting performance. However, a unique method to relate rock characteristics to rock cutting performance has not yet been developed. This is due to the complexity of interactions among the variables involved in the drilling process encompassing not only rock properties, but also the nature of drilling. Cost-effective drilling is achievable by allocating the available gross energy towards the drilling action and, at the same time, reducing systematically that energy consumed in frictional processes inherent to tool-rock interactions.

Several attempts have been made to assess drilling performance by correlating different rock properties with the drilling rate. For instance, rock texture, grain size, Unconfined Compressive Strength (UCS), Mohs hardness and rock mass structural parameters, and others have been used to build a number of drillability indices. However, not only rock properties, but also different sets of drilling parameters and drilling techniques have an impact on the drilling performance and efficiency of the process.

On one hand, to predict rock drilling performance and optimisation of drilling operation, tool-rock interaction laws, i.e. the relations between forces acting on the tool in contact with rock, are essential. For instance, through tool-rock interaction laws, it was found that during rotary drilling, the energy consumed in pure cutting action of rock is measured by the intrinsic specific energy. In the case of percussive drilling, tool-rock interactions are focused

mostly in the prediction of the penetration rate and the optimum thrust. On the other hand, rock failure characterised by rock brittleness is a concept yet to be investigated as there is not a unique criterion able to describe rock brittleness quantitatively nor consensus about the most suitable and reliable brittleness index to apply to different rock engineering works encountered in the field.

A new brittleness index upon fracture strain-energy quantities extracted from the area under complete stress-strain curve of rocks in uniaxial compressive tests is proposed herein to study drilling performance by rock brittleness capacity. This brittleness index takes into account post-peak instability in uniaxial compression as post-peak instability of rock during compression can be treated as a manifestation of rock brittleness. That is, an increase in the post-peak energy indicates an increase of stability (i.e. a decrease in brittleness or increase in ductility). In the same manner, a dramatic decrease of post-peak energy indicates less stability of the failure process (i.e. an increase in brittleness). In this view, advanced laboratory experiments on strength and deformability of soft-to-hard rock types (UCS is ranging from 7 to 215 MPa) were carried out. The compressive tests complied with the application of a prescribed constant lateral strain-rate as a feedback signal to control the axial load which was found to be a suitable loading rate to measure the complete stress-strain response for the rocks.

The new brittleness index developed herein describes a monotonic and unambiguous scale of brittleness with increasing pre-peak strength parameters such as crack damage stress and peak stress as well as deformation parameters such as the tangent Young's modulus of rock. This outcome becomes relevant in order to better understand material brittleness associated with the progressive fracture process characterised by the typical threshold damage stresses, peak stress and the elasticity parameters. The brittleness index scale indicates that a higher brittleness index means that rock is more brittle which corresponds to higher strength rocks.

In order to reliably estimate drilling performance both tool-rock interaction laws along with a proper rock brittleness index are required to be implemented. In this study the performance of a single PDC (Polycrystalline Diamond Compact) cutter cutting and different drilling methods including PDC rotary drilling, roller-cone rotary drilling and percussive drilling were investigated. To investigate drilling performance by rock strength properties, laboratory PDC cutting tests were performed on soft-to-hard rocks to obtain cutting parameters. In addition, results of laboratory and field drilling on different rocks found elsewhere in literature were used. Laboratory and field cutting and drilling test results were coupled with values of a new rock brittleness index proposed herein and developed upon energy dissipation extracted from the complete stress-strain curve in uniaxial compression. To quantify cutting and drilling performance, the intrinsic specific energy in rotary-cutting action, i.e. the energy consumed in pure cutting action, and drilling penetration rate values in percussive action were used. The results show that the new energy-based brittleness index successfully describes the performance of the studied cutting and drilling methods.

TABLE OF CONTENTS

LIST OF FIGURES

Pre-Peak and Post-Peak Rock Strain Characteristics during Uniaxial Compression by 3D Digital Image Correlation

Fracture Energy-Based Brittleness Index Development and Brittleness Quantification by Pre-Peak Strength Parameters in Rock Uniaxial Compression

Rock Cutting Characteristics on Soft-To-Hard Rocks under Different Cutter Inclinations

Rock Drilling Performance Evaluation by an Energy Dissipation Based Rock Brittleness Index

LIST OF TABLES

Pre-Peak and Post-Peak Rock Strain Characteristics during Uniaxial Compression by 3D Digital Image Correlation

Fracture Energy-Based Brittleness Index Development and Brittleness Quantification by Pre-Peak Strength Parameters in Rock Uniaxial Compression

Rock Cutting Characteristics on Soft-To-Hard Rocks under Different Cutter Inclinations

Rock Drilling Performance Evaluation by an Energy Dissipation Based Rock Brittleness Index

ACKNOWLEDGEMENTS

First and foremost, I would like to express my profound gratitude and thankfulness to my advisor A Prof Emmanuel Chanda for his support and superb guidance during my research tenure as a PhD student. Emmanuel took care of me before my arriving in Australia and throughout my stay in Australia.

I cannot fully express my gratitude to Dr Abbas Taheri, for his generosity, friendship and assistance to manage many aspects on my academic live. Abbas is a good long-time friend back in our research time at The Tokyo University of Science in Japan where we met for the first time. Abbas painstakingly guided each step to successfully complete my PhD work and we spent several hours together working on the quality of the publications resulting from this PhD work.

I would like to express my appreciation to Prof Richard Hillis, currently Professor at the Australian School of Petroleum at the University of Adelaide and CEO of the Deep Exploration Technologies CRC. Richard was my mentor during my PhD candidature. His very valuable advice aided to strengthen not only several aspects of my academic life but also my daily life and aspects related to my future career.

Furthermore, I want to thanks Dr Caroline Forbes, from the Department of Earth Sciences School of Physical Sciences at the University of Adelaide and Chair of the Educational Committee of Deep Exploration Technologies CRC. Caroline supported my internship tenure at the Earth Science and Resource Engineering Department of The Commonwealth Scientific and Industrial Research Organisation (CSIRO) and at the Australian Centre for Geomechanics of the University of Western Australia.

Special thanks are addressed to Dr Luiz Franca from (formerly) the Australian Resource Research Centre (ARRC), CSIRO Perth, for facilitating the cutting experiments, the fruitful discussions.

For their generous assistance, I would like to thanks to all the members of the Mining Laboratory who made the laboratory an ideal environment to work. Especial thanks are addressed to Ian Cates, Simon Golding and Adam Ryntjes who enthusiastically collaborated in many ways to complete the experimental tests I developed in this thesis work.

Last but not the least, the financial support to complete this PhD work provided by Deep Exploration Technologies CRC whose activities are funded by the Australian Government's Cooperative Research Centre Programme is deeply acknowledged.

THESIS DISSERTATION

Rock mass characterisation and classification to assess drilling performance have been undertaken previously by a number of researchers. However, a systematic classification method in this respect has not been achieved yet. This is due to the complexity of the variables involved in the drilling process which depends not only on a number of rock properties, but also on drilling parameters (i.e. the nature of drilling). Previous studies on rock drilling and rock characterisation were found to not take into account the tool-rock interaction laws to find the more relevant rock properties involved in the drilling process. In this context, tool-rock interaction laws need to be introduced to successfully characterise the rock drilling and optimise the drilling performance. Furthermore, as not all rock physical and mechanical properties may be relevant to characterise drilling, a proper rock parameter able to represent the strength and deformability properties of the rock in drilling, by rock brittleness, needs to be defined. In this regard, implementing a new rock brittleness index able to picture either ductile or brittle failure behaviour of rocks can serve to evaluate the drilling performance of rotary and percussive drilling methods.

Based on the comprehensive literature review presented in the introductory sections of four journal papers published as part of this thesis work, appended herein, it is evident that there is not a comprehensive study on rock strength and deformability and brittleness characterisation and their relation to drilling performance within the rock mechanics and drilling community. Therefore, the following are considered research gaps which are addressed in this thesis work.

1) There are few studies on complete stress-strain characteristics of rocks under uniaxial loading conditions along with mapping the strain field development of the specimen throughout the compressive test.

   The complete stress-strain characteristics of intact rock, i.e. the pre-peak and post-peak stress-strain regimes are relevant in the understanding of the total process of rock deformation. Pioneering studies on the complete stress-strain behaviour of rocks undergoing quasi-static compression loads suggest that rock can be classified into two categories, i.e. class I where fracture propagation is stable, and class II where fracture propagation is unstable.

   Few studies can be found in the literature dealing with post-peak measurements in the case of rocks following class II behaviour. In the first place, this limitation is due to the lack of implementation of a proper load-control method to respond accordingly to rock class II behaviour. The complete stress-strain curve for both class I and II rocks can be successfully obtained, depending on the brittleness of the rock, by implementing a closed-loop servo-controlled loading system having the feedback signal to control the applied axial load a prescribed constant lateral-strain rate. This method has been by far the most widely used to investigate the post-peak behaviour of quasi-brittle materials while another method based on a linear combination of stress and strain is also available.

   Rock behaviour under axial loading is generally studied in laboratory using load-controlled or displacement-controlled compressive loading systems. From here, load-controlled method can only measure pre-peak behaviour. To measure post-peak behaviour of rocks in unconfined and confined conditions, generally displacement-controlled method (i.e. axial-displacement or axial-

strain rate feedback to control axial load) is implemented in servo-controlled compressive machines. Nevertheless, displacement-controlled method is insufficient to measure post-peak regime for class II rocks because axial strain no longer monotonically increases from the moment rock behave as class II. As a result, following this method, a critical response of the rock takes place leading to rock drastic failure. Consequently, post-peak stress-strain behaviour is masked by a rapid strength reduction at constant displacement immediately after peak stress. However, this post-peak critical response may be a manifestation of axial displacement-control compliance and not true material behaviour. In this view, circumferential or lateral-strain controlled method is required mainly because lateral displacement (or lateral-strain) monotonically increases after peak stress even if axial displacement decreases.

Improper measurement of strains in the post-peak regime can lead to improper characterisation of the post-peak behaviour of rock useful to quantify post-peak fracture energy and rock brittleness on the ground of post-peak instability. Conventional strain measurement of rock specimen in uniaxial compression includes setting up external devices, e.g. Linear Variable Displacement Transducers (LVDT) and direct-contact extensometers or bonded strain gauges. In this respect, a major drawback using LVDT includes bedding error measurements. Although free from bedding errors, extensometers and strain gauge measurements are yet limited to a fixed gauge length and specific points of bonding, respectively. In addition, they may not capture entirely strains found in post-peak regime. In this case, extensometer misalignment and strain gauge damage are the major issues particularly when progressively growing cracks and localisation take place in the rock surface. Therefore, accurate non-contact strain measurements, via Three-Dimensional Digital Image

Correlation (3D DIC), becomes relevant to study strains in particular in post-peak regime.

3D DIC method is based on the calculation of surface deformation using a number of digital images from a reference undeformed and subsequent deformed states. This technique encompasses the use of two digital cameras positioned in the manner that the surface of the specimen is viewed from two different angles that allows full-field three-dimensional shape and displacement measurements. To study post-peak progressive failure behaviour of rock as well as strain pattern development on the rock surface, 3D DIC technique has not been implemented yet. Therefore, the application of 3D DIC technique in rock uniaxial compression is required.

2) There are few studies on the definition and development of a proper rock brittleness index from the complete stress-strain characteristics by fracture energy dissipation of rocks.

   Brittleness refers to deformation that involves hard, strong material that fractures and splits rather than staying whole while pliably deforming. Therefore, rock failure behaviour is defined by brittleness. However, rock brittleness is a concept yet to be developed as there is not a single and standard criterion (i.e. brittleness index) available to describe failure characteristics of different rocks. For instance, a number of different criteria to assess brittleness upon pre-peak stress-strain characteristics in uniaxial compression including ratios between elastic to plastic strains as well as fracture strain-energy relations in pre-peak regime are found to be insufficient to describe failure behaviour of rock. In the same manner, other brittleness indices developed based on ratios between uniaxial compressive to tensile strength are insufficient.

Post-peak fracture development characteristics are very complex as post-peak progressive fracture in the rock takes place at different shear-tensile extent and at different rates. Therefore, the post-peak stress-strain curve cannot be characterised simply by a single post-peak stress-strain modulus (i.e. class I characterised by a negative stress-strain post-peak slope and class II showing positive stress-strain post-peak slope) but by a combination of class I-II behaviour at different extent. Therefore, a single stress-strain post-peak modulus value may not be an accurate representation of the whole post-peak response.

In post-peak regime deformations, conventional local strain measurements by direct-contact extensometers and bonded strain gauges may not capture entirely the strains developed in post-peak regime. In this case, extensometer misalignment and strain gauge damage are the major issues. Particularly, these problems initiate when progressively growing cracks and localisation take place in a specimen. As a result, non-contact strain measurement via three-dimensional digital image correlation (3D DIC) becomes relevant to measure strains development in the rock surface in post-peak regime to study the deformation process.

In summary, there is not any study on rock brittleness assessment on the ground of post-peak instability taking into account fracture energy dissipation quantities from the complete stress-strain characteristics in uniaxial compression. In addition, an unambiguous brittleness scale against rock strength and deformation parameters such as crack damage stress, peak stress and elastic modulus, relevant to represent failure process development has not been developed yet.

3) There is not a comprehensive study on rock drilling performance assessment by a rock brittleness that takes into account fracture

energy dissipation quantities from the complete stress-strain characteristics.

A generalised method to relate drilling performance with rock strength characteristics has not been developed yet. This is due to the complexity of interactions among the variables involved in the drilling process encompassing not only rock properties, but also the nature of drilling. Therefore, not only rock properties, but also different sets of drilling forces acting on rock as well as drilling method all have impacts on the drilling performance. In this view, by coupling relevant drilling parameters with relevant rock properties, a reliable drilling performance prediction method can be developed.

On one hand, to predict rock drilling performance and optimisation of drilling operation, tool-rock interaction laws, i.e. the relations between forces acting on the tool in contact with rock, are essential. In this instance, the energy consumed in pure cutting action of rock is measured by the intrinsic specific energy that quantifies the maximum drilling efficiency. In the case of percussive drilling, tool-rock interactions are focused mostly in the prediction of the penetration rate and the optimum thrust. Therefore, the intrinsic specific energy and penetration rate can be used to study rotary and percussive drilling, respectively. On the other hand, a rock brittleness index sufficient to quantify unambiguously a scale from ductile to brittle failure for a wide range of rocks (i.e. from soft to hard rocks) is needed to be implemented.

Previous studies to assess rock brittleness have applied a number of different criteria primarily developed upon the pre-peak stress-strain characteristics from uniaxial compression experiments. In this regard, brittleness indices include ratios between elastic to plastic strain as well as strain-energy relations. In addition, other brittleness

indices defined upon relations between rock compressive strength, UCS, and tensile strength, TS, can be cited. Nonetheless, none of this brittleness indices can describe an unambiguous scale of brittleness from ductile to brittle failure.

Therefore, in order to predict drilling performance successfully, firstly tool-rock interaction laws should be implemented to quantify drilling. In this respect, it was found that there are very few studies that consider tool-rock interaction to characterise drilling performance. Secondly, a proper brittleness index is required to describe rock failure characteristics in drilling. As a result, the present study aims at evaluating drilling performance by taking into account both the drilling response from tool-rock interaction laws and by applying a newly developed energy-based rock brittleness index able to picture rock failure behaviour and describe an unambiguous brittleness scale.

On the research gaps presented above, the present PhD work addressed the following three research objectives:

1) To study the complete stress-strain characteristics of rocks under uniaxial loading conditions and strain field development.

   In this regard, the complete stress-strain behaviour of rock in uniaxial compression was studied through advanced laboratory testing and experimentation. This was successfully achieved by controlling the applied axial load to the rock specimens with a feedback signal based on monotonically-increased lateral-strain rate in a closed-loop system. The method proposed was efficient in capturing the post-peak characteristics of soft-to-hard rocks (i.e. sedimentary and igneous rocks with UCS ranging from 7 to 215 MPa). As shown later herein in the appended journal papers, the selected rocks sufficed to

successfully study brittleness and drilling performance for different rock types.

The rocks samples used in the present study were intact, uniform and isotropic in strength. Therefore, repeatability and consistency of the testing results were guaranteed. The diameter of the specimens tested under uniaxial compression was 42 mm that ultimately limited the maximum grain size of the specimens tested (i.e. fine to medium grain size) to satisfy the recommendations by the International Society for Rock Mechanics (ISRM). The capacity of the available compressive equipment limited the extent of the experiment program.

Non-contact strain measurement via three-dimensional digital image correlation (3D DIC) becomes relevant to measure strains development in post-peak regime. This technique was implemented to accurately measure rock deformation in pre-peak and post-peak regimes. Stresses in the rock samples were coupled with the field of strains, both axial and shear strains, obtained via 3D DIC that develops in the rock. Results of this synergy show that 3D DIC is a sound method to study the stress-strain characteristics of rocks under uniaxial compression tests.

2) To define and develop a proper rock brittleness index from the complete stress-strain characteristics by fracture energy dissipation of rocks under uniaxial compression conditions.

The present study aims to characterise complete stress-strain behaviour of soft-to-hard rocks (UCS is ranging from 7 to 215 MPa) in uniaxial compression and to define and to develop a brittleness index. Rock brittleness is developed upon pre-peak and post-peak stress-strain energy balance to describe unambiguously a brittleness

scale against rock mechanical parameters, i.e. rock brittleness against pre-peak rock strength and deformation parameters in uniaxial compression including crack damage stress, peak stress and Young's modulus. In this sense, the complete stress-strain characteristics in uniaxial compression become a fundamental piece of information to describe the total process of rock deformation and to assess brittleness based on post-peak failure behaviour. Non-contact strain measurement via 3D DIC technique was implemented to accurately measure rock deformation in pre-peak and post-peak regimes.

3) To study rock drilling performance assessment by a rock brittleness that takes into account fracture energy dissipation quantities from the complete stress-strain characteristics in uniaxial compression.

Therefore, in order to predict drilling performance successfully, firstly tool-rock interaction laws should be implemented to quantify drilling. Secondly, a proper brittleness index is required to describe rock failure characteristics in drilling. The present study aims at evaluating drilling performance by taking into account both the drilling response from tool-rock interaction laws and by defining a new energy-based rock brittleness index that considers rock failure behaviour which is able to describe an ambiguous brittleness scale from ductile to brittle.

The performance of two major mechanical drilling methods, namely rotary drilling and percussive drilling, are investigated against rock brittleness capacity by the new energy-based brittleness index. The intrinsic specific energy and rate of penetration, as two main drilling performance parameters, were coupled with rock brittleness.

To validate this proposal, cutting experiments with a single PDC (Polycrystalline Diamond Compact) and uniaxial compressive tests

were carried out on different rock types (i.e. fine-grained sedimentary, igneous and metamorphic rocks with UCS is ranging from 9 to 250 MPa) to quantify the intrinsic specific energy. The capacity of the available cutting equipment limited the extent of the experiment program. In addition, independent rotary drilling as well as percussive drilling results from laboratory and field tests (from the literature) were used.

Impregnated diamond drilling (micro-cutting at depths of cut in the order of 10 µm to 40 µm), where quartz content in the rock may be relevant to the drilling process, is out of the purview of the present study so does brittleness index, quartz content and drilling process relation.

Objectives 1 to 3 described above include the performance of both analytical and extensive advanced laboratory works including strength and deformation tests as well as rock cutting tests on soft-to-hard rocks (UCS is ranging from 7 to 250 MPa). The flow chart in Figure 1 depicts the methodology followed up in this research work to complete the objectives 1 to 3 mentioned above alongside with the outcomes reflected in the published papers.

This PhD thesis was completed by publishing four journal papers to meet the proposed research objectives. The papers have been published in leading journals in the Rocks Mechanics community, i.e. journals ranked as A+ and A according to the Excellence of Research for Australia (ERA) assessment in 2010. The material derived from this research work is as follows (Figure 1):

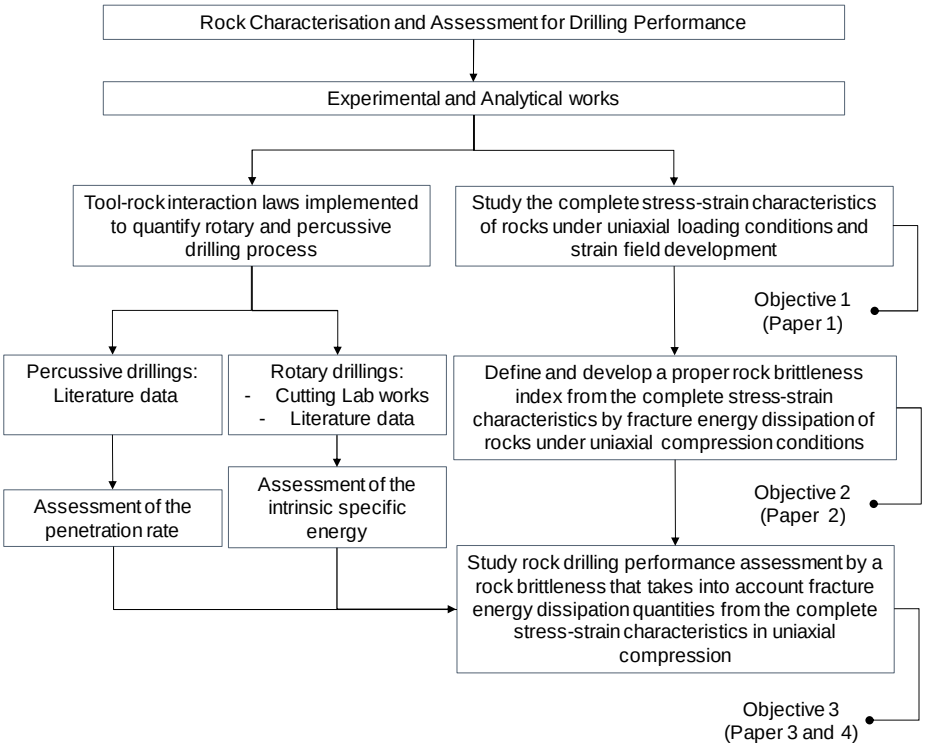

Figure 1. Flow chart of the methodology, objectives and outcomes of the research

1) To meet the objective 1 of this research work, i.e. to study the complete stress-strain characteristics of rocks under uniaxial loading conditions and strain field development, the following was produced (Munoz et al. 2016b):

   Paper 1:
   Munoz H, Taheri A, Chanda E (2016) Pre-Peak and Post-Peak Rock Strain Characteristics During Uniaxial Compression by 3D Digital Image Correlation. *Rock Mechanics and Rock Engineering:1-14 DOI:10.1007/s00603-016-0935-y*

   ERA: A, Impact Factor: 2.38, Journal with highest Impact Factor in Rock Mechanics journals.

2) To meet the objective 2 of this research work, i.e. to define and develop a proper rock brittleness index from the complete stress-strain characteristics by fracture energy dissipation of rocks under uniaxial compression conditions, the following was produced (Munoz et al. 2016a):

   Paper 2:
   Munoz H, Taheri A, Chanda E (2016) Fracture energy-based brittleness index development and brittleness quantification by pre-peak strength parameters in rock uniaxial compression. *Rock Mechanics and Rock Engineering DOI: 10.1007/s00603-016-1071-4*

   ERA: A, Impact Factor: 2.38. Journal with highest Impact Factor in Rock Mechanics journals.

3) To meet the objective 3 of this research work, i.e. to study rock drilling performance assessment by a rock brittleness that takes into account fracture energy dissipation quantities from the complete stress-strain characteristics in uniaxial compression, the following were published (Munoz et al. 2016d; Munoz et al. 2016e):

   Paper 3:
   Munoz H, Taheri A, Chanda E (2016) Rock Cutting Characteristics on Soft-to-Hard Rocks under Different Cutter Inclinations. *International Journal of Rock Mechanics and Mining Sciences: 85-89 DOI:10.1016/j.ijrmms.2016.05.014*

   ERA: A*, Impact Factor: 1.69. Journal of International Society of Rock Mechanics (ISRM).

Paper 4:

Munoz H, Taheri A, Chanda EK (2016) Rock Drilling Performance Evaluation by an Energy Dissipation Based Rock Brittleness Index. *Rock Mechanics and Rock Engineering:1-13 DOI:10.1007/s00603-016-0986-0*

ERA: A, Impact Factor: 2.38. Journal with highest Impact Factor in Rock Mechanics journals.

These papers were developed in strict sequential order as mention above. That is, firstly, in Paper 1 (Munoz et al. 2016b), a new method is developed to study the complete stress-strain characteristics of rocks under uniaxial loading conditions and the strain field. Secondly, after validating the work in Paper 1, Paper 2 (Munoz et al. 2016a) was produced on the development of an energy-based rock brittleness index from the complete stress-strain characteristics of rocks under uniaxial compression conditions. Subsequently, after validating the work in Paper 2, two papers referred to as Paper 3 (Munoz et al. 2016d) and Paper 4 (Munoz et al. 2016e) were produced on the evaluation of rock drilling performance by a the proposed fracture energy-based brittleness index.

In addition, it is noteworthy to mention that the results of this research has been delivered in a world-wide high standard conferences (Munoz et al. 2015; Munoz et al. 2016c; Munoz et al. 2016f; Munoz et al. 2014) through the following conference papers titles:

1) Munoz H, Taheri A, Chanda E (2016) Rock Brittleness Capacity upon Compressive Fracture Energy Dissipation to Assess Drilling Efficiency. *50th US Rock Mechanics/Geomechanics Symposium. ARMA 2016-2429, 16p*
2) Munoz H, Taheri A, Chanda E (2016) Strain Localisation Characteristics in Sandstone during Uniaxial Compression by 3D Digital Image Correlation. *ISRM International Symposium EUROCK 2016 1:356-362*

3) Munoz H, Taheri A, Chanda E (2015) Experiment Assessment of Rock-Cutting Characteristics by Strength-and-Fracture Driven *Mechanisms. Africa Australia Technical Mining Conference AusIMM 1:133-137*
4) Munoz H, Taheri A, Chanda E, Xu C, Grant D, Franca LFP (2014) Strain Rock Energy Approach to The Optimisation of Rock Drilling Processes. *Seventh International Conference on Deep and High Stress Mining. Australian Centre for Geomechanics 1:513-524*

CONCLUSIONS

The following general conclusion can be drawn from the present research work. Firstly, a non-contact optical method for strain measurement applying three-dimensional digital image correlation (3D DIC) in uniaxial compression was presented. Observations showed that, by 3D DIC technique relatively large strains developed in the post-peak regime, in particular within localised zones, difficult to capture by bonded strain gauges, can be measured in a straightforward manner. Field strain development in the rock samples suggested that strain localisation takes place progressively and develops at a lower rate in pre-peak regime. It is accelerated, otherwise, in post-peak regime associated with the increasing rate of strength degradation.

Secondly, new brittleness indices were developed based on fracture strain-energy quantities obtained from the complete stress-strain characteristics of rocks. In doing so, different rocks (UCS values ranging from 7 to 215 MPa) were examined in a series of quasi-static uniaxial compression tests after properly implementing lateral-strain control in a closed-loop system to apply axial load to rock specimen. This testing method was essential to capture post-peak regime of the rocks since a combination of class I-II or class II behaviour featured post-peak stress-strain behaviour. Further analysis on the post-peak strain localisation, stress-strain characteristics and the fracture pattern causing class I-II and class II behaviour were undertaken by analysing the development of field of strains in the rocks via three-dimensional digital image correlation

(3D DIC). Analyses of the experimental results demonstrated that brittleness indices proposed solely based on pre-peak stress-strain behaviour do not show strong correlation with any of the pre-peak rock mechanical parameters, otherwise they seemed to collapse in a single value irrespective of rock mechanical properties. On the other hand, the proposed brittleness indices based on pre-peak and post-peak stress-strain relations were found to competently describe an unambiguous brittleness scale against rock strength and deformation parameters such as crack damage stress, peak stress and elastic Young's modulus, relevant to represent failure process.

Finally, in order to reliably estimate drilling performance both tool-rock interaction laws along with a proper rock brittleness were implemented. In this study the performance of a single PDC (Polycrystalline Diamond Compact) cutter cutting and different drilling methods including PDC rotary drilling, roller-cone rotary drilling and percussive drilling were investigated against rock brittleness capacity. To investigate drilling performance by rock strength properties, laboratory PDC (Polycrystalline Diamond Compact) cutting tests were performed on different rocks (UCS values ranging from 9 to 250 MPa) to obtain cutting parameters and quantify the intrinsic specific energy. In addition, results of laboratory and field drilling on different rocks found elsewhere in literature were used. Laboratory and field cutting and drilling test results were coupled with values of a new rock brittleness index proposed herein and developed based on energy dissipation withdrawn from the complete stress-strain curve in uniaxial compression. To quantify cutting and drilling performance, the intrinsic specific energy in rotary-cutting action, i.e. the energy consumed in pure cutting action, and drilling penetration rate values in percussive action were used. The results show that the new energy-based brittleness index successfully describes the performance of the studied cutting and drilling methods.

REFERENCES

Munoz H, Taheri A, Chanda E (2015) Experiment assesment of rock-cutting characteristics by strengh-and-fracture driven mechanisms. Africa Australia Technical Mining Conference AusIMM 1:133-137

Munoz H, Taheri A, Chanda E (2016a) Fracture energy-based brittleness index development and brittleness quantification by pre-peak strength parameters in rock uniaxial compression. Rock Mechanics and Rock Engineering doi:DOI: 10.1007/s00603-016-1071-4

Munoz H, Taheri A, Chanda E (2016b) Pre-Peak and Post-Peak Rock Strain Characteristics During Uniaxial Compression by 3D Digital Image Correlation. Rock Mechanics and Rock Engineering:1-14 doi:10.1007/s00603-016-0935-y

Munoz H, Taheri A, Chanda E (2016c) Rock brittleness capacity upon compressive fracture energy dissipation to assess drilling efficiency. 50th US Rock Mechanics/Geomechanics Symposium: ARMA 2016-2429, 2016p

Munoz H, Taheri A, Chanda E (2016d) Rock Cutting Characteristics on Soft-to-Hard Rocks under Different Cutter Inclinations. International Journal of Rock Mechanics and Mining Sciences:85-89 doi:10.1016/j.ijrmms.2016.05.014

Munoz H, Taheri A, Chanda E (2016e) Rock Drilling Performance Evaluation by an Energy Dissipation Based Rock Brittleness Index. Rock Mechanics and Rock Engineering:1-13 doi:10.1007/s00603-016-0986-0

Munoz H, Taheri A, Chanda E (2016f) Strain localisation characteristics in sandstone during uniaxial compression by 3D digital image correlation. ISRM International Symposium EUROCK 2016 1:356-362

Munoz H, Taheri A, Chanda E, Xu C, Grant D, Franca LFP (2014) Strain rock energy approach to the optimisation of rock drilling processes. Seventh International Conference on Deep and High Stress Mining Australian Centre for Geomechanics 1:513-524

PUBLICATION IN JOURNALS

STATEMENT OF AUTHORSHIP

Statement of Authorship

Title of Paper	Pre-Peak and Post-Peak Rock Strain Characteristics during Uniaxial Compression by 3D Digital Image Correlation
Publication Status	☒ Published ☐ Accepted for Publication ☐ Submitted for Publication ☐ Unpublished and Unsubmitted w ork w ritten in manuscript style
Publication Details	Munoz, H., Taheri, A., Chanda, E. (2016) Pre-Peak and Post-Peak Rock Strain Characteristics during Uniaxial Compression by 3D Digital Image Correlation. Rock Mechanics and Rock Engineering DOI 10.1007/s00603-016-0935-y

Principal Author

Name of Principal Author (Candidate)	Henry Munoz
Contribution to the Paper	Overall paper preparation
Overall percentage (%)	85
Certification:	This paper reports on original research I conducted during the period of my Higher Degree by Research candidature and is not subject to any obligations or contractual agreements with a third party that would constrain its inclusion in this thesis. I am the primary author of this paper.
Signature	Date 28/06/16

Co-Author Contributions

By signing the Statement of Authorship, each author certifies that:

i. the candidate's stated contribution to the publication is accurate (as detailed above);
ii. permission is granted for the candidate in include the publication in the thesis; and
iii. the sum of all co-author contributions is equal to 100% less the candidate's stated contribution.

Name of Co-Author	Abbas Taheri
Contribution to the Paper	Paper review
Signature	Date 28/06/16

Name of Co-Author	Emmanuel Chanda
Contribution to the Paper	Paper review
Signature	Date 5/7/2016

Please cut and paste additional co-author panels here as required.

PRE-PEAK AND POST-PEAK ROCK STRAIN CHARACTERISTICS DURING UNIAXIAL COMPRESSION BY 3D DIGITAL IMAGE CORRELATION

H. Munoz[1], A. Taheri[2], E. K. Chanda[3]

[1]Deep Exploration Technologies Cooperative Research Centre DET CRC, Export Park, Adelaide Airport, SA 5950, Australia, and School of Civil, Environmental & Mining Engineering, The University of Adelaide, SA 5005, Australia, Ph: 61 8 8313 0591, Fax: 61 8 8313 4359, Email: henry.munozprincipe@adelaide.edu.au (corresponding author)

[2]Senior Lecturer, School of Civil, Environmental & Mining Engineering, The University of Adelaide, SA 5005, Australia, Ph: 61 8 8313 0906, Fax: 61 8 8313 4359, Email: abbas.taheri@adelaide.edu.au

[3]Associate Professor, School of Civil & Environmental & Mining Engineering, The University of Adelaide, SA 5005, Australia, Ph: 61 8 8313 7410, Fax: 61 8 8303 4359, Email: emmanuel.chanda@adelaide.edu.au

ABSTRACT

A non-contact optical method for strain measurement applying three-dimensional digital image correlation (3D DIC) in uniaxial compression is presented. A series of monotonic uniaxial compression tests under quasi-static loading conditions on Hawkesbury sandstone specimens were conducted. A prescribed constant lateral-strain rate to control the applied axial load in a closed-loop system allowed capturing the complete stress-strain behaviour of the rock, i.e. the pre-peak and post-peak stress-strain regimes. 3D DIC uses two-digital cameras to acquire images of the undeformed and deformed shape of an object

to perform image analysis and provides deformation and motion measurements. Observations showed that, 3D DIC provides strains free from bedding error in contrast to strains from LVDT. Erroneous measurements due to the compliance of the compressive machine are also eliminated. Furthermore, by 3D DIC technique relatively large strains developed in the post-peak regime, in particular within localised zones, difficult to capture by bonded strain gauges, can be measured in a straight forward manner.

Field of strains and eventual strain localisation in the rock surface were analysed by 3D DIC method, coupled with the respective stress levels in the rock. Field strain development in the rock samples, both in axial and shear strain domains suggested that strain localisation takes place progressively and develops at a lower rate in pre-peak regime. It is accelerated, otherwise, in post-peak regime associated with the increasing rate of strength degradation. The results show that a major failure plane, due to strain localisation, becomes noticeable only long after the peak stress took place. In addition, post-peak stress-strain behaviour, was observed to be either in a form of localised strain in a shearing zone or inelastic unloading outside of the shearing zone.

KEYWORDS

Uniaxial compression test, post-peak behaviour, strain localisation, digital image correlation

INTRODUCTION

The mechanical properties of intact rock extracted from the stress-strain curve in uniaxial compression tests have major implications on civil engineering projects, mining engineering and mineral exploration related operations. In this sense, the complete stress-strain characteristics of intact rock, i.e. the pre-peak and post-peak stress-strain regimes are relevant in the understanding of the total process of rock deformation (Fairhurst and Hudson 1999; Hashiba et al. 2006; He et al. 1990; Hudson et al. 1971; Okubo and Nishimatsu 1985; Vasconcelos et al. 2009; Wawersik and Brace 1971; Wawersik and Fairhurst 1970).

Pioneering studies on the complete stress-strain behaviour of rocks undergoing quasi-static compression loads (Hudson et al. 1971; Rummel and Fairhurst 1970; Wawersik and Brace 1971; Wawersik and Fairhurst 1970) suggest that rock can be classified into two categories as shown in Figure 1.1 (Hudson et al. 1971), i.e. class I where fracture propagation is stable, and class II where fracture propagation is unstable. The complete stress-strain curve for both class I and II rocks can be successfully obtained, depending on the brittleness of the rock, by implementing a closed-loop servo-controlled loading system having the feedback signal to control the applied axial load a prescribed constant lateral-strain rate (Hudson et al. 1971). This method has been by far the most widely used to investigate the post-peak behaviour of quasi-brittle materials (Amann et al. 2011; Daniel C. Jansen and Edwin 1995; Fairhurst and Hudson 1999; Hudson et al. 1971; Vasconcelos et al. 2009); the other method is based on a linear combination of stress and strain (He et al. 1990; Okubo and Nishimatsu 1985; Okubo et al. 1990).

The compressive loading process of quasi-brittle materials, such as rock and concrete, leads to localisation of macro cracks when peak stress is attained (Jansen and Shah 1997; Markeset and Hillerborg 1995). According to the compressive damage zone (CDZ) crack model (Markeset and Hillerborg 1995), failure of quasi-brittle materials, takes place within a damage zone, limited by the length of the damage zone L_d as shown in Figure 1.2. In this framework, the stress-strain curve (in the region before peak stress) describes the compressive behaviour of the material in the whole specimen. Immediately after peak stress is reached and strain localisation takes place unloading happens in the material outside of the damage zone (see Figure 1.2). In this regime, the post-peak curve describes the deformation at the damage zone, which encompasses deformations associated with the formation and coalescence of distributed longitudinal cracks and deformations at localised zone.

Improper measurement of strains in the post-peak regime can lead to improper characterisation of the post-peak behaviour of rock useful to quantify post-peak fracture energy (Bažant 1989; Jansen and Shah 1997; Markeset and

Hillerborg 1995) and rock brittleness on the ground of post-peak instability (Tarasov and Potvin 2013). Conventional strain measurement of rock specimen in uniaxial compression includes setting up external devices, e.g. Linear Variable Displacement Transducers (LVDT) and direct-contact extensometers or strain gauges. In this respect, a major drawback using LVDT includes bedding error measurements (Taheri and Tani 2008). Although free from bedding errors, extensometers and strain gauge measurements are yet limited to a fixed gauge length and specific points of bonding, respectively. In addition, they may not capture entirely strains found in post-peak regime. In this case, extensometer misalignment and strain gauge damage are the major issues particularly when progressively growing cracks and localisation take place in the rock surface. Therefore, accurate non-contact strain measurements, via three-dimensional digital image correlation (3D DIC), becomes relevant to study strains in particular in post-peak regime.

Digital image correlation (DIC) refers to the class of non-contact methods that acquire images of an object, store images in digital form and perform image analysis to extract full-field shape, deformation and motion measurements (Sutton et al. 2009). Two-dimensional (2D) DIC technique was the foundation of early applications of DIC in the stress-strain characterisation of a wide variety of materials including polymers, metals, wood, composites, asphalt, ceramics, soils, concrete, rock, and so forth in specimens assumed to be nominally planar and deforming within the object plane (Sutton et al. 2009). Since 2D DIC requires predominantly in-plane displacements and strains, relatively small out-of-plane motions introduce errors in the measurement of in-plane displacements. Furthermore, it is impractical to apply 2D DIC to rock cylinders in uniaxial compression. In essence, 3D DIC solves the limitations of 2D DIC. 3D DIC method is based on the calculation of surface deformation using a number of digital images from a reference undeformed and subsequent deformed states (Chu et al. 1985; Sutton et al. 2009). This technique encompasses the use of two digital cameras positioned in the manner that the surface of the specimen is viewed from two different angles that allows full-field

three-dimensional shape and displacement measurements. 3D DIC has been used to study deformation of different materials, e.g. (Heinz and Wiggins 2010). To study post-peak failure behaviour of rock material, 3D DIC technique, however, has not been implemented yet.

This research focusses on the application of 3D DIC technique in rock uniaxial compression. In this research, the complete stress-strain behaviour of Hawkesbury sandstone in uniaxial compression was studied through laboratory testing and experimentation. Controlling the applied axial load to the rock specimens with a feedback signal based on monotonically-increased lateral-strain rate in a closed-loop system was efficient in capturing the post-peak characteristics of the rock. Stresses in the rock samples were coupled with the field of strains, both axial and shear strains, obtained via 3D DIC that develops in the rock. Results of this synergy show that 3D DIC is a sound method to study the stress-strain characteristics of rocks under uniaxial compression tests.

EXPERIMENTAL STUDY

ROCK TYPE AND CORE PREPARATION

Hawkesbury sandstone was used in the experiments. This rock is an early Middle Triassic (Anisian) formation widely exposed in the Sydney Basin in Australia (Brian R. Rust and Jones 1987). The rock presents inherent bedding planes due to its natural sedimentary formation. Cylindrical specimens were retrieved from coring rock blocks in a way that the bedding plane orientation, defined as the angle between the bedding plane and the horizontal, was about 30º-40º in the cores tested here.

The diameter of specimens was 42 mm and their aspect ratio (i.e. length to diameter ratio) was maintained at 2.4. A visual inspection shows that specimen diameter was more than 20 times bigger than the rock grains size satisfying the recommendations by the International Society for Rock Mechanics (ISRM) (Bieniawski and Bernede 1979; Fairhurst and Hudson 1999). The end faces and sides of the specimen were prepared smooth and straight according to

the ISRM standard (Fairhurst and Hudson 1999; ISRM 1981). The rock samples correspond to fine-grain size rock having a density of 2.20 g/cm^3.

In total five rock samples were examined. In four of them, strains were measured by 3D DIC method. On the other hand, in one sample strains were measured by bonded strain gauges. Table 1.1 lists the mechanical properties of Hawkesbury sandstone, including the uniaxial compressive strength (UCS), Young's modulus (E), Poisson's ratio (υ) and the ratio of threshold stresses for fracture damage in the pre-peak regime. The UCS of the rock is 33.5 MPa, while E, is about 10.1 GPa.

SPECKLE PATTERN PREPARATION

3D DIC method relies on a contrasting random texture as speckle pattern in the surface of the specimen (Sutton et al. 2009). The pattern used in digital image correlation adheres to the surface of the object in study and it deforms as the surface does, therefore no loss of correlation occurs even under large translations and deformations the object may experience. Although some materials such as wood or concrete may display an inherent speckle pattern, a hand-made speckle pattern is usually needed for optimal measurement (Dautriat et al. 2011; Sutton et al. 2009). The latter was the case for Hawkesbury sandstone. So, a speckle pattern was thoroughly created by firstly spraying ordinary white paint on the rock surface in order to make a solid white basecoat and then spray-tarnishing black paint which created black speckles (Heinz and Wiggins 2010; Song et al. 2013; Yang et al. 2015). To achieve effective correlation, the speckle pattern was non-repetitive, isotropic and high in contrast, i.e. random pattern exhibiting no bias to an orientation and showing dark blacks and bright whites, adequate in size for high-strain resolution. By doing so, very sensitive defocus was avoided (Sutton et al. 2009). A typical speckle pattern on Hawkesbury sandstone is shown in Figure 1.3.

ROCK INSTRUMENTATION

The rock specimens having speckle pattern were instrumented by a direct-contact lateral extensometer placed along the perimeter and mounted at

mid-length of the rock specimens so that end-edge friction effects were eliminated (Hawkes and Mellor 1970). The lateral extensometer type used was 632.12F20-series manufactured by MTS Systems Co, as depicted in Figure 1.3, was used to record lateral strains, ε_L.

Additionally, a rock specimen without speckle pattern was instrumented by six strain gauges orientated in the axial direction to measure the respective axial strain ε_A. Strain gauges, either types KFG-30-120-C1 (30 mm gauge length) or KFG-10-120-C1 (10 mm gauge length) manufactured by Tokyo Sokki Kenkyujo Co., were used. The strain gauges were bonded in different locations in each quarter on the lateral surface of the rock sample as shown in Figure 1.4 (letters A, B, C, D, E and F refer to the strain gauge location). This arrangement was made to capture strains in different rock location to later collate them with those obtained by the 3D DIC measurement. Similar to 3D DIC method, strains measured by strain gauges are free from bedding errors in contrast to LVDTs readings.

LOADING SET-UP AND TESTING METHOD

The rock specimens were subjected to a quasi-static monotonic axial loading by a closed-loop servo-controlled hydraulic compressive machine stiff enough to not allow the elastic energy to accumulate in the machine (i.e. Instron-1342 model manufactured by Instron Inc). The testing machine has a loading capacity of 250 kN. The closed-loop control system is fully digital and it is capable and flexible to operate loading control under either axial-load rate control, axial-strain rate control or lateral-strain rate control feedback signal using an in-built computer system. Applying uniform load to sample was ensured in all the tests. This is critical to avoid premature specimen failure due to machine platen or specimen surface misalignment.

In this study, the applied axial load was controlled in a way keeping lateral strain-rate constant by the lateral extensometer. The electronics and computer program allows the hydraulic system to be adjusted continuously and automatically to ensure load to response accordingly with feedback signal and

damage extent to the specimen. A closed loop servo-controlled load system having the axial-strain rate feedback signal, provided sufficiently low rate and monotonic strain increase, can only capture post-peak behaviour if rock obviously follows class I behaviour (Rummel and Fairhurst 1970). This loading arrangement, however, cannot capture post-peak behaviour of most of strong and medium-strong rocks which generally follow class II mode or a combination of class I and class II behaviour (Hudson et al. 1971).

Figure 1.5a shows the time history of loading (F), axial strain (ε_A), and lateral strain (ε_L) in a typical test carried out herein. At a regime approaching to the peak stress, where load-lateral strain curve, i.e. F-ε_L, becomes less steep, axial-strain rate ($d\varepsilon_A/dt$) decreases significantly so loading rate (dF/dt) does. During axial loading, the lateral strain ε_L is increased monotonically and linearly with time producing a constant lateral-strain rate throughout the test, i.e. $d\varepsilon_L/dt = 0.02\text{x}10^{-4}$/s in Figure 1.5b. From this figure, it can be observed that the axial-strain rate fluctuates from $d\varepsilon_A/dt = 0.17\text{x}10^{-4}$ decreasing fast to about $5\text{x}10^{-7}$/s at the peak stress and then fluctuating to rates from about $1\text{x}10^{-8}$/s - $2\text{x}10^{-6}$/s satisfying static to quasi-static loading conditions in uniaxial compression tests for quasi-brittle materials (Hudson et al. 1971; P. H. Bischoff and Perry 1991; Wawersik and Brace 1971; Wawersik and Fairhurst 1970). In the same manner, the loading rate fluctuates from $dF/dt = 1.7\text{x}10^{-1}$ kN/s to about $1\text{x}10^{-4}$ - $1\text{x}10^{-3}$ kN/s at peak stress and thereafter, experiencing rates up to 0.02 kN/s.

Axial load (by a load cell), axial strain (by both strain gauges and external LVDTs) and lateral strain (by a ring extensometer) values were acquired continuously by a data acquisition system at a rate of 4 data points per second. Digital images taken automatically by the digital cameras were recorded simultaneously pairing the applied axial load with the respective instant image by an analog data recording.

3D DIGITAL IMAGE CORRELATION METHOD

The principle of 3D computer rests on recovering the three-dimensional position by recording simultaneous image points using two cameras (C and C'), as shown schematically in Figure 1.6 (Sutton et al. 2009). For instance, two 3D points Q and R on the same projective ray (C, p) demonstrate that there exists an infinity of 3D points that correspond to the image point p. On the other hand, if two image points are (p, q'), then the unique 3D point correspond to Q. Similarly, image points (p, r') correspond to a unique 3D point R.

Then, the sensor positions for a common 3D point $\widetilde{M}$, the scaled sensor location in the left camera, $\widetilde{m}$, and the corresponding scaled sensor location in right camera, $\widetilde{m}'$, are related directly related through transformation matrices ([K], [T]) to transforms vectors in the world coordinate system, into the pinhole system located in the left and right camera by

$$m = [\mathrm{K}] \bullet [\mathrm{T}] \bullet \{\widetilde{M}\}$$

$$\widetilde{m}' = [\mathrm{K}'] \bullet [\mathrm{T}'] \bullet \{\widetilde{M}\} \qquad (1)$$

The matrices [K] and [T] (or [K′] and [T′]) take into account elementary transformations of the pinhole camera model and the associated coordinate systems based on pure perspective projection concepts of a coordinate point. The first transformation relates the world coordinate system of a scene point to coordinates in the camera system which requires rotation and translation operations associated to [T] (or [T′]). A second and subsequent transformations are the projection of this point onto the image coordinate system (retinal plane) to later transform this point into the sensor coordinate system (pixel units) both associated to [K] (or [K′]).

3D DIGITAL IMAGE CORRELATION SET UP AND MEASUREMENT

3D DIC method is based on the calculation of surface deformation of an object by using a number of digital images from a reference undeformed and subsequent deformed states. This technique encompasses setting up two digital

cameras pointing at the specimen from two different angles and capturing a series of grey-scale images of the surface pattern. In this manner, a three-dimensional measurement of the specimen shape and displacements is created.

As it is shown in Figure 1.3, during test the cameras, positioned on the left and right sides, were symmetrically focusing on rock specimen to capture digital grey-scale images. The cameras consisted of two high-resolution monochrome stereo cameras (i.e. Fujinon HF75SA-1, 1:1.8/75mm, 5 Megapixels resolution) deemed suitable for quasi-static load testing. Continuous and uniform illumination across the entire rock specimen was provided by a conveniently adjusted goose-neck halogen light to ensure adequate contrast with minimal rock heating.

The images were captured by Vic-Snap software (produced by Correlated Solutions Inc.) using an exposure time of 37 ms. For quasi-static loading conditions, the primary function of the exposure time is to reduce the required object illumination for adequate image contrast (Sutton et al. 2009). Prior to the compression tests, each camera was stereo calibrated using a 30-mm standard target having uniformly spaced markers. Calibration of the cameras was done by taking at least 30 image pairs at the calibration target. To do so, as it is shown in Figure 1.7a, the calibration target was positioned and orientated differently, i.e. tilted and rotated, in and out of plane, close to the speckled rock specimen.

Typical image pairs obtained by the left and right side cameras during calibration are shown in Figure 1.7a. The total images acquired during calibration were computed and analysed by VIC-3D software. VIC-3D software has been used effectively in a number of DIC material testing, e.g. (Sutton et al. 2009). Stereo calibration results produced a standard deviation of residuals of 0.020 (in pixels), in general for all the tests. This value represents the difference between the position where a target point was found in the image and the theoretical position where the mathematical calibration model places the point. The value 0.020 suggests that the calibration of the cameras is adequate for

measurements (Sutton et al. 2009). Therefore, the camera set up was ready for starting the compressive test.

During the loading tests, the digital cameras were programmed to capture the images automatically at a frame rate of a picture each 0.5 seconds, from the start of loading for during the first 30 minutes, and thereafter a picture each 5 seconds until the end of the tests. This frame rate results suitable to capture and store a large number of images for further analysis. In this manner, digital data file size and subsequent computation time were minimised. Digital images were stored for post-test processing and analysis.

Data acquisition systems of Vic-Snap and Instron 1342 were connected via an analog data recording and instantaneous axial deformation, lateral deformation, applied load and instantaneous pair images were synchronously acquired. A one-to-one correspondence between load, deformation and respective digital images during the compressive tests allowed assigning a specific image to a specific stress to study strain development with stresses.

Deformation field study was concentrated within a portion of the specimen in each image (i.e. the area of interest) as shown in Figure 1.7b. VIC-3D software (produced by Correlated Solutions Inc.) was used for the analysis. This software implements image processing algorithms for tracking surface coordinates and deformation from image to image. For deformation and strain analysis, a start image, when the axial load was not applied yet to the rock, was selected. The start image provides a reference for VIC-3D software to recreate the deformation field on subsequent images. Upon completion of image processing, the field of strains of the specimen surface was obtained. Strain measurement accuracy by computing confidence margins gets values in the order of 0.03×10^{-4}.

TEST RESULTS AND DISCUSSION

ROCK STRESS-STRAIN CHARACTERISTICS

Figure 1.4 shows a shear failure plane oriented about 30º-40º formed after the end of the compressive loading. As it can be seen in Figure 1.4, shear failure plane is not affected by any bedding plane. The inherent bedding planes represent the texture of the sandstone rock rather than some weak planes which control shear failure. Previous studies on sandstone have shown the bedding plane upon UCS relation is complex and not unique, e.g. a W or U shape variation of UCS as the bedding orientation is increased from 0º to 90º (Al-Harthi 1998), a monotonic decrease in UCS with increasing the bedding orientation (Gatelier et al. 2002), etc. In this study, all the samples were cores in the same direction; therefore, effect of anisotropic properties, if any, was eliminated. Results of UCS tests on five specimens which are shown in Table 1.1 confirm this statement.

Figure 1.8, Figure 1.9 and Figure 1.10 show the typical stress-strain curves for Hawkesbury sandstone. In these figures, stress-strain relations are given in terms of the axial stress q and respective axial strain ε_A and lateral strain ε_L. In the pre-peak regime, the characteristics threshold stresses for fracture damage of rock associated with crack closure (q_{cc}), crack initiation (q_{ci}), crack damage (q_{cd}) and peak stress (q_{peak}), were identified from the typical stress-strain curves. The following expressions were used (Martin and Chandler 1994):

$$\varepsilon_{vol} = \varepsilon_A + 2\varepsilon_L \tag{2}$$

$$\varepsilon_{vol}^{e} = \frac{1-2\upsilon}{E} q \tag{3}$$

$$\varepsilon_{vol}^{c} = \varepsilon_{vol} - \varepsilon_{vol}^{e} \tag{4}$$

Where ε_{vol} is the volumetric strain, and ε_{vol}^{e} and ε_{vol}^{c} are the elastic volumetric strain and the crack-induced volumetric strain, respectively. ε_A is the average axial strain obtained by strain gauges. ε_L is the lateral strain from the lateral extensometer.

The initial region of the stress-strain curve bound by q_{cc} represents the stress level where closure of existing micro cracks in the rock takes place. Once the existing cracks are closed, the rock is assumed to behave elastic until the onset of dilation at q_{ci}. Cracking associated with axial stresses slightly above q_{ci} does not result in reduced rock strength (Martin and Chandler 1994). q_{cd} represents the onset of unstable crack growth characterised by significant structural changes to the rock (Hallbauer et al. 1973), while q_{peak} marks the onset of the post-peak behaviour.

Figure 1.10 shows the location of the threshold stresses for fracture damage in a typical stress-strain curve of Hawkesbury sandstone. It was found that, on average q_{cc} takes place at a stress of $0.29q_{peak}$, and q_{ci} and q_{cd} occur at $0.52q_{peak}$ and $0.67q_{peak}$ respectively .Young´s modulus (E) and Poisson's ratio (υ) for the rock were extracted from the linear-elastic portion of the stress-strain curves limited by q_{cc} and q_{ci} with respective values $dq/d\varepsilon_A$ and $-\varepsilon_L/\varepsilon_A$. In general, it was observed that the tangent modulus of the rock is at its highest value at relatively low axial strains and subsequently, the tangent modulus decreases progressively as the rock is reaching the peak stress. Table 1.1 summarises the threshold stresses of the tested rock samples.

It was observed that after the peak stress (q_{peak}) took place, progressive drop of stress was followed associated with the progressive strength degradation of the rock. The respective post-peak stress-strain curve of Hawkesbury sandstone was characterised by both class I (i.e. $M = dq/d\varepsilon_A < 0$) and class II rock (i.e. $M > 0$) if post-peak behaviour is classified similar to Wawersik and Fairhurst (Wawersik and Fairhurst 1970) (see Figure 1.1). That is, a negative post-peak slope immediately after the onset of peak stress and then a positive post-peak slope taking place at a stage where the compressive stress was about $0.7q_{peak}$ - $0.8q_{peak}$ up until the end of the test where residual stress was close to zero.

Hawkesbury sandstone show no sign of perceptible major cracking detected in pre-peak regime. This evidence is well supported by the field of

strains in the rock surface obtained by 3D DIC as shown later. Localisation occurred in the post-peak regime in the form of a predominant single shear-failure plane.

POST-PEAK STRAIN MEASUREMENT METHOD

Figure 1.8a and Figure 1.8b compare the stress-strain curves generated from three different methods for axial and lateral strain measurements. That is, the axial strain by the vertical displacement of the machine platen, the average readings of a couple of LVDTs, and by a virtual extensometer E0 (extracted from 3D DIC analysis) located vertically along the rock sample, as shown in Figure 1.7b. In lateral strain, strains from the chain extensometer strain and virtual extensometer E5 and E6 located horizontally in the rock sample, as shown in Figure 1.7b, are compared.

Figure 1.8a suggests that strains from 3D DIC technique are independent and free from bedding error, in contrast to LVDT strains, and free from any apparent additional strain due to machine displacements compliance. In fact, strains from 3D DIC measures only the actual strain deformations of the specimen under compression. Previous researches on material testing using DIC technique on rocks (Nguyen et al. 2011; Song et al. 2013; Zhang et al. 2012) and polymers (Heinz and Wiggins 2010) support this finding. Figure 1.8b shows a nearly single curve characterising the stress-lateral strain behaviour of the rock in pre-peak regime independent on the measurement device.

Strains from 3D DIC virtual extensometers and strain gauges are in well agreement in magnitude as shown in Figure 1.9 and Figure 1.10. The Young's modulus of Hawkesbury sandstone in Figure 1.9, with strains measured by strain gauges, yielded 10.4 GPa on average, as shown in Table 1.1. Similarly, the Young's modulus of the rock from 3D DIC analysis in the four tests yielded 10.0 GPa on average as presented in Table 1.1. The threshold stresses yielded nearly the same values after stress-strain curves with strain gauges and 3D DIC measurements were analysed, as shown in Table 1.1.

In general, in the post-peak regime, progressive and generalised fractures in the rock surface may either break or detach bonded strain gauges from the rock surface making post-peak strains reading difficult or impossible as shown in the incomplete stress-strain curves in Figure 1.9. In this figure, labels A, B, D, and F refer to the strain gauge location in the rock sample as depicted in Figure 1.4 (C and E are not shown in Figure 1.9 to avoid overcrowding the figure). On the other hand, the post-peak strains, free from bedding error, were captured straightforward with 3D DIC as shown in Figure 1.10. In this figure, labels DIC-E0, DIC-E1, and DIC-E2 refer to the virtual extensometers location in the rock sample as depicted in Figure 1.7b (DIC-E3, and DIC-E4 are not shown in Figure 1.10 to avoid overcrowding the figure).

In Figure 1.9, curves B and F, which demonstrate results of those strain gauges that were not damaged in post-peak regime (see Figure 1.4), all experienced inelastic unloading. 3D DIC proved to be useful for studying the pre-peak and more importantly the post-peak strain behaviour of rock in uniaxial compression. Figure 1.10 shows different post-peak curves, characterised by either inelastic unloading or localised strain depending on the virtual extensometer length and location in the rock surface with respect to the localised zone. In this similar manner, Figure 1.8b shows different post-peak curves by labels DIC-E5 and DIC-E6, characterised by either inelastic unloading or localised strain, in stress-lateral strain space.

In Figure 1.10, a portion of the rock outside the localised zone (taking place as a shear-failure plane) where strains were measured by DIC-E1, experiences inelastic unloading. In this case, the area under the stress-strain curve enclosed by the loading-unloading path is the pre-peak energy per unit volume of rock, which is dissipated due to micro cracking during the loading process up to the peak. On the other hand, both DIC-E0 and DIC-E2 encountered the localised zone at different extent, experiencing post-peak paths differently. So the energy from the post-peak stress-strain curve is associated with additional energy dissipated locally in the damage zone, e.g. (Bažant 1989; Jansen and Shah 1997; Markeset and Hillerborg 1995).

FIELD STRAIN PATTERNS

Digital image correlation analysis provided quantitative evidence on the nature of field strains developed in the rock surface throughout the compressive test. In Figure 1.10, different loading stages along the stress-strain curve were identified to further examine field strain patterns both in axial and shear-strain domains. In pre-peak state, the threshold stress values for fracture damage of rock at $0.29q_{peak}$, 0.52 q_{peak} and $0.67q_{peak}$, corresponding to cack closure, crack initiation and crack damage respectively, together with the peak stress q_{peak} were selected. In post-peak state a number of specific stresses from $0.95q_{peak}$ to $0.15q_{peak}$ were selected.

Figure 1.11a shows the field of axial strains within the area of interest analysed during pre-peak regime at the threshold stresses for fracture damage and peak stress. The field of axial strains suggests the specimen does deform at a uniform strain rate as axial strains start increasing uniformly with increasing axial load until peak stress was reached, as shown by colour gradient in Figure 1.11a. In correspondence with uniform development of the field of axial strains, the axial strains measured by the virtual extensometers DIC-E0, DIC-E1, DIC-E2, DIC-E3,DIC-E4, and DIC-E5, location depicted in Figure 1.7b, produces nearly a single stress-strain curve as shown in Figure 1.10 and Figure 1.8a. Finally, Figure 1.11a shows no sign of perceptible cracking in pre-peak regime.

Figure 1.11b and Figure 1.11c show the field of axial strains in the rock surface during post-peak regime at selected stress levels. In the post-peak regime the axial-strain field does not increase uniformly, but progressively at different rates with large deformations localising around the future failure plane. The results suggest that deviation from strain uniformity begins progressively after peak stress was reached. This phenomenon has shown clearly by colour gradient in Figure 1.11b for stresses relatively immediately after q_{peak} at $0.95q_{peak}$ to $0.75q_{peak}$. Thereafter, as shown by colour gradient in Figure 1.11c for stresses ranging from $0.70q_{peak}$ to $0.15q_{peak}$ strain localisation is accelerated which resulted in increasing the rate of strength degradation. As shown in Figure 1.10,

from the onset of post-peak, the virtual extensometers DIC-E0, DIC-E1, DIC-E2, DIC-E3, DIC-E4, and DIC-E5 experience either inelastic unloading or localised irreversible strain at different extent. Furthermore, comparison of Figure 1.8 and Figure 1.10 indicates that the local strains in the localisation zone may be much larger than the nominal average strain obtained from LVDT or lateral extensometer. Finally, it was observed that the failure plane became noticeable at the naked eye only long after the peak stress took place, on average at $0.45q_{peak}$ - $0.55q_{peak}$, as shown in Figure 1.11c.

Figure 1.12a shows the field of shear strains within the area of interest analysed at the threshold stresses (i.e. q_{cc}, q_{ci}, q_{cd}) and the peak stress, q_{peak}, in the pre-peak regime. In the shear-strain field strains, with values of about $5x10^{-4}$, are marginal (see nearly a single colour gradient in Figure 1.12a). In conjunction with the field of axial strains discussed above, no localised shear strains into a failure plane was observed in the pre-peak regime.

Figure 1.12b shows the field of shear strains in the rock surface during post-peak regime at selected stress levels. In the post-peak regime the shear strains are localised progressively along the future failure plane. First, the rate of shear strain development was slow, and then it accelerated with the increasing rate of strength degradation. The field of shear strains, within the area of interest, shows that shear strains are slightly localised along the future failure plane. Barely noticeable colour gradient even at a stress level of $0.7q_{peak}$ and $0.6q_{peak}$ was noticed. As it may be seen in Figure 1.12b, localised shear strains becomes clear only from stress levels about $0.45q_{peak}$ - $0.55q_{peak}$, where the failure plane becomes noticeable at the naked eye. Thereafter, a more significant shear strain gradient in the specimen was noticed.

CONCLUSIONS

In this study, three-dimensional digital image correlation (3D DIC) method was used to study the pre-peak and post-peak stress-strain characteristics of Hawkesbury sandstone in a series of uniaxial compression under quasi-static

loading conditions. 3D DIC is a non-contact method that provides deformation and motion measurements of an object undergoing external load. Post-peak stress-strain of the rock was successfully captured by controlling the applied axial load with prescribed constant lateral-strain rate from monotonically increased lateral strains. The following conclusions have been drawn from this study.

Post-peak strain measurement with strain gauges bonded to the specimen surface is very difficult due to strain gauge damage caused by post-peak large crack propagations and strain localisation. In general, it was noticed that the strain gauges will either damage or exhibit unloading behaviour. It was found that using 3D DIC method, relatively large strains developed in the rock, in particular within localised zones, can be captured successfully.

In addition, 3D DIC method shows major advantages in contrast with conventional external strain measurements. Firstly, by providing strains free from bedding errors unlike LVDT, and secondly by generating the field of strain development relevant for strain localisation insights.

In post-peak regime, different stress-strain curves, characterised by either local inelastic unloading or localised strain, can be produced depending on the gauge length and gauge location with respect to the compression damage zone (CDZ) and the localised zone. 3D DIC method serves well for strain measurement inside and outside the CDZ.

Field strain development, both in axial and shear strain domains, in the rock suggests that strain localisation takes place progressively and develops at a lower rate in the pre-peak regime. Strain localisation, however, is accelerated in the post-peak regime associated with accelerating rate of strength degradation. The results show that the major failure plane became noticeable only long after the peak stress was reached.

ACKNOWLEDGEMENT

The work has been supported by the Deep Exploration Technologies Cooperative Research Centre whose activities are funded by the Australian Government's Cooperative Research Centre Programme. This is DET CRC Document 2015/781.

REFERENCES

Al-Harthi AA (1998) Effect of planar structures on the anisotropy of Ranyah sandstone, Saudi Arabia Engineering Geology 50:49-57 doi:http://dx.doi.org/10.1016/S0013-7952(97)00081-1

Amann F, Button E, Evans K, Gischig V, Blümel M (2011) Experimental Study of the Brittle Behavior of Clay shale in Rapid Unconfined Compression Rock Mechanics and Rock Engineering 44:415-430 doi:10.1007/s00603-011-0156-3

Bažant Z (1989) Identification of strain softening constitutive relation from uniaxial tests by series coupling model for localisation Cement and Concrete Research 19:973-997

Bieniawski ZT, Bernede MJ (1979) Suggested methods for determining the uniaxial compressive strength and deformability of rock materials: Part 1. Suggested method for determination of the uniaxial compressive strength of rock materials International Journal of Rock Mechanics and Mining Sciences & Geomechanics Abstracts 16:137 doi:http://dx.doi.org/10.1016/0148-9062(79)91450-5

Brian R. Rust, Jones BG (1987) The Hawkesbury Sandstone South of Sydney, Australia: Triassic analogue for the deposit of a large, braided river Journal of Sedimentary Petrology 57:222-233

Chu TC, Ranson WF, Sutton MA (1985) Applications of digital-image-correlation techniques to experimental mechanics Experimental Mechanics 25:232-244 doi:10.1007/BF02325092

Daniel C. Jansen SPS, Edwin CR (1995) Stress-Strain Results of Concrete from Circumferential Strain Feedback Control Testing Materials Journal 92 doi:10.14359/9774

Dautriat J, Bornert M, Gland N, Dimanov A, Raphanel J (2011) Localized deformation induced by heterogeneities in porous carbonate analysed by multi-scale digital image correlation Tectonophysics 503:100-116 doi:http://dx.doi.org/10.1016/j.tecto.2010.09.025

Fairhurst CE, Hudson JA (1999) Draf ISRM suggested method for the complete stress-strain curve for intact rock in uniaxial compression International Journal of Rock Mechanics and Mining Sciences 36:279-289 doi:http://dx.doi.org/10.1016/S0148-9062(99)00006-6

Gatelier N, Pellet F, Loret B (2002) Mechanical damage of an anisotropic porous rock in cyclic triaxial tests International Journal of Rock Mechanics and Mining Sciences 39:335-354 doi:http://dx.doi.org/10.1016/S1365-1609(02)00029-1

Hallbauer DK, Wagner H, Cook NGW (1973) Some observations concerning the microscopic and mechanical behaviour of quartzite specimens in stiff, triaxial compression tests International Journal of Rock Mechanics and Mining Sciences & Geomechanics Abstracts 10:713-726 doi:http://dx.doi.org/10.1016/0148-9062(73)90015-6

Hashiba K, Okubo S, Fukui K (2006) A new testing method for investigating the loading rate dependency of peak and residual rock strength International Journal of Rock Mechanics and Mining Sciences 43:894-904 doi:http://dx.doi.org/10.1016/j.ijrmms.2005.12.005

Hawkes I, Mellor M (1970) Uniaxial testing in rock mechanics laboratories Engineering Geology 4:179-285 doi:http://dx.doi.org/10.1016/0013-7952(70)90034-7

He C, Okubo S, Nishimatsu Y (1990) A study of the class II behaviour of rock Rock Mechanics and Rock Engineering 23:261-273 doi:10.1007/BF01043307

Heinz SR, Wiggins JS (2010) Uniaxial compression analysis of glassy polymer networks using digital image correlation Polymer Testing 29:925-932 doi:http://dx.doi.org/10.1016/j.polymertesting.2010.08.001

Hudson JA, Brown ET, Fairhurst C (1971) Optimizing the control of rock failure in servo-controlled laboratory tests Rock mechanics 3:217-224 doi:10.1007/BF01238181

ISRM (1981) Rock characterization testing and monitoring—ISRM suggested methods. Oxford

Jansen DC, Shah S (1997) Effect of Length on Compressive Strain Softening of Concrete Journal of Engineering Mechanics 123:25-35 doi:doi:10.1061/(ASCE)0733-9399(1997)123:1(25)

Markeset G, Hillerborg A (1995) Softening of concrete in compression — Localization and size effects Cement and Concrete Research 25:702-708 doi:http://dx.doi.org/10.1016/0008-8846(95)00059-L

Martin C, Chandler N The progressive fracture of Lac du Bonnet granite. In: International Journal of Rock Mechanics and Mining Sciences & Geomechanics Abstracts, 1994. vol 6. Elsevier, pp 643-659

Nguyen TL, Hall SA, Vacher P, Viggiani G (2011) Fracture mechanisms in soft rock: Identification and quantification of evolving displacement discontinuities by extended digital image correlation Tectonophysics 503:117-128 doi:http://dx.doi.org/10.1016/j.tecto.2010.09.024

Okubo S, Nishimatsu Y (1985) Uniaxial compression testing using a linear combination of stress and strain as the control variable International Journal of Rock Mechanics and Mining Sciences & Geomechanics Abstracts 22:323-330 doi:http://dx.doi.org/10.1016/0148-9062(85)92064-9

Okubo S, Nishimatsu Y, He C (1990) Loading rate dependence of class II rock behaviour in uniaxial and triaxial compression tests—an application of a proposed new control method International Journal of Rock Mechanics and Mining Sciences & Geomechanics Abstracts 27:559-562 doi:http://dx.doi.org/10.1016/0148-9062(90)91007-T

P. H. Bischoff, Perry SH (1991) Compressive behaviour of concrete at high strain rates Materials and Structures 24:425--450

Rummel F, Fairhurst C (1970) Determination of the post-failure behavior of brittle rock using a servo-controlled testing machine Rock mechanics 2:189-204 doi:10.1007/BF01245574

Song H, Zhang H, Kang Y, Huang G, Fu D, Qu C (2013) Damage evolution study of sandstone by cyclic uniaxial test and digital image correlation Tectonophysics 608:1343-1348 doi:http://dx.doi.org/10.1016/j.tecto.2013.06.007

Sutton MA, Orteu JJ, Schreier H (2009) Image Correlation for Shape, Motion and Deformation Measurements. Springer US,

Taheri A, Tani K (2008) Use of down-hole triaxial apparatus to estimate the mechanical properties of heterogeneous mudstone International Journal of Rock Mechanics and Mining Sciences 45:1390-1402 doi:http://dx.doi.org/10.1016/j.ijrmms.2008.01.017

Tarasov B, Potvin Y (2013) Universal criteria for rock brittleness estimation under triaxial compression International Journal of Rock Mechanics and Mining Sciences 59:57-69 doi:http://dx.doi.org/10.1016/j.ijrmms.2012.12.011

Vasconcelos G, Lourenço P, Alves C, Pamplona J (2009) Compressive Behavior of Granite: Experimental Approach Journal of Materials in Civil Engineering 21:502-511 doi:doi:10.1061/(ASCE)0899-1561(2009)21:9(502)

Wawersik WR, Brace WF (1971) Post-failure behavior of a granite and diabase Rock mechanics 3:61-85 doi:10.1007/BF01239627

Wawersik WR, Fairhurst CA (1970) A Study of Brittle Rock Fracture in Laboratory Compression Experiments Int J Rock Mech Min Sci 7:561-575

Yang G, Cai Z, Zhang X, Fu D (2015) An experimental investigation on the damage of granite under uniaxial tension by using a digital image correlation method Optics and Lasers in Engineering 73:46-52 doi:http://dx.doi.org/10.1016/j.optlaseng.2015.04.004

Zhang H, Huang G, Song H, Kang Y (2012) Experimental investigation of deformation and failure mechanisms in rock under indentation by digital image correlation Engineering Fracture Mechanics 96:667-675 doi:http://dx.doi.org/10.1016/j.engfracmech.2012.09.012

LIST OF SYMBOLS AND NOMENCLATURE

F	Applied axial load
t	Time
q	Differential stress
q_{peak}	Peak stress
q_{cc}	Crack closure stress
q_{ci}	Crack initiation stress
q_{cd}	Crack damage stress
ε_A, ε_L	Axial and lateral strains
ε_{vol}	Volumetric strain
ε_{vol}^{e}	Elastic volumetric strain
ε_{vol}^{c}	Crack-induced volumetric strain, respectively.
E	Young´s modulus
υ	Poisson's ratio
$\mathrm{d}F/\mathrm{dt}$	Rate of loading
$\mathrm{d}\varepsilon_A/\mathrm{dt}$	Rate of axial strain
$\mathrm{d}\varepsilon_\mathrm{L}/\mathrm{dt}$	Rate of lateral strain
LVDT	Linear Variable Displacement Transducers
UCS	Unconfined Compressive Strength
3D DIC	Three-dimensional digital image correlation

CDZ Compression Damage Zone

LIST OF FIGURES

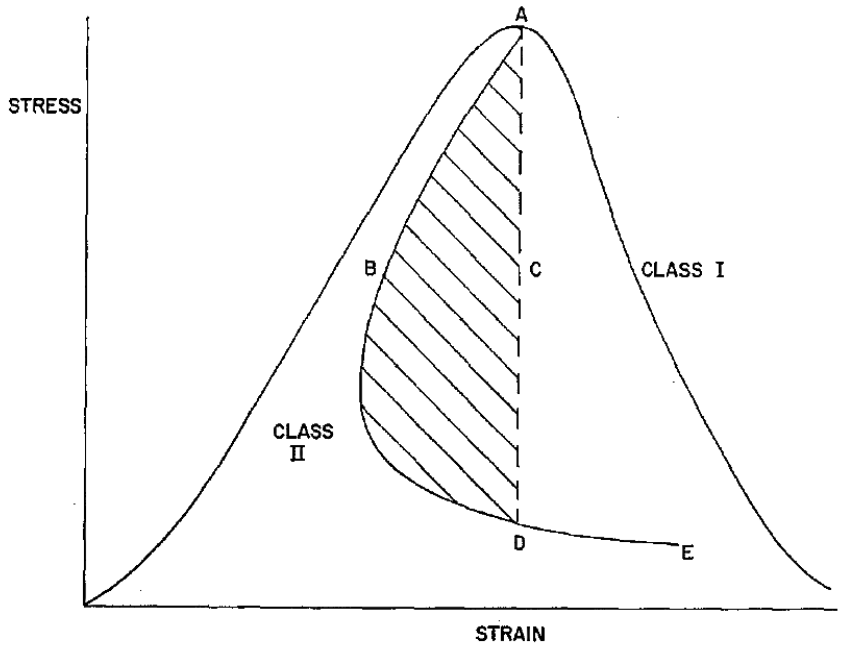

Figure 1.1 Classification of class I and class II behaviour of rock failure in uniaxial compression (Hudson et al. 1971)

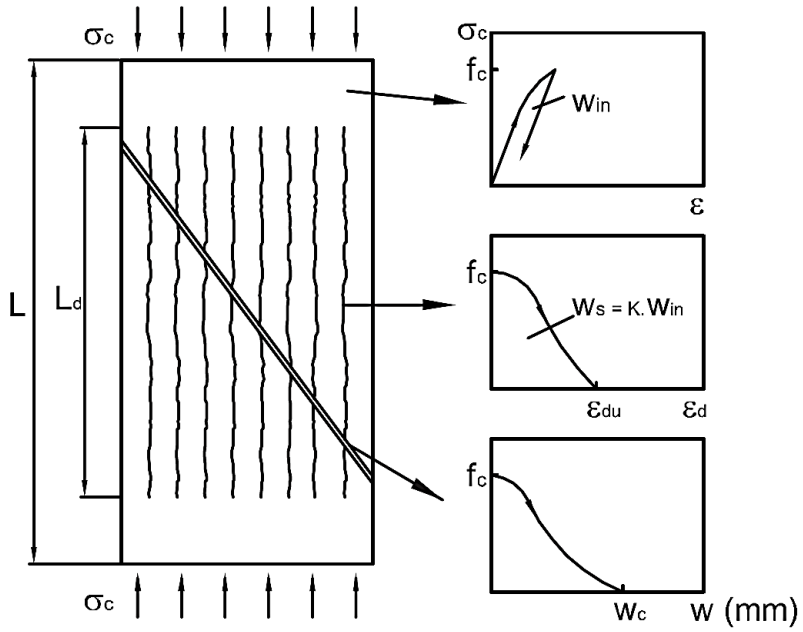

Figure 1.2 Identification of the compression zone damage model and deformation of a specimen loaded in uniaxial compression (Vasconcelos et al. 2009)

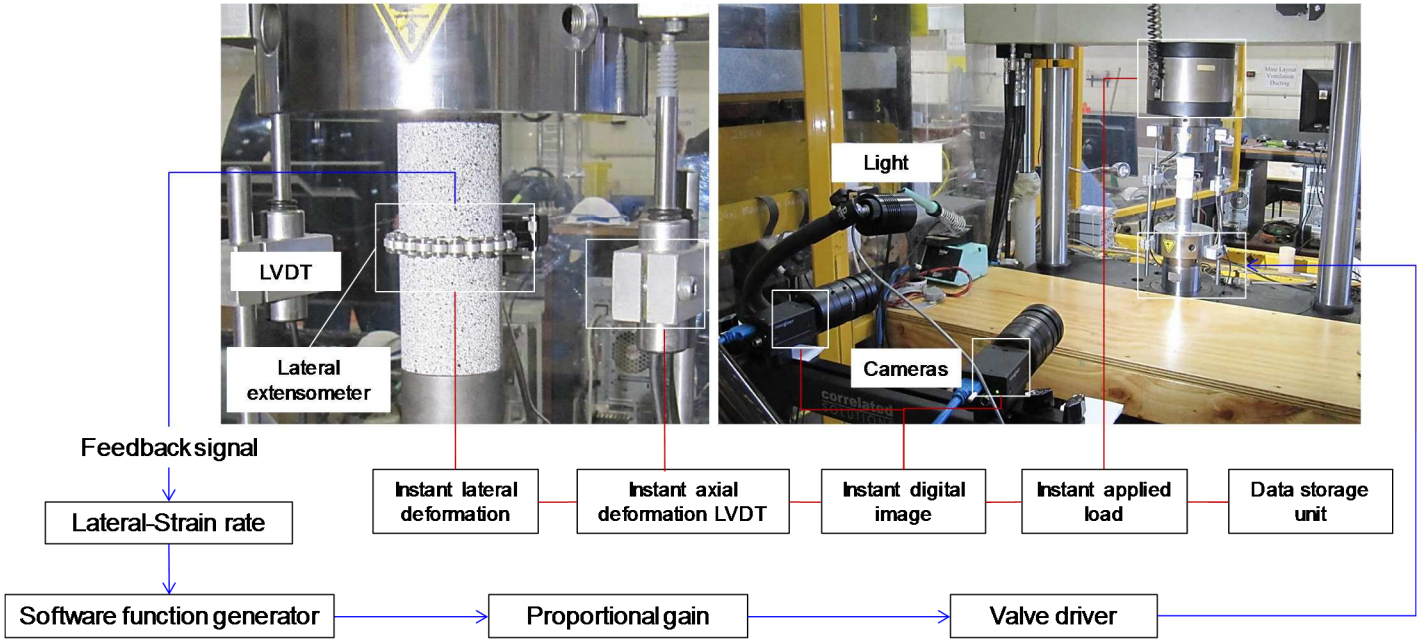

Figure 1.3 Experimental set up: servo-controlled closed-loop testing system and two-camera stereo system for 3D DIC in uniaxial compression loading

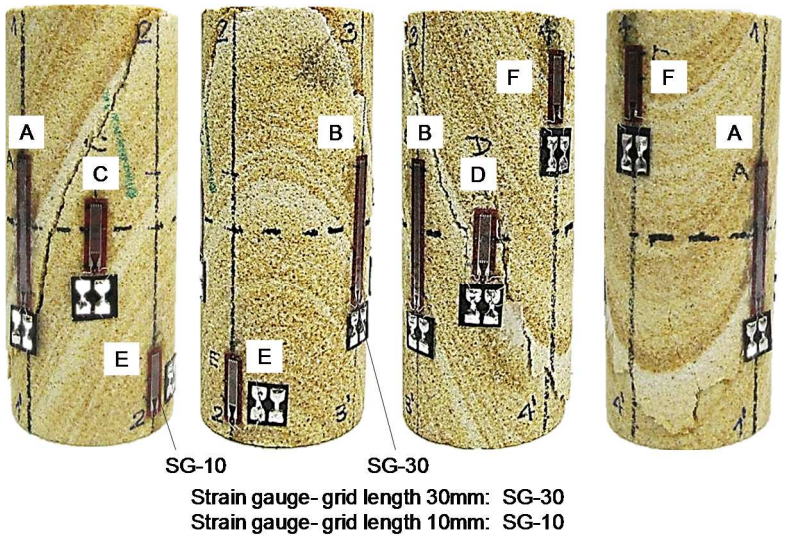

Figure 1.4 Strain gauge instrumentation arrangement and typical failure pattern of Hawkesbury sandstone. A, B, C, D and E refer to the location of strain gauges

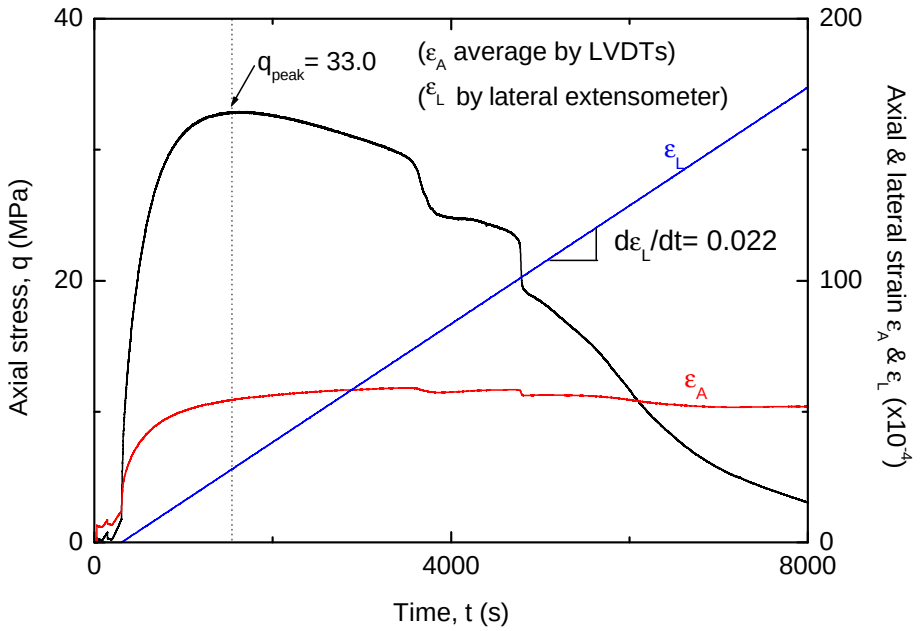
40
20
0
0
4000
8000
200
100
0
Axial stress, q (MPa)
Axial & lateral strain ε_A & ε_L (x10^-4)
Time, t (s)
q_peak = 33.0
(ε_A average by LVDTs)
(ε_L by lateral extensometer)
ε_L
dε_L/dt= 0.022
ε_A

a)

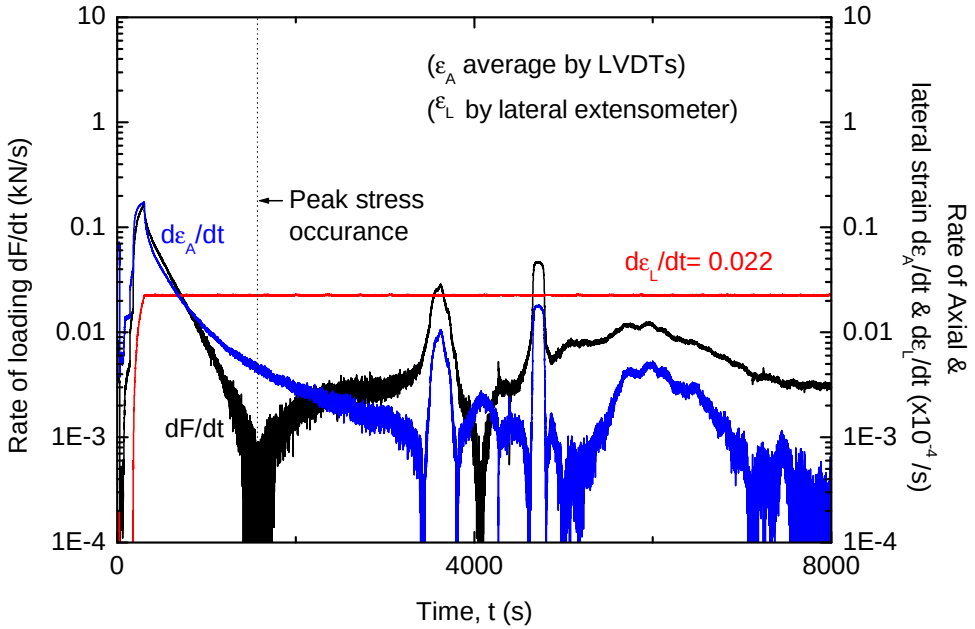

b)

Figure 1.5 Typical time history of a) loading and strains and b) loading rate and strain rate in uniaxial compression tests with lateral-strain rate feedback signal

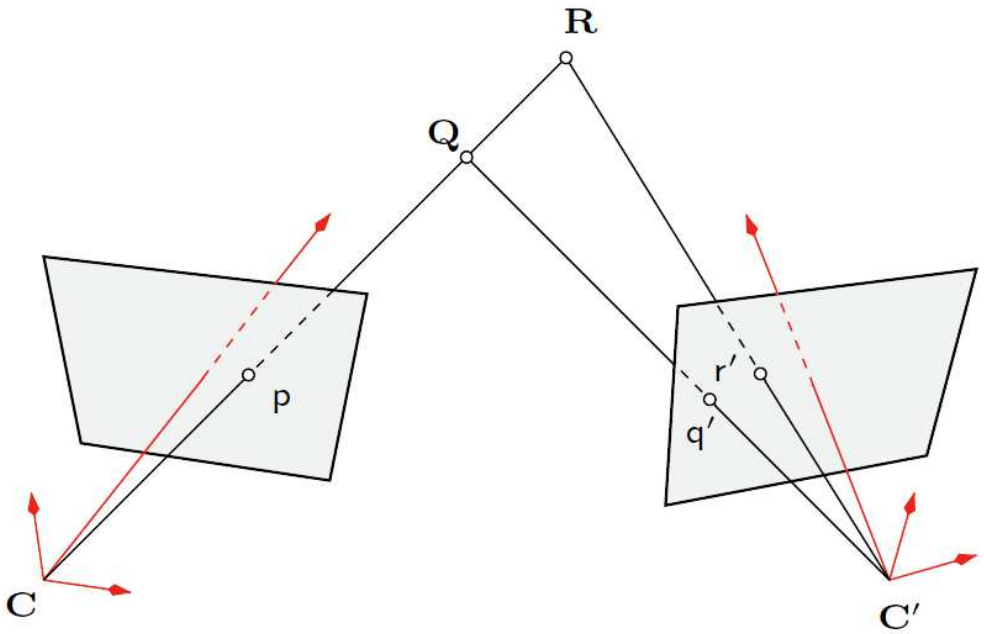

Figure 1.6 Recovering the third dimension by using two cameras (Sutton et al. 2009)

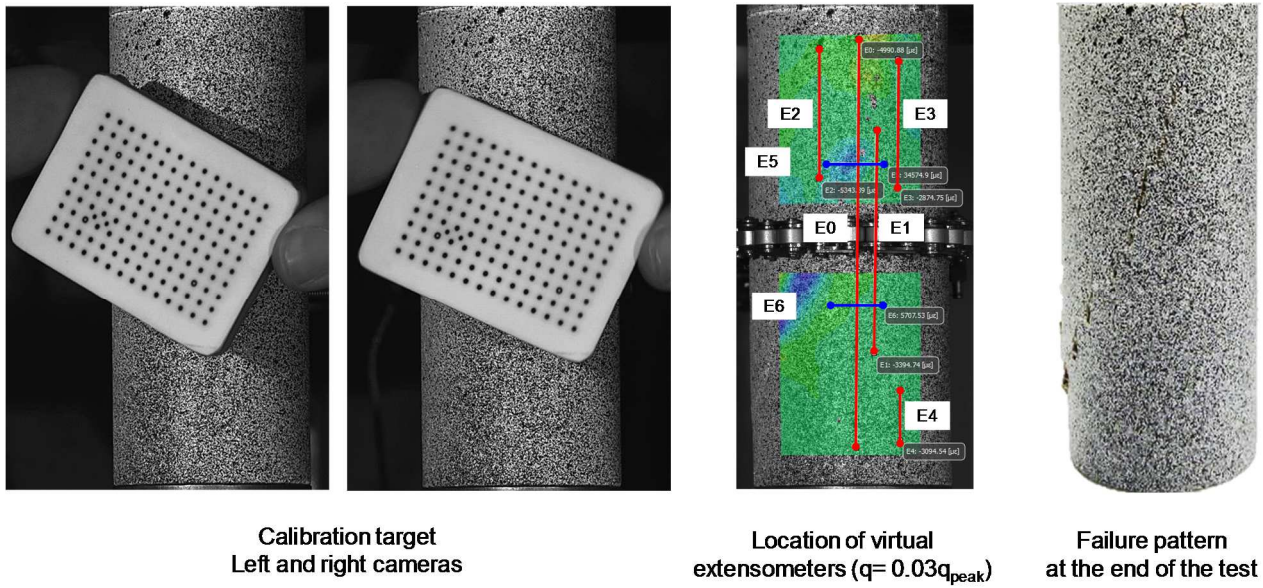

a) b)

Figure 1.7 a) Calibration procedure for the stereo cameras left and right pair imaging and b) location of the virtual extensometers within the area of interest and rock at the end of the compression test

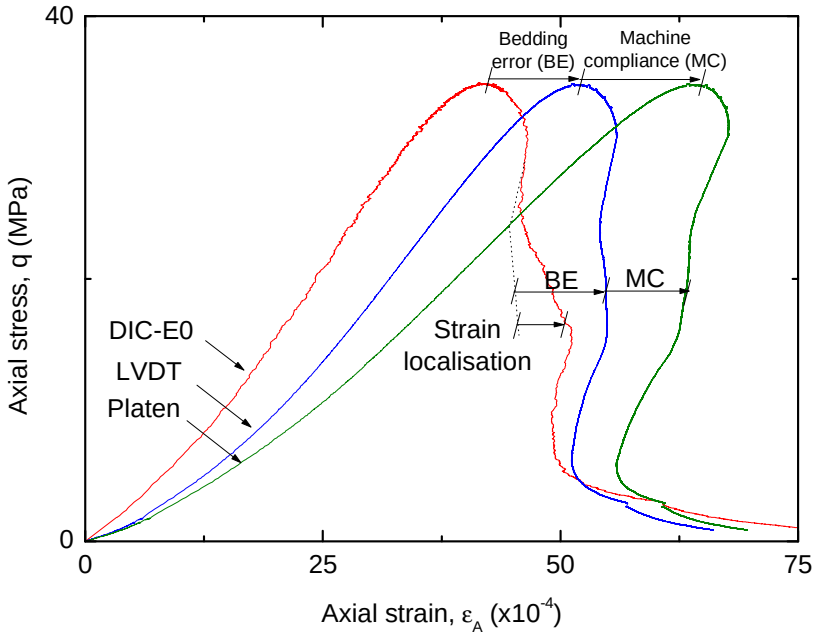
40
0
0
25
50
75
Axial stress, q (MPa)
Axial strain, ε_A (x10^-4)
Bedding error (BE)
Machine compliance (MC)
BE
MC
Strain localisation
DIC-E0
LVDT
Platen

a)

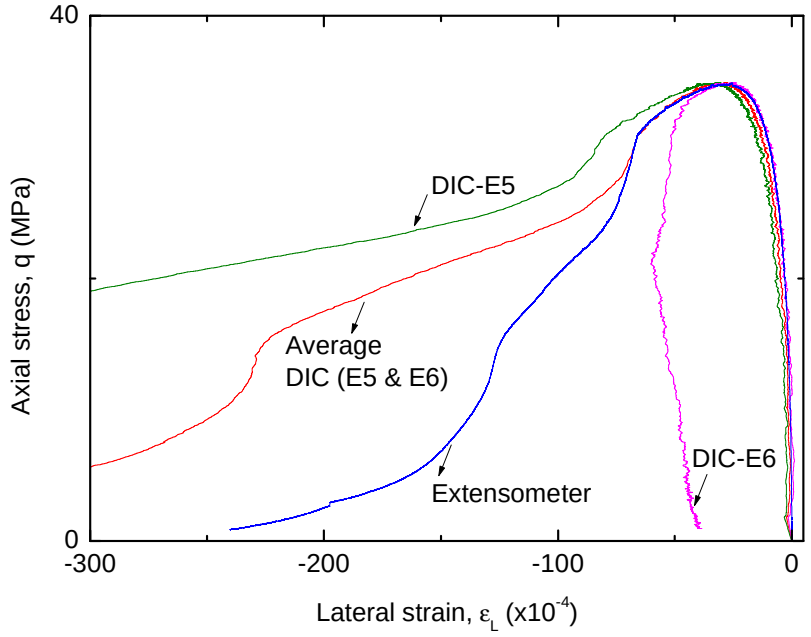

b)

Figure 1.8 a) Stress-axial strain curves from platen displacement, external LVDT and DIC measurements (DIC-E0) and b) Stress-lateral strain curves from lateral extensometer and DIC measurements (DIC-E5 and E6)

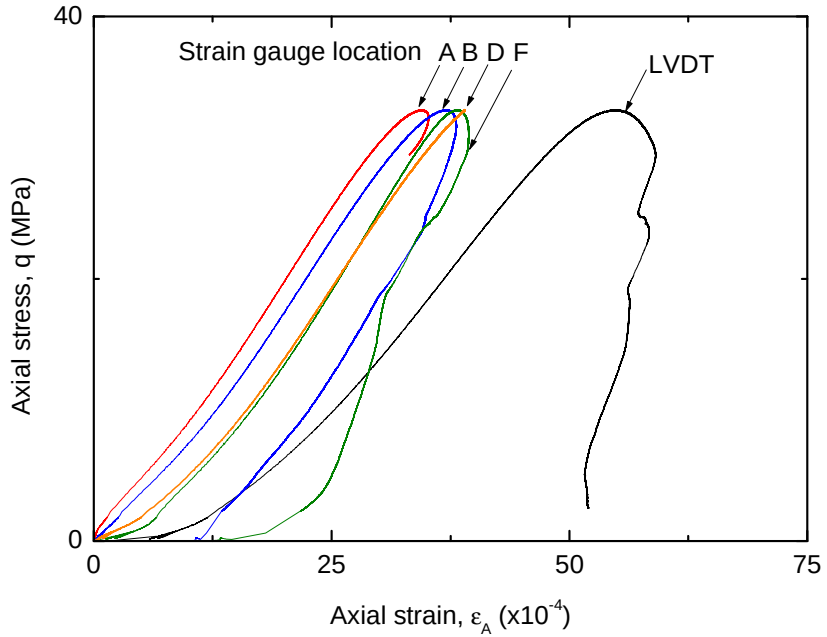

Figure 1.9 Typical stress-strain curves with axial strains obtained from external LVDT and strain gauges

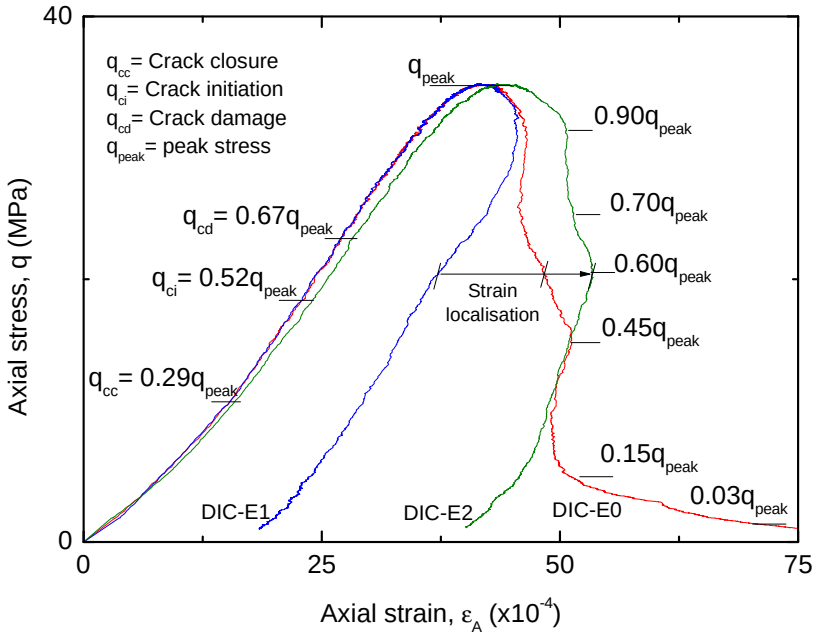

Figure 1.10 Typical stress-strain curves obtained from DIC for virtual extensometers DIC-E0, DIC-E1 and DIC-E2

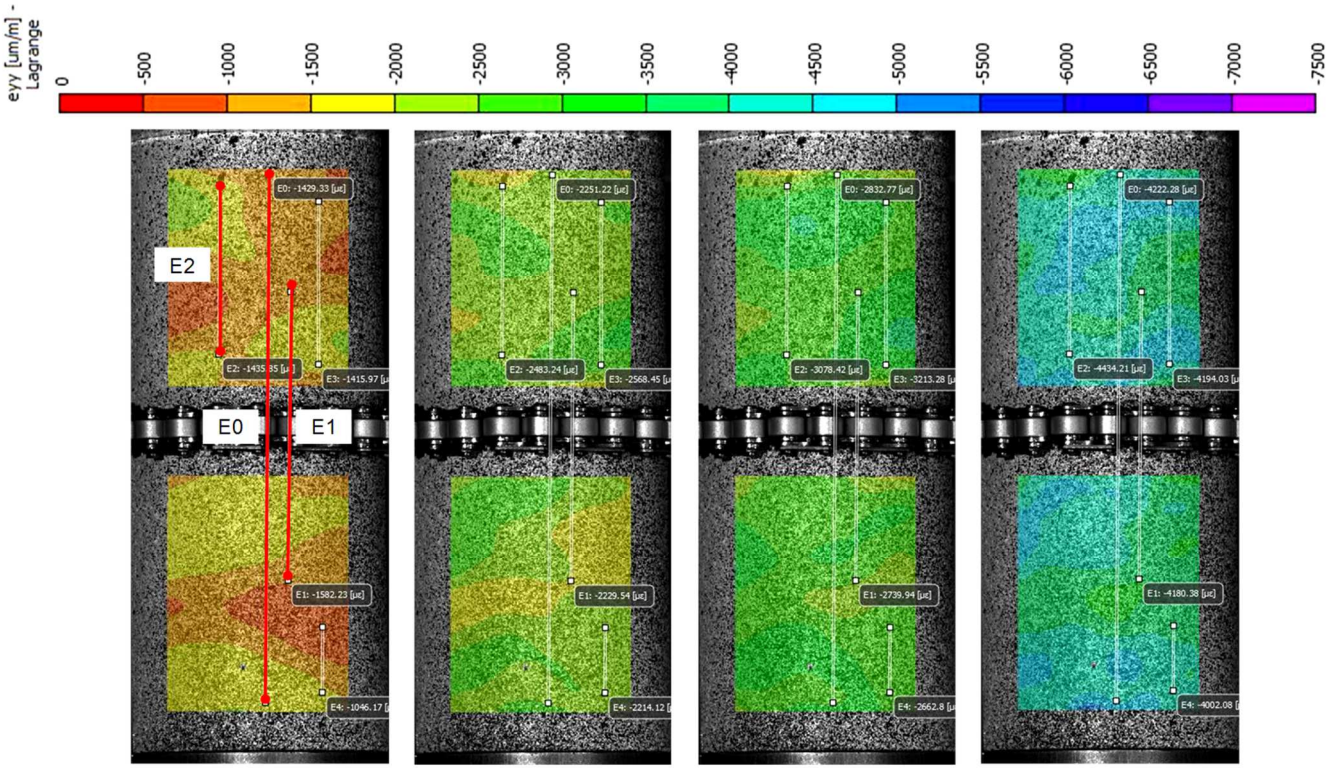

$q_{cc}= 0.29q_{peak}$ $q_{ci}= 0.52q_{peak}$ $q_{cd}= 0.67q_{peak}$ q_{peak}

a)

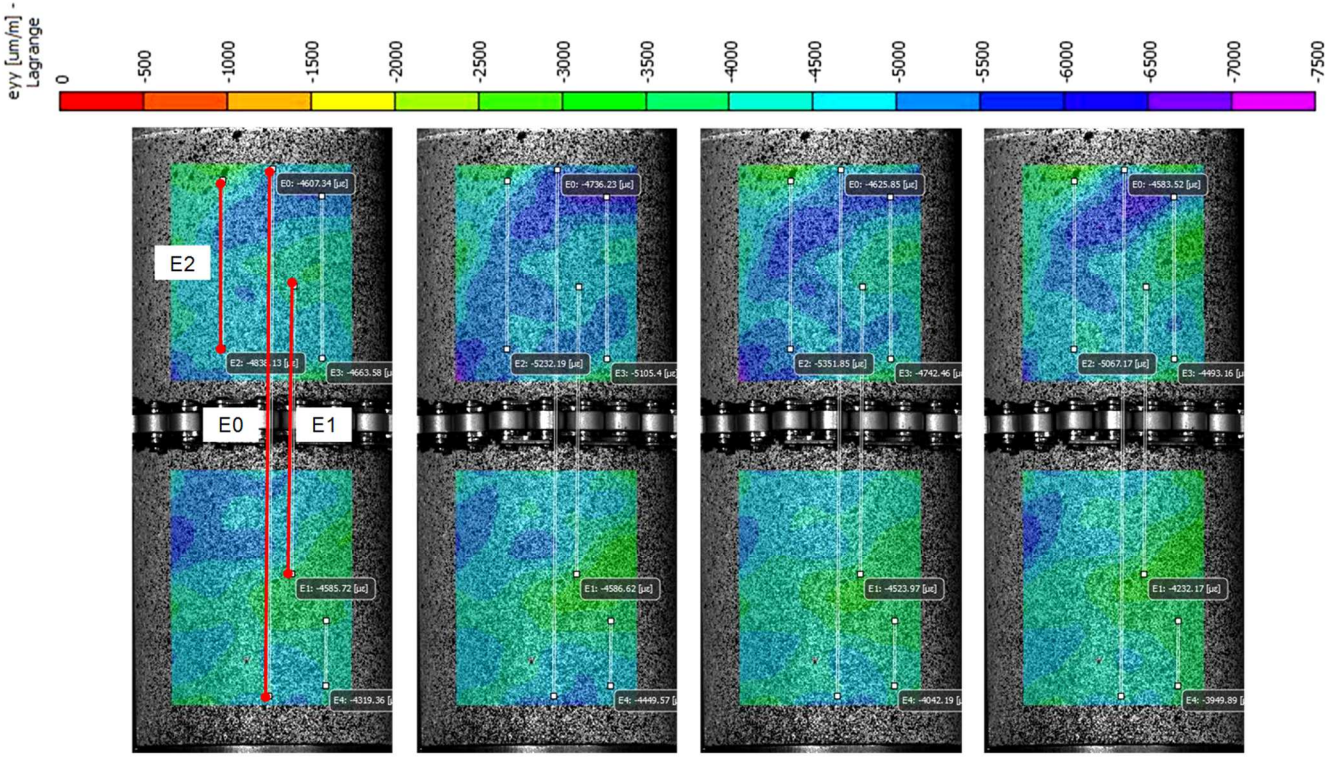
eyy [um/m] - Lagrange
0
-500
-1000
-1500
-2000
-2500
-3000
-3500
-4000
-4500
-5000
-5500
-6000
-6500
-7000
-7500
E2
E0
E1
E0: -4607.34 [με]
E2: -4836.13 [με]
E3: -4663.58 [με]
E1: -4585.72 [με]
E4: -4319.36 [με]
E0: -4736.23 [με]
E2: -5232.19 [με]
E3: -5105.4 [με]
E1: -4586.62 [με]
E4: -4449.57 [με]
E0: -4625.85 [με]
E2: -5351.85 [με]
E3: -4742.46 [με]
E1: -4523.97 [με]
E4: -4042.19 [με]
E0: -4583.52 [με]
E2: -5067.17 [με]
E3: -4493.16 [με]
E1: -4232.17 [με]
E4: -3949.89 [με]
0.95qpeak
0.90qpeak
0.85qpeak
0.75qpeak

b)

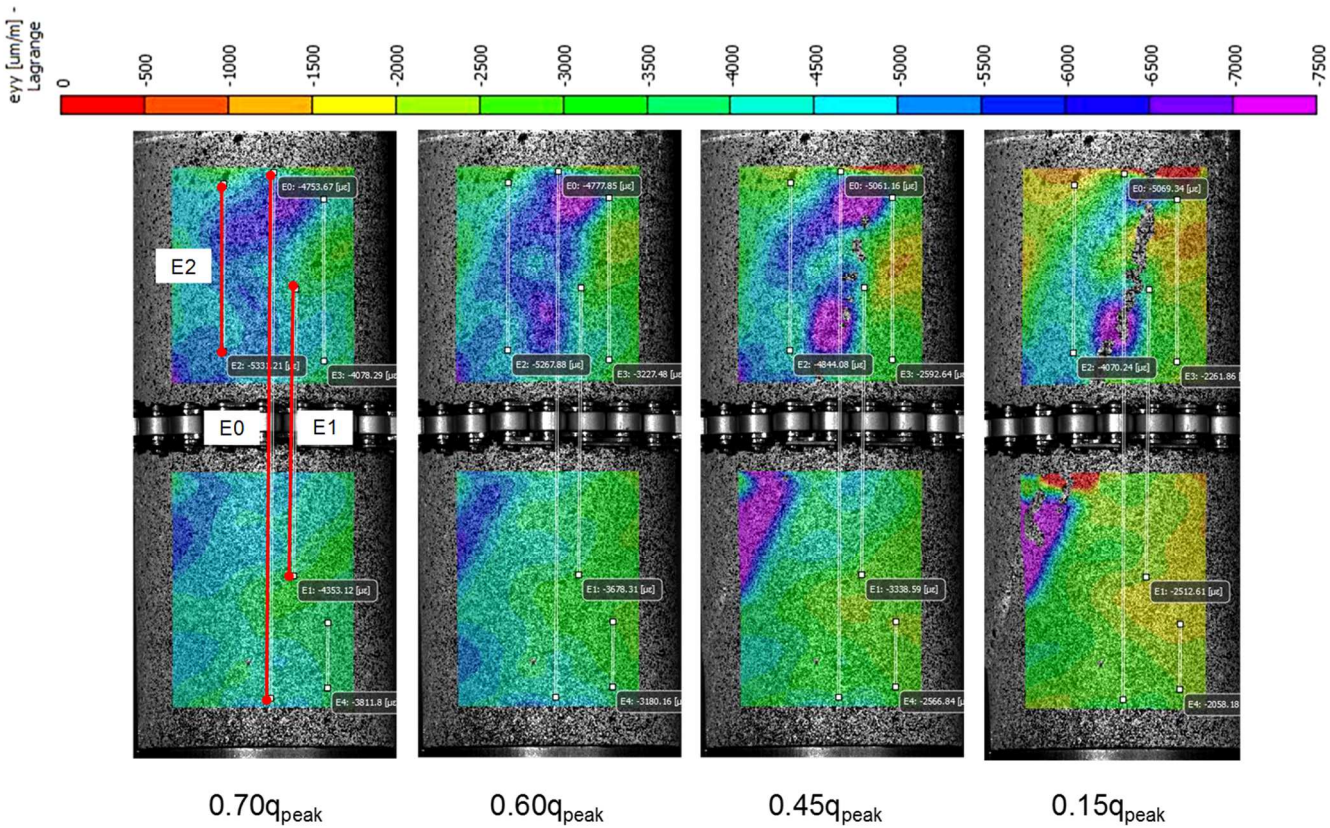

c)

Figure 1.11 Field of axial strains developed at different stress levels in a) pre-peak regime and b) and c) post-peak regime

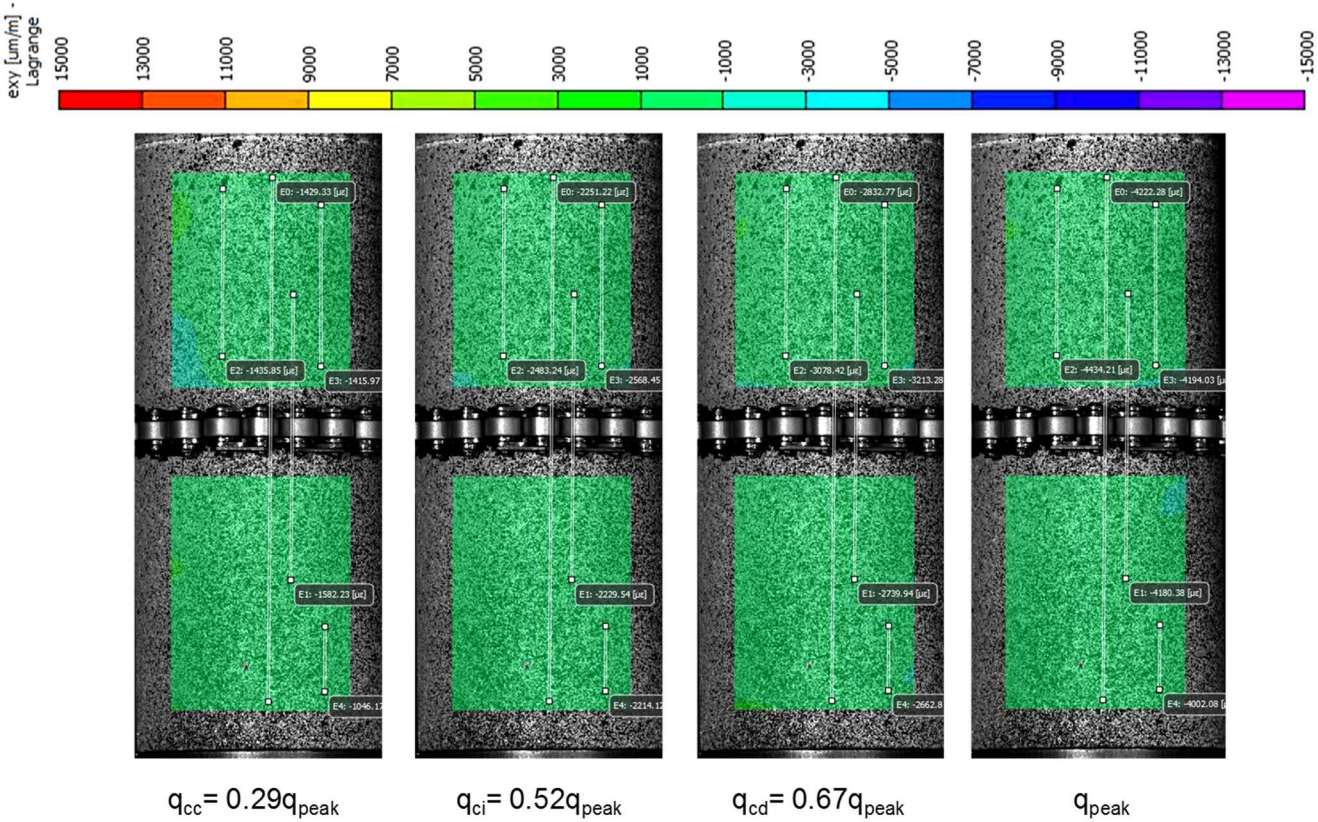

$q_{cc}= 0.29q_{peak}$ $q_{ci}= 0.52q_{peak}$ $q_{cd}= 0.67q_{peak}$ q_{peak}

a)

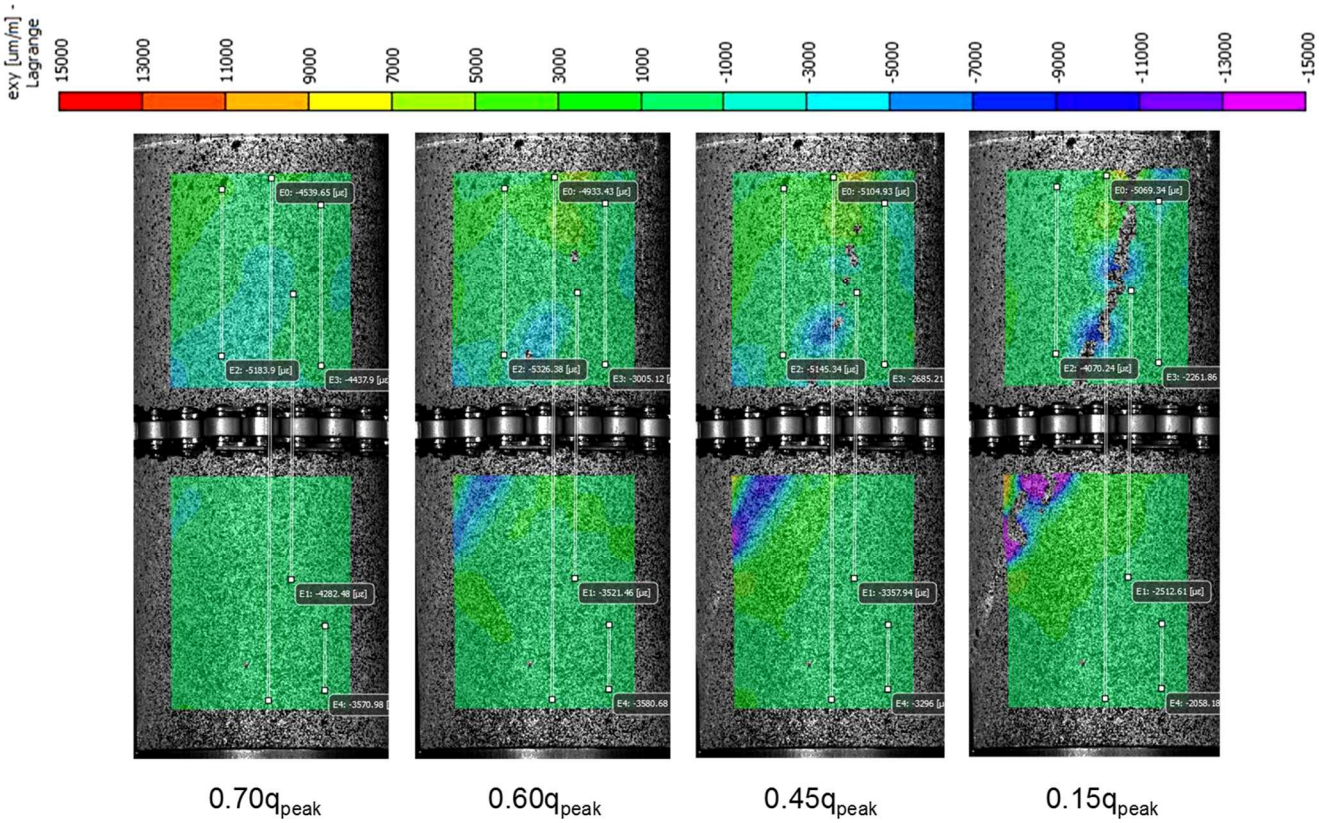

b)

Figure 1.12 Field of shear strains developed at different stress levels in a) pre-peak regime and b) post-peak regime

LIST OF TABLES

Table 1.1 Hawkesbury sandstone properties and threshold stresses for fracture damage

Sample No.	Strain measurement	q_{peak} or UCS (MPa)	Young's modulus E (GPa)	Poisson's ratio (υ)	q_{cc}/q_{peak}	q_{ci}/q_{peak}	q_{cd}/q_{peak}
1	Strain gauge	32.7	10.4	0.15	0.27	0.47	0.67
2	DIC	36.1	10.3	0.16	0.28	0.52	0.67
3	DIC	31.2	9.9	0.19	0.30	0.57	0.69
4	DIC	32.9	9.5	0.16	0.32	0.53	0.70
5	DIC	34.8	10.2	0.15	0.27	0.52	0.68
Average		33.5	10.1	0.17	0.29	0.52	0.68
SD		±1.7	±0.3	±0.015	±0.02	±0.03	±0.01

q_{peak} : Peak stress, UCS: Unconfined Compressive Strength, q_{cc} : Crack closure stress, q_{ci} : Crack initiation stress, q_{cd} : Crack damage stress. SD: Standard deviation

STATEMENT OF AUTHORSHIP

Statement of Authorship

Title of Paper	Fracture Energy-Based Brittleness Index Development and Brittleness Quantification by Pre-Peak Strength Parameters in Rock Uniaxial Compression
Publication Status	☒ Published ☐ Accepted for Publication ☐ Submitted for Publication ☐ Unpublished and Unsubmitted w ork w ritten in manuscript style
Publication Details	Munoz, H., Taheri, A., Chanda, E. (2016) Fracture Energy-Based Brittleness Index Development and Brittleness Quantification by Pre-Peak Strength Parameters in Rock Uniaxial Compression. Rock Mechanics and Rock Engineering DOI: 10.1007/s00603-016-1071-4

Principal Author

Name of Principal Author (Candidate)	Henry Munoz		
Contribution to the Paper	Overall paper preparation		
Overall percentage (%)	85		
Certification:	This paper reports on original research I conducted during the period of my Higher Degree by Research candidature and is not subject to any obligations or contractual agreements with a third party that would constrain its inclusion in this thesis. I am the primary author of this paper.		
Signature		Date	05/10/16

Co-Author Contributions

By signing the Statement of Authorship, each author certifies that:

i. the candidate's stated contribution to the publication is accurate (as detailed above);
ii. permission is granted for the candidate in include the publication in the thesis; and
iii. the sum of all co-author contributions is equal to 100% less the candidate's stated contribution.

Name of Co-Author	Abbas Taheri		
Contribution to the Paper	Paper review		
Signature		Date	06/10/16

Name of Co-Author	Emmanuel Chanda		
Contribution to the Paper	Paper review		
Signature		Date	06 Oct. 2016

Please cut and paste additional co-author panels here as required.

FRACTURE ENERGY-BASED BRITTLENESS INDEX DEVELOPMENT AND BRITTLENESS QUANTIFICATION BY PRE-PEAK STRENGTH PARAMETERS IN ROCK UNIAXIAL COMPRESSION

H. Munoz[1], A. Taheri[2], E. K. Chanda[3]

[1]Deep Exploration Technologies Cooperative Research Centre DET CRC, Export Park, Adelaide Airport, SA 5950, Australia, and School of Civil, Environmental & Mining Engineering, The University of Adelaide, SA 5005, Australia, Ph: 61 8 8313 0591, Fax: 61 8 8313 4359, Email: henry.munozprincipe@adelaide.edu.au (corresponding author)

[2]Senior Lecturer, School of Civil, Environmental & Mining Engineering, The University of Adelaide, SA 5005, Australia, Ph: 61 8 8313 0906, Fax: 61 8 8313 4359, Email: abbas.taheri@adelaide.edu.au

[3]Associate Professor, School of Civil & Environmental & Mining Engineering, The University of Adelaide, SA 5005, Australia, Ph: 61 8 8313 7410, Fax: 61 8 8303 4359, Email: emmanuel.chanda@adelaide.edu.au

ABSTRACT

Brittleness is a fundamental mechanical rock property critical to many civil engineering works, mining development projects and mineral exploration operations. However, rock brittleness is a concept yet to be investigated as there is not any unique criterion available, widely accepted by rock engineering community able to describe rock brittleness quantitatively. In this study new brittleness indices were developed based on fracture strain-energy quantities obtained from the complete stress-strain characteristics of rocks. In doing so, different rocks having Unconfined Compressive Strength values ranging from 7 to 215 MPa, were

examined in a series of quasi-static uniaxial compression tests after properly implementing lateral-strain control in a closed-loop system to apply axial load to rock specimen. This testing method was essential to capture post-peak regime of the rocks since a combination of class I-II or class II behaviour featured post-peak stress-strain behaviour. Further analysis on the post-peak strain localisation, stress-strain characteristics and the fracture pattern causing class I-II and class II behaviour were undertaken by analysing the development of field of strains in the rocks via three-dimensional digital image correlation (3D DIC). Analysis of the results demonstrated that pre-peak stress-strain brittleness indices proposed solely based on pre-peak stress-strain behaviour do not show any correlation with any of pre-peak rock mechanical parameters. On the other hand, the proposed brittleness indices based on pre-peak and post-peak stress-strain relations were found to competently describe an unambiguous brittleness scale against rock deformation and strength parameters such as the elastic modulus, the crack damage stress and the peak stress relevant to represent failure process.

KEYWORDS

Brittleness index, fracture energy, post-peak energy, uniaxial compression, digital image correlation

INTRODUCTION

Brittleness refers to deformation that involves hard, strong material that fractures and splits rather than staying whole while pliably deforming. Therefore, rock failure behaviour is defined by brittleness. Brittleness is an essential mechanical rock property critical to many civil engineering works, mining development projects and mineral exploration operations. Rock brittle fracture damage, detrimental to stability of surface and underground rock excavations rock breakage and drilling, are amongst major practical applications. However, rock brittleness is a concept yet to be investigated as there is not any standard criterion (i.e. brittleness index) available to describe failure characteristics of different rocks. For instance, a number of different criteria to assess brittleness upon pre-peak stress-strain characteristics in uniaxial compression including ratios between elastic

to plastic strain as well as fracture strain-energy relations, e.g. (Hucka and Das 1974; Kidybiński 1981), are found to be insufficient to describe failure behaviour of rock (Tarasov and Potvin 2013). In the same manner, other brittleness indices are developed based on ratios between uniaxial compressive to tensile strength, e.g. (Altindag 2002; Hucka and Das 1974; Kahraman 2002). In this respect, in the present study rock brittleness is developed upon pre-peak and post-peak stress-strain energy balance to describe rock brittleness against pre-peak rock strength parameters in uniaxial compression including Young's modulus, crack damage stress and peak strength. In this sense, the complete stress-strain characteristics in uniaxial compression become a fundamental piece of information to describe the total process of rock deformation to assess brittleness based on post-peak failure behaviour.

Pioneering studies on the complete stress-strain behaviour of rocks undergoing quasi-static compression (Hudson et al. 1971; Wawersik and Brace 1971; Wawersik and Fairhurst 1970) classify rocks into two categories: class I, characterised by a negative post-peak slope, where fracture propagation is stable, and class II, showing positive post-peak slope, where fracture propagation is unstable. Nonetheless, few studies can be found in the literature dealing with post-peak measurements in the case of rocks following class II behaviour. In the first place, this limitation is due to the lack of implementation of a proper load-control method to respond accordingly to rock class II behaviour. That is, rock behaviour under axial loading is generally studied in laboratory using load-controlled or displacement-controlled compressive loading systems. From here, load-controlled method can only measure pre-peak behaviour. To measure post-peak behaviour of rocks in unconfined and confined conditions, e.g. (Gowd and Rummel 1980; Kumar et al. 2010), generally displacement-controlled method (i.e. axial-displacement or axial-strain rate feedback to control axial load) is implemented in servo-controlled compressive machines, e.g. (Bieniawski and Bernede 1979). Nevertheless, displacement-controlled method is insufficient to measure post-peak regime for class II rocks because axial strain no longer monotonically increases from the moment rock behave as class II. As a result, following this method, a critical

response of the rock takes place leading to rock drastic failure. Consequently, post-peak stress-strain behaviour is masked by a rapid strength reduction at constant displacement immediately after peak stress, e.g. (Labuz and Biolzi 2007). However, this post-peak critical response may be a manifestation of axial displacement-control compliance and not true material behaviour. In this view, circumferential or lateral-strain controlled method is suggested by some researchers to measure post-peak stress-strain for brittle rocks (Fairhurst and Hudson 1999; Hudson et al. 1971). This is mainly because lateral displacement monotonically increases after peak stress even if axial displacement decreases.

In the present study, fracture energies, obtained from the complete stress-strain curve and dissipated during crack development which is associated with decreasing of load-carrying capacity in post-peak regime, are the basis to develop brittleness indices. Fracture energy obtained from the complete stress-strain curve (i.e. pre-peak and post-peak energy) following either class I or class II behaviour can be estimated by taking into account the actual shape of complete stress-strain curve (Jansen and Shah 1997; Markeset and Hillerborg 1995). Alternatively, fracture energy can be estimated by some simplified expressions taking into account both the elastic Young's modulus and a single linear post-peak modulus to represent the complete stress-strain curves of rock (Tarasov and Potvin 2013; Tarasov and Potvin 2012; Xue-bin and Yi-shan 2003). However, in general, the actual features of pre-peak and post-peak stress-strain curves of rock may be overly simplified if fracture energy is obtained in this manner by using single values of Young's modulus and post-peak modulus. In addition, post-peak fracture development characteristics are very complex and they cannot be characterised simply by a single post-peak modulus as post-peak progressive fracture in the rock takes place at different shear-tensile extent and at different rates. Furthermore, post-peak behaviour can consist of not only class I or class II behaviour, i.e. class I, characterised by a negative post-peak slope and class II, showing positive post-peak slope, but it can be endowed by a combination of class I-II behaviour at different extent. Therefore, a single post-peak modulus value may not be an accurate representative of the whole post-peak response.

In this respect, Wawersik and Fairhurst (Wawersik and Fairhurst 1970), for instance, observed in uniaxial compressive test on granite, limestone, basalt and marble, (UCS between 35 and 350 MPa) that none of the post-failure curves could be approximated by a linear fitting. They pointed out that it is difficult to conceive intuitively how a simple approximately linear form of stress-strain relationship was obtained in the post-failure curves of norite, quartzite, and an unidentified soft rock by Bieniawski (Bieniawski 1967) as fracture in these materials consisted of a combination of slabbing and faulting. Unlike the study undertaken by Tarasov and Potvin (Tarasov and Potvin 2013) which shows a simple approximately linear form of post peak stress-strain relations for a sandstone, a quartzite and a dolerite (UCS between 180 to 380 MPa) all following class I behaviour in unconfined compression tests, studies on the post-peak curves on granite (UCS between 40 to 340 MPa) conducted by Vasconcelos et al. and Wawersik and Brace (Vasconcelos et al. 2009; Wawersik and Brace 1971) show successive drops and recoveries of the load-carrying capacity at different extent, i.e. class I and class II behaviour at different extent. In this case, as indicated by Vasconcelos et al. and Wawersik and Brace, crack propagation process is deemed as the main characteristic of post-peak behaviour that may be responsible to define the final shape of the stress-strain curve. Therefore, the post-peak stress strain curve may result on either type a smooth or irregular saw-shape curve associated with the mechanism of recovery of stress provided by grain interlocking in between the sides of macro cracks.

In post-peak regime deformations associated with the formation and coalescence of distributed longitudinal cracks and faulting localisation of quasi-brittle materials takes place within a damage zone which is limited by the length of the damage zone (Bažant 1989; Jansen and Shah 1997; Markeset and Hillerborg 1995). In this condition, conventional local strain measurements by extensometers and strain gauges cannot entirely capture the strains developed in post-peak regime. In this case, extensometer misalignment and strain gauge damage are the major issues. Particularly these problems initiate when progressively growing cracks and localisation take place in specimen. As a result, non-contact strain measurement via three-dimensional digital image correlation (3D DIC) becomes relevant to measure

strains development in post-peak regime. Digital image correlation (DIC) refers to the class of non-contact methods that acquire images of an object, store images in digital form and perform image analysis to extract full-field shape, deformation and motion measurements (Chu et al. 1985; Sutton et al. 2009). 3D DIC has been used to study deformation of different materials (Heinz and Wiggins 2010; Song et al. 2013; Yang et al. 2015). This technique was implemented in this study to accurately measure rock deformation in pre-peak and post-peak regimes.

In summary, there is not any study on rock brittleness assessment on the ground of post-peak instability taking into account the complete stress-strain characteristics in uniaxial compression. In addition, an unambiguous brittleness scale against rock strength parameters such as elastic modulus, crack damage stress and peak stress relevant to represent failure process development has not been developed yet. In view of the above, the present study aims to characterise complete stress-strain behaviour of different soft, medium-strong and strong rocks (UCS is ranging from 7 to 215 MPa) in uniaxial compression. Another objective is to develop a brittleness index based on fracture energy dissipation resulted from the complete stress-strain curve in uniaxial compression able to describe unambiguously a brittleness scale against rock mechanical parameters.

EXPERIMENTAL STUDY

ROCK MATERIAL AND PREPARATION

A series of uniaxial compressive tests under quasi-static monotonic loading conditions were carried out on different rock samples including five limestones (Tuffeau, Savonniere, Massangis, Chassagne and Rocheron), a sandstone (Hawkesbury) and two granites (Alvand and Harcourt) presented in Table 2.1. At least three specimens have been tested for each rock sample. It is anticipated that stress-strain parameters shown in the present study are representative values of a group of tests. The limestones, which are sources from different quarries in France, all belong to Middle Jurassic. Hawkesbury sandstone is an early Middle Triassic rock sources from New South Wales, Australia. Alvand granite, a late Paleogene rock, is known as a typical strong rock in western Iran. The Upper Devonian

Harcourt granite was sourced from Mount Alexander in Victoria, Australia. The rock samples correspond to fine to medium grain size rock having densities varying from 1.40 to 2.70 g/cm^3 (Table 2.1).

The rocks were quarried and prepared in blocks otherwise were collected from the field as cores retrieved during drilling. Cylindrical specimens were prepared by coring the rock blocks. The diameter of the specimens was 42 mm. A visual inspection shows that the specimens' diameters was from 10 to more than 20 times bigger than the rock grains size satisfying recommendations given by the International Society for Rock Mechanics (ISRM) (Bieniawski and Bernede 1979; Fairhurst and Hudson 1999). The end faces and sides of the specimen were prepared smooth and straight according to the ISRM standard (Fairhurst and Hudson 1999; ISRM 1981). The aspect ratio (i.e. length to diameter ratio) of the samples was maintained at 2.4 for all the rock samples.

ROCK INSTRUMENTATION

The rock specimens were instrumented locally by six strain gauges orientated in the axial direction, as depicted in Figure 2.1a (letters A, B, C, D, E and F refer to the strain gauge location), to measure the respective axial strains ε_A. The strain gauges used were both KFG-30-120-C1 (30 mm gauge length) and KFG-10-120-C1 (10 mm gauge length) types manufactured by Tokyo Sokki Kenkyujo Co. Axial extensometers type 632.12F20-series manufactured by MTS Systems Co were attached to the samples as well, as depicted in Figure 2.1a. Additionally, axial deformation of the specimens was measured externally by a pair of axial linear variable displacement transducers (LVDTs) mounted at both left and right sides to the rock specimen. Axial strains ε_A were calculated for strain gauges, extensometers and LVDTs readings.

Additionally, the rock specimens were instrumented by a direct-contact lateral extensometer (lateral ring-shape extensometer) wrapped around the cylindrical sample, see Figure 2.1a. This device was essential to control the axial load by lateral strain. The lateral extensometer was mounted at mid-length of the rock specimens so that end-edge friction effects (Hawkes and Mellor 1970) and

confined zones due to boundary conditions (Van Vliet and Van Mier 1995) on the measurements were eliminated. Lateral strains (ε_L) were calculated from the change in diameter length of the sample induced by axial load. The lateral extensometer type used in the tests was that 632.12F20-series manufactured by MTS Systems Co.

3D DIGITAL IMAGE CORRELATION METHOD

As the details of DIC application to uniaxial compression tests are given by Munoz et al. (Munoz et al. 2016a), herein only a brief description of the methodology is presented. This technique encompasses setting up two digital cameras pointing at the specimen from two different angles and capturing a series of grey-scale images of the specimen surface pattern to create three-dimensional measurement of shape and displacements of the specimen. Figure 2.1b shows the experimental set up used in this study for three-dimensional (3D) DIC measurements.

Rock surface deformations induced by the compressive load throughout the tests were captured by taking a significant number of images of the speckle surface of the specimens by using a couple of digital cameras (i.e. Fujinon HF75SA-1, 1:1.8/75mm, 5 Megapixels resolution) suitable for quasi-static load testing. The speckle pattern on the rocks, created by firstly spraying ordinary white paint and then spray-tarnishing black paint, e.g. (Heinz and Wiggins 2010; Song et al. 2013; Yang et al. 2015), was non-repetitive, isotropic and high in contrast, i.e. random pattern exhibiting no bias to an orientation and showing dark blacks and bright whites, adequate in size for high-strain resolution (Sutton et al. 2009). Prior to the compression tests, each camera was calibrated using a 30-mm standard target having uniformly spaced markers. Calibration results produced a standard deviation of residuals of 0.020 (in pixels). This value suggests that the calibration of the cameras is adequate for measurements (Sutton et al. 2009).

Images of undeformed and deformed states of the specimen were captured automatically by Vic-Snap software at a frame rate of an image each 0.5 seconds, from the start of loading for during the first 30 minutes, and thereafter an image each 5 seconds until the end of the tests. This frame rate results suitable to capture

and store a large number of images for further analysis. Instantaneous axial deformation, lateral deformation, applied load and instantaneous images were synchronously acquired to ensured one-to-one correspondence between load, deformation and respective images. Imaging data processing of the area of interest was conducted by VIC-3D software.

LOADING SET-UP AND TESTING METHOD

The rock specimens were subjected to a quasi-static monotonic axial loading by a compressive machine which was stiff enough to not allow the elastic energy to be accumulated in the machine (i.e. Instron-1342 and 1282 models manufactured by Instron Inc.). The closed-loop servo control system of the compressive machine is fully digital and it is capable and flexible to control the applied axial load by an in-built computer system as a function of lateral-strain feedback signal. Thus, the applied axial load was controlled in a way keeping lateral strain-rate constant. In this sense, the electronics and computer program allowed the hydraulic system to be adjusted continuously and automatically to ensure the load to respond accordingly with the feedback signal and with the damage extent to the specimen. Axial load (by a load cell), axial strain (by strain gauges, extensometers and external LVDTs) and lateral strain (by a ring extensometer) were acquired continuously by a data acquisition system at a rate of 4 data points per second.

Different load cells having capacities of 100, 250 or 1000 kN were installed in the compressive machine depending on the strength of rock. Applying uniform load to the rock samples, essential to avoid premature failure of the specimens, was ensured in all the tests by using a hinge-type pedestal that adjusted the specimens centre line to fit perpendicular to the loading platen and avoid misalignments. In all the tests, no additional friction-reducing layers in contact between the specimens and the loading platen were used. In this case, the platen was in direct contact with the specimens.

COMPRESSIVE TEST RESULTS

LATERAL-STRAIN CONTROLLED TEST

The application of a proper loading method in the compression tests was critical in order to obtain the complete post-peak stress-strain response of the rocks as post-peak stress-strain characteristics are the main component to develop the brittleness indices proposed herein. In this respect, Figure 2.2 shows the normalised stress-strain curves for Hawkesbury sandstone under uniaxial compression loading following load-controlled, axial-strain controlled and lateral-strain controlled loading methods. Tests were performed under a constant axial-load increment of 0.026 kN/s (or 0.016 MPa/s), a constant axial strain increment of $6x10^{-6}$/s and a constant lateral-strain increment of $2x10^{-6}$/s, respectively, to satisfy static to quasi-static loading conditions (Bischoff and Perry 1991; Hudson et al. 1971; Wawersik and Brace 1971; Wawersik and Fairhurst 1970). Normalisation was done by dividing stresses and strains (here strains comes from LVDT readings) by the peak stress and the strain at the peak stress, respectively. Figure 2.2 shows, on one hand, that pre-peak curves nearly overlap to each other irrespective of the loading method used in the tests. On the other hand, in the tests following axial load-controlled and axial-strain controlled methods, it was not possible to capture the complete post-peak stress-strain curves as Hawkesbury sandstone behaved at some moments as class II. In general, this outcome clearly indicates that if rock follows class II or a combination of class I-II mode behaviour, as observed in the rest of the rocks tested here, the compressive tests end prematurely at the moment that class II behaviour start dominating post-peak regime.

Unlike load-controlled and axial-strain controlled methods, lateral-strain controlled method was successfully implemented to measure pre-peak and post-peak stress-strain relation of all the rocks introduced in Table 2.1. A constant lateral-strain increment of $2x10^{-6}$/s was applied to all the rocks throughout the compressive tests. Axial-strain rate varied from $1.7x10^{-5}$ /s to $2x10^{-6}$ /s at the beginning to the end of the test with axial-rate fluctuations. Figure 2.3a and Figure 2.3b show the time history of stress and strains and stress and strain rates of Hawkesbury sandstone, respectively. As it can be seen in Figure 2.3b, from the

moment that lateral-strain control takes over the test, at nearly the beginning of loading, the axial-load rate and the axial-strain rate were about 0.2 kN/s and $1.7x10^{-5}$ /s, respectively, and thereafter they start to decrease gradually as the stress in the rock reaches peak stress. After peak stress, the axial strain and load rate experienced fluctuations as the result of the strength response of the rock and the automatic adjustment of applied loading upon the damage extend induced in the sample. In other words, post-peak regime was characterised by progressively dropping and minor recoveries, if any, of the load-carrying capacity accompanied with crack propagation process and localisation.

Rock samples tested following lateral-controlled method failed very smoothly, i.e. an eruptive failure was not observed in any sample at the end of the tests. Cracks growing and shear zone localisation were the main failure characteristics of rock samples (see Figure 2.1a). Essentially axial splitting of the sample by macroscopic crack (or cracks) extending in the direction of axial load and faulting or macroscopic shear failure was observed depending on rock type and strength. For instance, in Hawkesbury sandstone, faulting was observed. For limestones and granites, predominantly distributed longitudinal cracks were observed at the end of the tests.

COMPLETE AVERAGE STRESS-STRAIN CURVES

In post-peak regime, local strain measurement (by extensometers and strain gauges) is insufficient to capture strains when progressively growing cracks and localisation took place. In this case, extensometer misalignment and strain gauge damage make post-peak strains reading difficult or impossible, thus incomplete stress-strain curves may be resulted. For instance, in Figure 2.4 LVDT captured the complete stress-strain curve (average strain) while curves labelled A and D (see strain gauge location in Figure 2.1a) were damaged at or immediately after peak stress and, therefore, they did not capture post-peak strains. This is very common for the strain gauges attached to specimen. Also, strain gauges C and E only captured pre-peak strains (curves C and E are not shown in Figure 2.4). Furthermore, strain gauges B and F which were not damaged during the compressive loading (i.e. B and F were out of the localised shear zones) only

measured local inelastic unloading after peak stress. Therefore, discussions given here are based on axial strains ε_A obtained from LVDTs or DIC measurements. Although LVDT's readings contained bedding error (Taheri and Tani 2008), they can be used to describe the post-peak characteristics of rocks with sufficient accuracy, see (Jansen and Shah 1997; Markeset and Hillerborg 1995). Results obtained by DIC measurement, however, are free from this experimental error (Munoz et al. 2016a). In this view, axial strains ε_A from LVDTs, both in pre-peak and post-peak regime are presented in Figure 2.5 for all the rocks tested in this study.

In general, it was observed that immediately after the peak stress q_{peak} took place, progressive drop of stress was followed associated with the progressive strength degradation of the rock. Upon strength and rock type, post-peak regime complied with either a combination of class I-II behaviour, or otherwise class II behaviour. Successively sudden drops and recoveries of the load-carrying capacity at different extent shaped post-peak stress-strain curves from smooth-type to irregular saw-shape as shown in Figure 2.5. The former may be associated with the internal bonding connections breakage and the favourable shear strain localisation. On the contrary, the latter, stress-strain curves may be associated with the mechanism of recovery of the stress provided by interlocking in between the sides of the macro cracks as suggested in previously studies on granite and high strength concrete, e.g. (Jansen and Shah 1997; Vasconcelos et al. 2009). It is noteworthy that no sign of perceptible major crack in the specimen was noticed during pre-peak regime neither at peak stress. It was only after peak stress was reached that the rocks experienced progressively macro cracking growth from coalescence of micro cracks.

A major cracking in the form of a predominant single shear-failure plane took place in the case of Hawkesbury sandstone. For the rest of the rocks, as shown in Figure 2.1a combination of shear cracks and distributed longitudinal cracks at different extent gradually happened during post-peak loading. Microscopic studies, not conducted in the present study, suggest that macroscopic shear failure initially involves uniform nucleation and growth of micro crack throughout the sample

followed by accelerated cracking over a central region of sample as the peak stress is approached to eventually form a macroscopic large shear plane (Horii and Nemat-Nasser 1986; Wong 1982). On the other hand, if the axial compression is accompanied by large amount of lateral expansion, crack growth becomes unstable after a certain crack length is attained, resulting in axial splitting (Horii and Nemat-Nasser 1986).

PRE-PEAK STRESS-STRAIN QUANTITIES

In general, the stress-strain curves follow stages distinguished by: i) an initial region bound by q_{cc} where existing micro cracks are closed during initial loading; ii) once existing cracks are closed, rock is assumed to behave linear elastic until the onset of q_{ci} (Martin and Chandler 1994). Random stable axial cracking associated with axial stresses slightly above q_{ci} are considered to not reduce the rock strength (Bieniawski 1967); iii) q_{cd} is associated to the reversal point of the total volumetric strain at the onset of dilation generated by crack development and represents the onset of unstable crack growth (Bieniawski 1967) which is characterised by significant structural changes to the rock (Hallbauer et al. 1973); iv) while q_{peak} marks the onset of the post-peak behaviour. After peak-stress is attained, macro cracks growing, coalescence of cracks and localisation characterise the post-peak regime (Bieniawski 1967). These typical characteristic stresses were well observed in the rocks tested in the present study and extracted from the stress-strain curves according to Martin and Chandler (Martin and Chandler 1994).

Table 2.2 summarises the average values of q_{peak} (i.e. UCS), Young´s modulus (E_{LVDT}) and normalised crack damage stresses q_{cd}/q_{peak} of the rocks tested here. The values of E_{LVDT} were extracted from the linear-elastic portion of the stress-strain curves limited by q_{cc} and q_{ci}. Here, strains were obtained from LVDTs and lateral-extensometer readings. Elastic modulus values ranged from 1.90 to 48.8 GPa, while the UCS of the rocks ranged from 7 to 215 MPa. Crack damage stress values q_{cd} occurred at 0.66 to 0.99 q_{peak} depending on rock type and its strength. Figure 2.6 shows the relationships between E_{LVDT} and q_{cd} with

q_{peak} for all the rocks tested in this study. A sound linear correlation was found in both cases.

POST-PEAK LOCAL STRAIN FEATURES

Digital image correlation analysis provided quantitative evidence on the nature of field strains developed in the rock surface throughout the compressive test. In Figure 2.7, Figure 2.8, and Figure 2.9 different loading stages along the stress-strain curve including crack closure q_{cc}, crack initiation q_{ci}, crack damage q_{cd} and the peak stress q_{peak} in pre-peak as well as post-peak stresses at $0.70q_{peak}$ to $0.15q_{peak}$ were selected of representative rocks to examine field of axial strain patterns.

The field of strains within the area of interest Figure 2.7, Figure 2.8, and Figure 2.9 demonstrate that the specimens do deform uniformly in pre-peak regime, i.e. axial strains start increasing uniformly, provided relatively homogenous intact rock and uniform load, as axial load increases until peak stress, as shown by colour gradient in the samples at pre-peak stress levels. On the other hand, in post-peak regime the field of strains increased progressively at different rates with large deformations localising around the future failure plane or along axial macro cracks extending in the direction of the axial load. The results indicate that deviation from strain uniformity begins progressively after peak stress was reached. Thereafter, as shown by gradient colour in Figure 2.7, Figure 2.8, and Figure 2.9 strains start extending rapidly as the rate of strength degradation is accelerated.

Uniform development of strains in the samples, explained in the above paragraph by Figure 2.7, Figure 2.8, and Figure 2.9, produced a single stress-strain curve in pre-peak regime, i.e. a single stress-strain curve in pre-peak regime was extracted from the virtual extensometers (i.e. E0, E1 and E2) irrespective of their length and location within the study area in the sample. See the length and location of E0, E1 and E2 in Figure 2.7, Figure 2.8, and Figure 2.9. This observation confirms that the stress-strain curve before peak stress describes the overall compressive behaviour of the material. Failure mode features of a given rock, be either class I-II or class II, were captured globally by LVDTs and locally by virtual

extensometers (i.e. E0, E1 and E2, see Figure 2.7, Figure 2.8, and Figure 2.9). The results indicate that a set of different local post-peak moduli in the specimen can be expected as local post-peak strains responded differently when deformation, encountered by local gauges, associated to axial cracking or faulting developed at different extent. Therefore, the average axial strain obtained from LVDTs in post-peak regime may be much lower than local axial strains measured at localised zones as shown for instance by E1 in Figure 2.8. This is mainly because after peak stress is reached, areas of sample which are located outside of the localised zone undergo inelastic unloading, making the average axial strain smaller that the strain measured in the localised zone.

FRACTURE ENERGY IN COMPRESSION

The complete stress-strain curves allowed assessing the total fracture energy per unit volume of rock dissipated throughout the compressive tests. Local stress-strain curves extracted from the virtual extensometers E0, E1 and E2 as shown in Figure 2.7, Figure 2.8, and Figure 2.9 do yield local fracture energy as fracture energy is calculated by the area under the respective local stress-strain curves. Therefore, it is expected to have a distribution of local fracture energy upon the length and location of local extensometers with respect to localised zones within the area of interest in the rock sample.

In this respect, Figure 2.9 shows the local stress-strain and energy characteristics in a Hawkesbury sandstone sample. Figure 2.9a shows the location and length of virtual extensometers E0, E(A), E(B) and E(C) and Figure 2.9b shows their respective stress-strain curves. The stress-strain curves by E(A), E(B) and E(C) present a transition from damaged to undamaged zones in different areas of the specimen. This behaviour is also shown by the colour gradient in Figure 2.9a. The post-peak curves presented in Figure 2.9b were characterised by either i) local inelastic unloading in the material outside of the damaged zone or ii) localised strain in the material inside of the damaged zone. For instance, in Figure 2.9b, E(C) unloaded at the peak stress level unlike E(A) and E(B) which encountered the failure plane and experienced localised strains. Overall behaviour of the

Hawkesbury sandstone sample is captured by E0 which include localised damaged zone and undamaged zone which experiences unloading in post-peak regime. The distribution of the locally dissipated fracture energy is depicted in Figure 2.9c. From Figure 2.9c, it can be observed that the dissipated local energy in the damage zone in the specimen by E(A) is obviously the highest when compared with withdrawn energies from E(B) and E(C) and even with the energy withdrawn from the total length E0. This is mainly because, unlike other virtual extensometers, E(A) captures most of the strains in the localised zone. In this instance, energy by E0 can be calculated by summing up the local energy in each portion of the specimen following studies on localisation, e.g. (Markeset and Hillerborg 1995; Watanabe et al. 2004) as,

$$U_{total-E0} = U_{total-E(A)} \frac{\ell E(A)}{\ell E0} + U_{total-E(B)} \frac{\ell E(B)}{\ell E0} + U_{total-E(C)} \frac{\ell E(C)}{\ell E0} \quad (1)$$

Where $\ell E(A)$, $\ell E(B)$, $\ell E(C)$ and $\ell E0$ are the gauge length of virtual extensometers E(A), E(B), E(C) and E0, respectively. Correctness of this relation is proved by the experimental results of energy consumed locally by E(A), E(B) and E(C) and the average consumed energy by E0 presented in Figure 2.9c. Furthermore, energy quantities, from DIC extensometer E0 (see location of E0 in Figure 2.7, Figure 2.8, and Figure 2.9) and LVDT differed by only 2 to 7% in this study. This suggests that although LVDT strains contain bedding errors, they can be used with enough accuracy to assess fracture energy quantities of the rocks. Therefore, compression fracture energy for the rocks was estimated from the stress-strain curves with LVDTs depicted in Figure 2.5 which represent the total average strains of the entire rock specimen.

The total fracture energy (U_{total}) comprises of pre-peak energy (U_{pre}) and post-peak energy (U_{pre}) and it is expressed by the following equation:

$$U_{total} = U_{pre} + U_{post} \quad (2)$$

Pre-peak energy per unit volume of rock is estimated as the area under the stress-strain curve enclosed by loading the specimen up to the peak stress and then unloading it completely. In Figure 2.10a, the unloading path was assumed to be linear with a slope equal to E_{LVDT} (i.e. the Young modulus obtained by LVDTs), see Table 2.2 for the values of E_{LVDT} of the rocks. On the other hand, post-peak energy was calculated taking into account the area under the post-peak stress-inelastic strain. That is the area under the unloaded pre-peak stress-strain curve (assuming that unloading curve's Young's modulus, E_{un}, is equal to loading curve's Young's modulus, E_{LVDT}) and under the post-peak stress-inelastic strain as shown in Figure 2.10a. Herein, the post-peak fracture energy was defined until a post-peak stress level equal to about one third of the peak stress, i.e. $0.33q_{peak}$, a stress level where the stress-strain curve is terminated by drawing a linear unloading following a slope equal to E_{LVDT} (Jansen and Shah 1997; Jansen et al. 1995).

The quantities of U_{total}, U_{pre} and U_{post} for the rocks studied here are reported in Table 2.3. Furthermore, Table 2.3 also reports the values of elastic energy (U_e) at peak stress (see Figure 2.10b for the notation of U_e) where U_e is obtained as follows:

$$U_e = \frac{q_{peak}^2}{2E_{LVDT}} \tag{3}$$

Figure 2.10c shows the relationship of U_{pre}, U_{post}, U_{total} and U_e with their respective peak stress q_{peak} for the rocks studied here. This figure shows that U_e obviously increases in a linear fashion with an increase in q_{peak}. Unlike the values of U_e, U_{post} and U_{total} energies increase with an increase in q_{peak} until q_{peak}= 180 MPa and then decreases smoothly when q_{peak} increases. This trend clearly complies with low energy enclosed in the stress-strain curve of rocks that follow class I-II or class II post-peak behaviour. Figure 2.5 clearly shows this behaviour in rocks with higher peak strength. In addition, in Figure 2.10c, U_{pre} seems to increase slightly as q_{peak} increases, although, the results does not show any conclusive trend.

ENERGY-BASED BRITTLENESS INDEX

In this section, firstly, a number of brittleness indices, which were developed previously based on the pre-peak rock fracture energy, are examined to evaluate their capacity to measure brittleness and their relation with strength parameters. Then, a number of brittleness indices based on the pre-peak and the post-peak fracture energy in uniaxial compression are proposed. Finally, it is attempted to find correlations between the proposed brittleness indices with the pre-peak strength parameters of rock including the elastic modulus (E_{LVDT}), the crack damage stress (q_{cd}) and peak stress (q_{peak}). Brittleness indices that take into account only pre-peak stress-strain characteristics, namely, B_1 upon strain ratio (Hucka and Das 1974) and upon energy ratios B_2 (Hucka and Das 1974) and B_3 (Kidybiński 1981), see expressions below, were investigated.

$$B_1 = \frac{\varepsilon_{A-e}}{\varepsilon_{A-ir}+\varepsilon_{A-e}} \tag{4}$$

$$B_2 = \frac{U_e}{U_{peak}} \tag{5}$$

$$B_3 = \frac{U_{pre}}{U_e} \tag{6}$$

Where ε_{A-e} is the elastic axial strain and ε_{A-ir} is the irreversible axial strain. U_{peak} is the strain energy until peak stress ($U_{peak}. = \ U_{pre} + U_e$). These quantities are summarised in Table 2.3.

Figure 2.11, Figure 2.12 and Figure 2.13 show the plot relation of brittleness indices B_1, B_2 and B_3 with strength parameters q_{peak}, q_{cd}, and E_{LVDT}. Figure 2.11a, b and c demonstrate that B_1 was not able to correlate well with three pre-peak rock parameters. Furthermore, brittleness index B_1 for most of the rocks shows a single value, about 0.8 on average, irrespective of rock increasing strength trend.

Similarly, as can be seen in Figure 2.12a, b and c, the brittleness index B_2, which is developed based on energy ratios in pre-peak regime, does not show an acceptable correlation with rock pre-peak parameters. In this case, although the

coefficient of correlation R^2 is relatively high for the overall data (i.e. about 0.8 in Figure 2.12a, b and c) the following was observed: the correlation was scatter for the rocks having peak strengths of 7 to 84 MPa. For the rest of the rocks, having peak strengths higher than 84 MPa, B_2 is almost a constant value, in a broad sense about 0.9, which does not increase with an increase in mechanical properties values of rocks.

In Figure 2.13a, b and c, the brittleness index B_3, which is defined using pre-peak stress-strain results was not able to show a strong correlation with pre-peak mechanical rock parameters. In this case, similar to B_2, although the coefficient of correlation R^2 is relatively high for the overall data (i.e. about 0.9 in Figure 2.13a, b and c) the following was observed: the brittleness index B_3 was scatter for the rocks having peak strengths of 7 to about 84 MPa. On the other hand, for the rocks having peak strengths higher than 84 MPa, B_3 slightly decreases and its value almost remains constant at 0.1.

The above discussion on three brittleness indices based on the pre-peak stress-strain relations clearly shows that, pre-peak rock behaviour may not be sufficient to generate a rock brittleness index capable of describing rock failure behaviour with the required accuracy. As a result, in this study, a number of brittleness indices are proposed based on energy quantities from pre-peak and post-peak stress-strain characteristics following energy balance and post-peak instability. That is, an increase in the post-peak energy indicates an increase of stability (i.e. a decrease in brittleness). By the same argument, a dramatic decrease of post-peak energy indicates less stability of the failure process (i.e. an increase in brittleness). Figure 2.5 and Figure 2.10c clearly support these arguments. The following energy-based brittleness indices are proposed:

$$B_{U-I} = \frac{U_e}{U_{total}} \tag{7}$$

$$B_{U-II} = \frac{U_e}{U_{post}} \tag{8}$$

$$B_{U-III} = \frac{U_{peak}}{U_{total}} \tag{9}$$

Table 2.3 summarises the strain energy quantities U_{total} and U_{post} for the rocks studied here. In Table 2.4 the values of B_{U-I}, B_{U-II} and B_{U-III} are presented for the rocks.

As demonstrated in Figure 2.14, Figure 2.15 and Figure 2.16 the proposed brittleness indices B_{U-I}, B_{U-II} and B_{U-III} were able to describe properly a monotonic and unambiguous scale of brittleness with increasing pre-peak strength parameters of the rocks. In these figures, the brittleness indices clearly increase monotonically in a non-linear fashion with the peak stress q_{peak}, the crack damage stress q_{cd}, and the tangent Young's modulus E_{LVDT}. Then, obviously B_{U-I}, B_{U-II} and B_{U-III} applied to Tuffeau limestone (UCS= 7 MPa) yielded relatively the lowest values. On the other hand, Rocheron limestone (UCS= 215 MPa) produced the highest values of B_{U-I}, B_{U-II} and B_{U-III} . That is, the higher the brittleness index means that rock is more brittle. The rest of the rocks fell in between complying with the proposed brittleness scale.

From the results presented in Figure 2.14, Figure 2.15 and Figure 2.16, a number of non-linear relationships between brittleness indices and pre-peak mechanical parameters are established as follows:

$$B_{U-I} = 0.563e^{0.0056q_{peak}} \ , R^2 = 0.955 \quad (10a)$$

$$B_{U-I} = 0.581e^{0.0058\,q_{cd}} \ , R^2 = 0.956 \quad (10b)$$

$$B_{U-I} = 0.510e^{0.0251\,E_{LVDT}} \ , R^2 = 0.953 \quad (10c)$$

And

$$B_{U-II} = 0.832e^{0.0041q_{peak}} \ , R^2 = 0.903 \quad (11a)$$

$$B_{U-II} = 0.847e^{0.0043\,q_{cd}} \ , R^2 = 0.927 \quad (11b)$$

$$B_{U-II} = 0.792e^{0.0173\,E_{LVDT}} \ , R^2 = 0.820 \quad (11c)$$

And

$$B_{U-III} = 0.792e^{0.0173q_{peak}} \ , R^2 = 0.820 \quad (12a)$$

$$B_{U-III} = 0.867e^{0.0038\,q_{cd}} \ , R^2 = 0.925 \quad (12b)$$

$$B_{U-III} = 0.818e^{0.0154\,E_{LVDT}}\ ,\ R^2 = 0.801 \qquad (12c)$$

The above result clearly suggests that pre-peak parameters are well related to brittleness capacity of rock. This outcome becomes relevant in order to better understand material brittleness associated with the progressive fracture process characterised by the typical threshold damage stresses and the elasticity parameters. For instance, rock damage stress, q_{cd} has been proposed to better quantify the in situ state of damage surrounding tunnel excavation (Eberhardt et al. 1999; Martin 1997). Furthermore, as noted by Hudson et al. (Hudson et al. 1974) and Martin and Chandler (Martin and Chandler 1994), q_{cd} can be considered as intrinsic material property. Coefficient of correlations for B_{U-I}, B_{U-II} and B_{U-III} against rock strength parameters, indicate that in general B_{U-I} has the highest correlations in contrast to B_{U-II} and B_{U-III} for an exponential fitting. In summary, expressions 10-12 above may become relevant for further geotechnical applications. The developed brittleness index, B_{U-I}, recently successfully has been implemented to evaluate the drilling performance of different drilling methods (Munoz et al. 2016b)

CONCLUSIONS

In this study three brittleness indices were developed based on not only pre-peak but also post-peak stress-strain characteristics upon fracture energy balance and post-peak instability response. In this sense, obtaining the complete stress-strain characteristics of rock was fundamental to characterise pre-peak and post-peak rock properties. This was achieved by implementing properly lateral-strain controlled loading method in the uniaxial compression tests. Furthermore post-peak deformation characteristics were also examined by three-dimensional digital image correlation (3D DIC). Different soft, medium-strong and strong rocks (UCS is ranging from 7 to 215 MPa) were tested and analysed. Using results of DIC measurement, the post-peak relations of the rocks were characterised by either a local inelastic unloading in the material outside of the damaged zone (localized zone) or a localised strain in the material inside of the damaged zone.

Analyses of the experimental results demonstrated that brittleness indices proposed solely based on pre-peak stress-strain behaviour do not show any strong

correlation with any of the pre-peak rock mechanical parameters, otherwise they seemed to collapse in a single value irrespective of rock mechanical properties. On the other hand, the proposed brittleness indices based on the pre-peak and the post-peak stress-strain relations were strongly correlated with the pre-peak mechanical parameters including the tangent Young's modulus, the crack damage stress and the peak stress. This outcome is relevant to suggest the pre-peak rock parameters as potential indicators for assessing and predicting rock brittleness. Therefore, the pre-peak strength parameters can be suggested as potential indicators for assessing rock brittleness for further geotechnical applications.

ACKNOWLEDGEMENT

The work has been supported by the Deep Exploration Technologies Cooperative Research Centre whose activities are funded by the Australian Government's Cooperative Research Centre Programme. This is DET CRC Document 2016/105.

REFERENCES

Altindag R (2002) The evaluation of rock brittleness concept on rotary blast hole drills Journal-South African Institute of Mining and Metallurgy 102:61-66

Bažant Z (1989) Identification of strain softening constitutive relation from uniaxial tests by series coupling model for localisation Cement and Concrete Research 19:973-997

Bieniawski ZT (1967) Mechanism of brittle fracture of rock International Journal of Rock Mechanics and Mining Sciences & Geomechanics Abstracts 4:395-406 doi:http://dx.doi.org/10.1016/0148-9062(67)90030-7

Bieniawski ZT, Bernede MJ (1979) Suggested methods for determining the uniaxial compressive strength and deformability of rock materials: Part 1. Suggested method for determination of the uniaxial compressive strength of rock materials International Journal of Rock Mechanics and Mining Sciences & Geomechanics Abstracts 16:137 doi:http://dx.doi.org/10.1016/0148-9062(79)91450-5

Bischoff PH, Perry SH (1991) Compressive behaviour of concrete at high strain rates Materials and Structures 24:425--450

Chu TC, Ranson WF, Sutton MA (1985) Applications of digital-image-correlation techniques to experimental mechanics Experimental Mechanics 25:232-244 doi:10.1007/BF02325092

Eberhardt E, Stead D, Stimpson B (1999) Quantifying progressive pre-peak brittle fracture damage in rock during uniaxial compression International Journal of Rock Mechanics and Mining Sciences 36:361-380 doi:http://dx.doi.org/10.1016/S0148-9062(99)00019-4

Fairhurst CE, Hudson JA (1999) Draf ISRM suggested method for the complete stress-strain curve for intact rock in uniaxial compression International Journal of Rock Mechanics and Mining Sciences 36:279-289 doi:http://dx.doi.org/10.1016/S0148-9062(99)00006-6

Gowd TN, Rummel F (1980) Effect of confining pressure on the fracture behaviour of a porous rock International Journal of Rock Mechanics and Mining Sciences & Geomechanics Abstracts 17:225-229 doi:http://dx.doi.org/10.1016/0148-9062(80)91089-X

Hallbauer DK, Wagner H, Cook NGW (1973) Some observations concerning the microscopic and mechanical behaviour of quartzite specimens in stiff, triaxial compression tests International Journal of Rock Mechanics and Mining Sciences & Geomechanics Abstracts 10:713-726 doi:http://dx.doi.org/10.1016/0148-9062(73)90015-6

Hawkes I, Mellor M (1970) Uniaxial testing in rock mechanics laboratories Engineering Geology 4:179-285 doi:http://dx.doi.org/10.1016/0013-7952(70)90034-7

Heinz SR, Wiggins JS (2010) Uniaxial compression analysis of glassy polymer networks using digital image correlation Polymer Testing 29:925-932 doi:http://dx.doi.org/10.1016/j.polymertesting.2010.08.001

Horii H, Nemat-Nasser S (1986) Brittle Failure in Compression: Splitting, Faulting and Brittle-ductile Transition Philosophical Transactions of the Royal Society of London Series A, Mathematical and Physical Sciences 319 (1549) The Royal Society:337–374

Hucka V, Das B (1974) Brittleness determination of rocks by different methods International Journal of Rock Mechanics and Mining Sciences & Geomechanics Abstracts 11:389-392 doi:http://dx.doi.org/10.1016/0148-9062(74)91109-7

Hudson JA, Brown ET, Fairhurst C (1971) Optimizing the control of rock failure in servo-controlled laboratory tests Rock mechanics 3:217-224 doi:10.1007/BF01238181

Hudson JA, Brown ET, Fairhurst C (1974) Shape of the complete stress-strain curve for rock : Hudson, JA Univ. Minnesota, Minneapolis, USA Brown, ET James Cook Univ. Queensland, AUS Fairhurst, C Univ. Minnesota, Minneapolis, USA Symposium. In Stability of rock slopes. 8F, 2T, 14R. 13TH SYMPOSIUM ON ROCK MECHANICS ASCE, NEW YORK, 1972, P773–795 International Journal of Rock Mechanics and Mining Sciences & Geomechanics Abstracts 11:A6 doi:http://dx.doi.org/10.1016/0148-9062(74)92247-5

ISRM (1981) Rock characterization testing and monitoring—ISRM suggested methods. Oxford

Jansen DC, Shah S (1997) Effect of Length on Compressive Strain Softening of Concrete Journal of Engineering Mechanics 123:25-35 doi:doi:10.1061/(ASCE)0733-9399(1997)123:1(25)

Jansen DC, Shah SP, Rossow EC (1995) Stress-Strain Results of Concrete from Circumferential Strain Feedback Control Testing Materials Journal 92 doi:10.14359/9774

Kahraman S (2002) Correlation of TBM and drilling machine performances with rock brittleness Engineering Geology 65:269-283 doi:10.1016/S0013-7952(01)00137-5

Kidybiński A (1981) Bursting liability indices of coal International Journal of Rock Mechanics and Mining Sciences & Geomechanics Abstracts 18:295-304 doi:http://dx.doi.org/10.1016/0148-9062(81)91194-3

Kumar R, Sharma KG, Varadarajan A (2010) Post-peak response of some metamorphic rocks of India under high confining pressures International

Journal of Rock Mechanics and Mining Sciences 47:1357-1362 doi:http://dx.doi.org/10.1016/j.ijrmms.2010.08.016

Labuz JF, Biolzi L (2007) Experiments with rock: Remarks on strength and stability issues International Journal of Rock Mechanics and Mining Sciences 44:525-537 doi:http://dx.doi.org/10.1016/j.ijrmms.2006.09.005

Markeset G, Hillerborg A (1995) Softening of concrete in compression — Localization and size effects Cement and Concrete Research 25:702-708 doi:http://dx.doi.org/10.1016/0008-8846(95)00059-L

Martin C, Chandler N The progressive fracture of Lac du Bonnet granite. In: International Journal of Rock Mechanics and Mining Sciences & Geomechanics Abstracts, 1994. vol 6. Elsevier, pp 643-659

Martin CD (1997) Seventeenth Canadian Geotechnical Colloquium: The effect of cohesion loss and stress path on brittle rock strength Canadian Geotechnical Journal 34:698-725 doi:10.1139/t97-030

Munoz H, Taheri A, Chanda EK (2016a) Pre-Peak and Post-Peak Rock Strain Characteristics During Uniaxial Compression by 3D Digital Image Correlation Rock Mechanics and Rock Engineering:1-14 doi:10.1007/s00603-016-0935-y

Munoz H, Taheri A, Chanda EK (2016b) Rock Drilling Performance Evaluation by an Energy Dissipation Based Rock Brittleness Index Rock Mechanics and Rock Engineering:1-13 doi:10.1007/s00603-016-0986-0

Song H, Zhang H, Kang Y, Huang G, Fu D, Qu C (2013) Damage evolution study of sandstone by cyclic uniaxial test and digital image correlation Tectonophysics 608:1343-1348 doi:http://dx.doi.org/10.1016/j.tecto.2013.06.007

Sutton MA, Orteu JJ, Schreier H (2009) Image Correlation for Shape, Motion and Deformation Measurements. Springer US,

Taheri A, Tani K (2008) Use of down-hole triaxial apparatus to estimate the mechanical properties of heterogeneous mudstone International Journal of Rock Mechanics and Mining Sciences 45:1390-1402 doi:http://dx.doi.org/10.1016/j.ijrmms.2008.01.017

Tarasov B, Potvin Y (2013) Universal criteria for rock brittleness estimation under triaxial compression International Journal of Rock Mechanics and Mining Sciences 59:57-69 doi:http://dx.doi.org/10.1016/j.ijrmms.2012.12.011

Tarasov BG, Potvin Y (2012) Absolute, relative and intrinsic rock brittleness at compression Transactions of the Institutions of Mining and Metallurgy, Section A: Mining Technology 121:218-225

Van Vliet M, Van Mier J (1995) Softening behaviour of concrete under uniaxial compression

Vasconcelos G, Lourenço P, Alves C, Pamplona J (2009) Compressive Behavior of Granite: Experimental Approach Journal of Materials in Civil Engineering 21:502-511 doi:doi:10.1061/(ASCE)0899-1561(2009)21:9(502)

Watanabe K, Niwa J, Yokota H, Iwanami M (2004) Experimental study on stress-strain curve of concrete considering localized failure in compression Journal of Advanced Concrete Technology 2:395-407

Wawersik WR, Brace WF (1971) Post-failure behavior of a granite and diabase Rock mechanics 3:61-85 doi:10.1007/BF01239627

Wawersik WR, Fairhurst CA (1970) A Study of Brittle Rock Fracture in Laboratory Compression Experiments Int J Rock Mech Min Sci 7:561-575

Wong TF (1982) Micromechanics of faulting in westerly granite International Journal of Rock Mechanics and Mining Sciences & Geomechanics Abstracts 19:49-64 doi:http://dx.doi.org/10.1016/0148-9062(82)91631-X

Xue-bin W, Yi-shan P (2003) Effect of relative stress on post-peak uniaxial compression fracture energy of concrete J Wuhan Univ Technol-Mat Sci Edit 18:89-92 doi:10.1007/BF02838401

Yang G, Cai Z, Zhang X, Fu D (2015) An experimental investigation on the damage of granite under uniaxial tension by using a digital image correlation method Optics and Lasers in Engineering 73:46-52 doi:http://dx.doi.org/10.1016/j.optlaseng.2015.04.004

LIST OF FIGURES

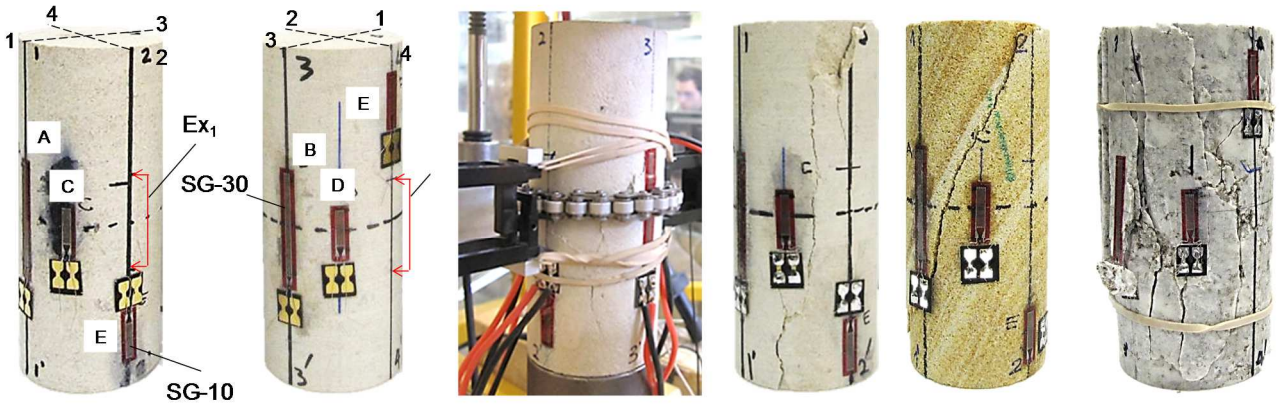

a)

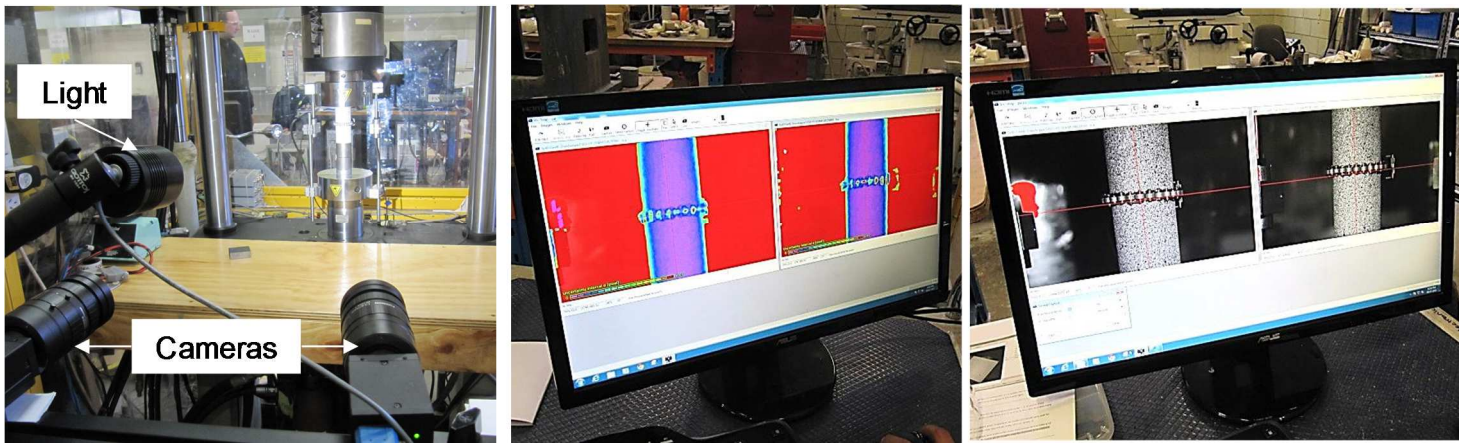

b)

Figure 2.1 a) Rock instrumentation (Massangis limestone) and rocks at the end of the test (Tuffeau limestone, Hawkesbury sandstone and Alvand granite) and b) servo-controlled closed-loop testing system and 3D DIC set up

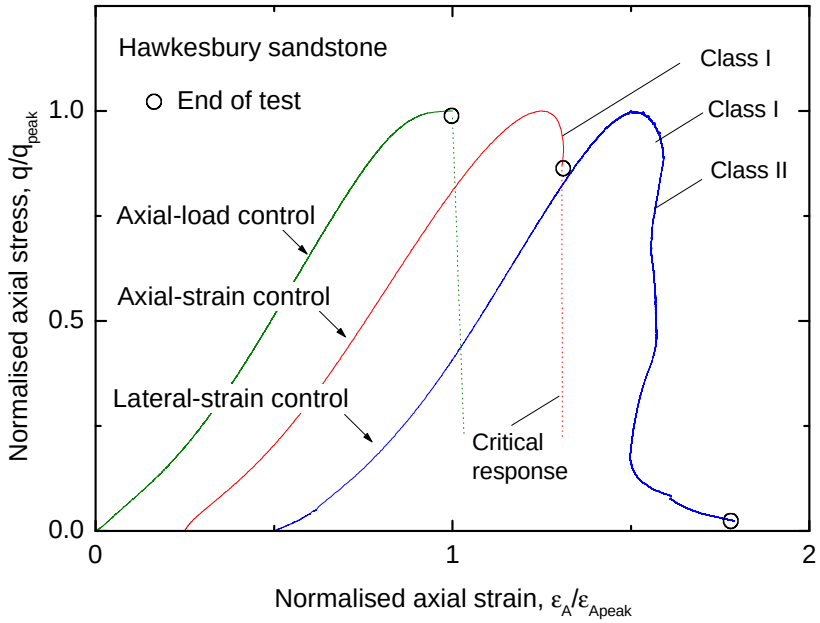

Figure 2.2 Normalised stress-strain relations of Hawkesbury sandstone under axial-load, axial-strain and lateral-strain control (the origin of the curves were shifted horizontally to not overcrowd the figure)

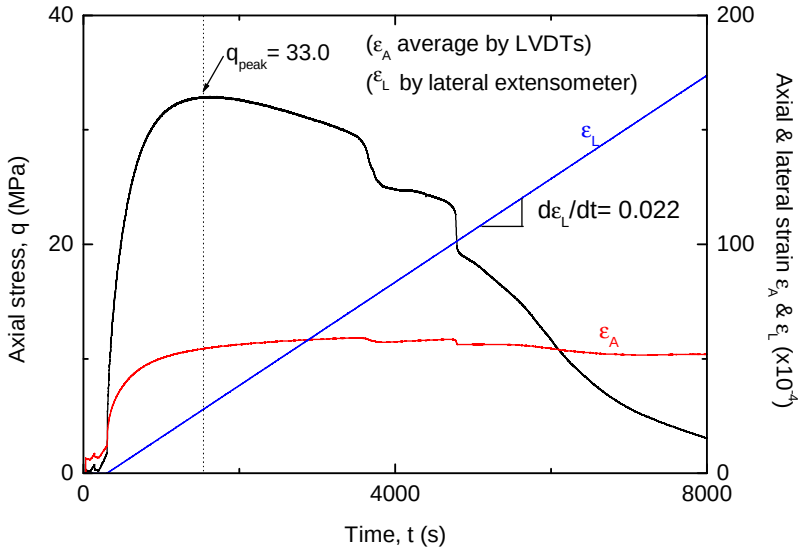

a)

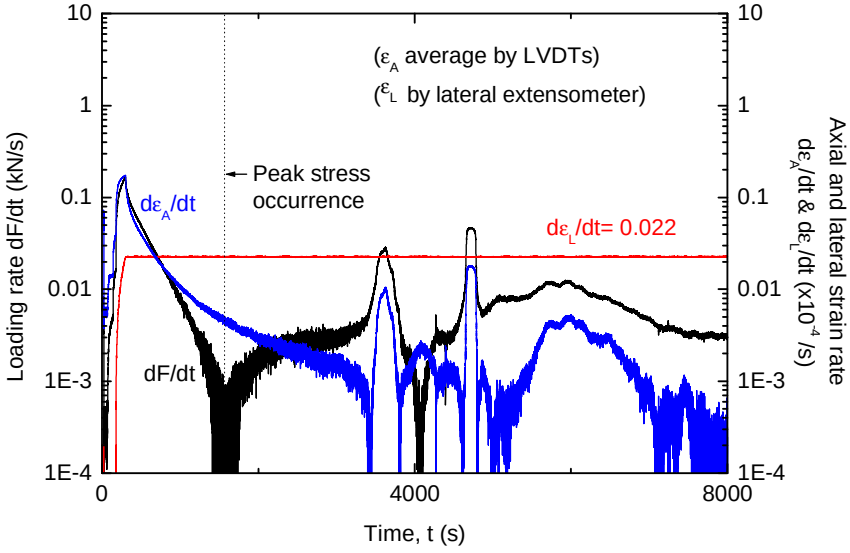

b)

Figure 2.3 Typical time history of a) loading and strains and b) loading and strain rates in uniaxial compression tests (Hawkesbury sandstone) with lateral-strain control feedback

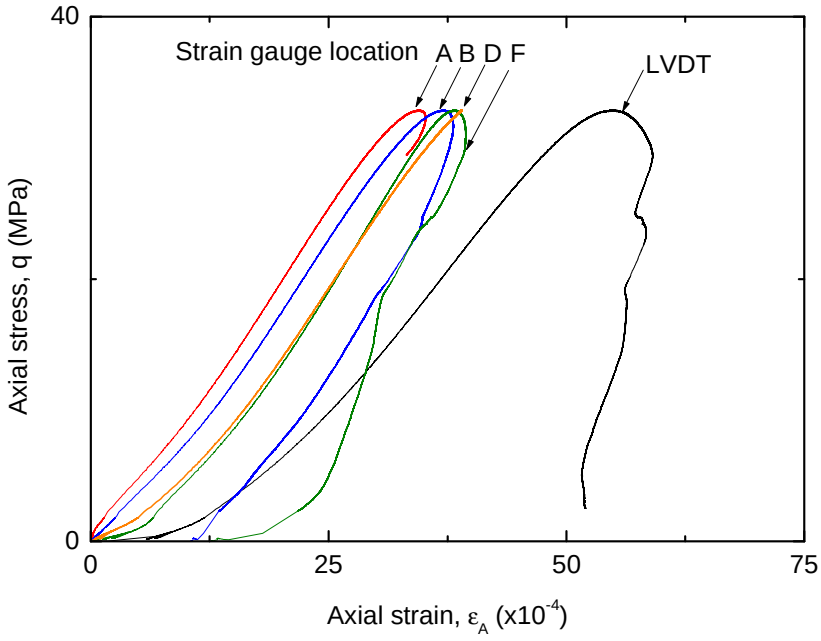

Figure 2.4 Typical stress-strain curves with axial strains obtained from external LVDT and strain gauges in Hawkesbury sandstone

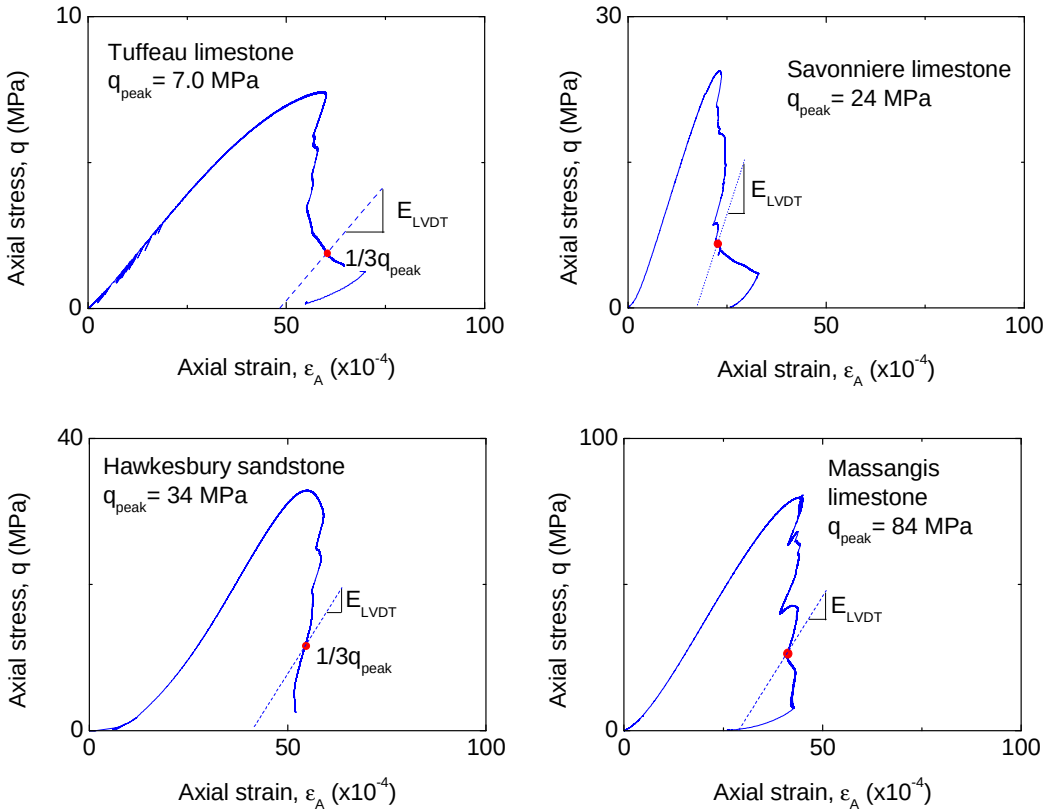
Tuffeau limestone
q_{peak}= 7.0 MPa
E_{LVDT}
1/3q_{peak}
Axial stress, q (MPa)
Axial strain, ε_A (x10^{-4})
0
50
100
10
Savonniere limestone
q_{peak}= 24 MPa
30
Hawkesbury sandstone
q_{peak}= 34 MPa
40
Massangis
limestone
q_{peak}= 84 MPa
100

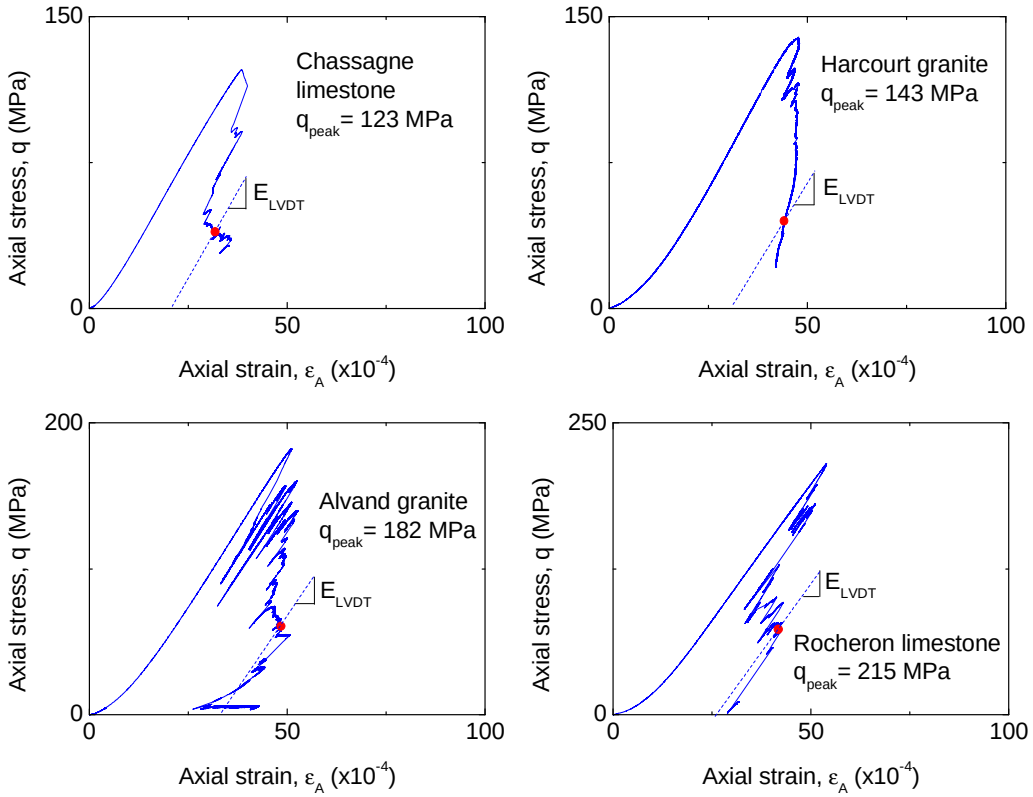

Figure 2.5 Typical complete stress-strain curves for different rocks under lateral strain-rate control

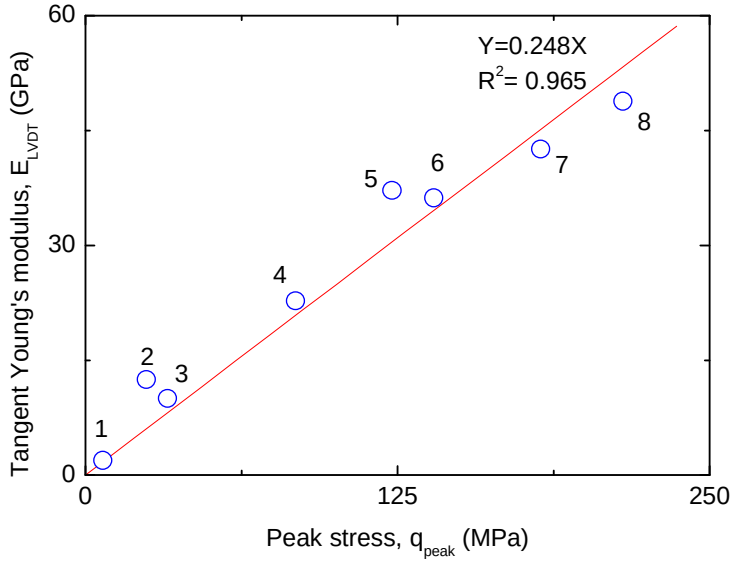

a)

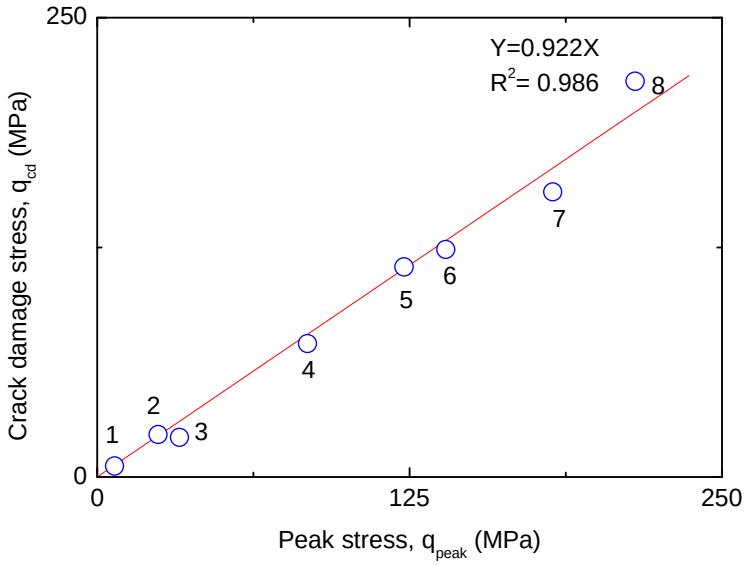

b)

Figure 2.6 Pre-peak stress-strain quantities: a) tangent Young's modulus and b) crack damage stress relations with peak stress for different rock types. Numbers 1 to 8 refer to the rock type in Table 2.1

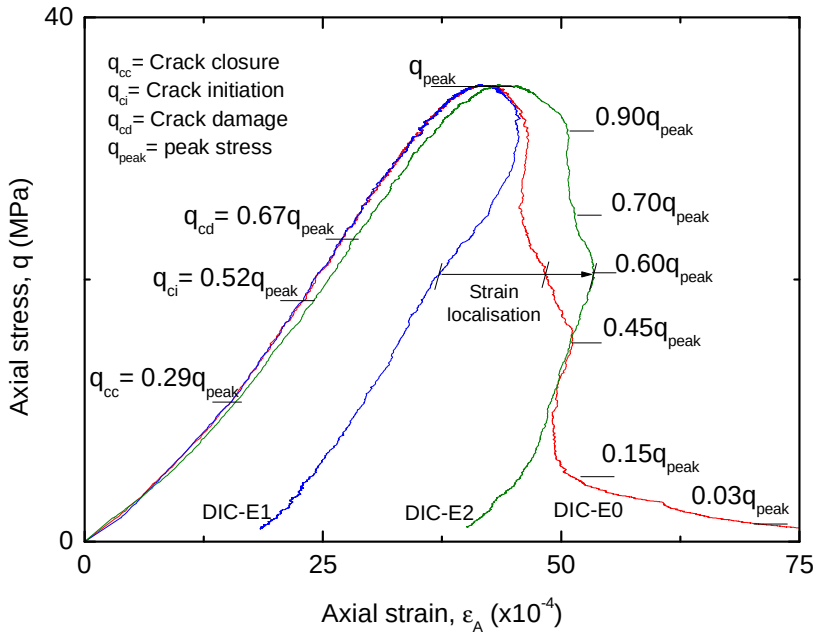
40
0
0
25
50
75
Axial stress, q (MPa)
Axial strain, ε_A (x10^-4)
q_cc= Crack closure
q_ci= Crack initiation
q_cd= Crack damage
q_peak= peak stress
q_peak
0.90q_peak
0.70q_peak
0.60q_peak
0.45q_peak
0.15q_peak
0.03q_peak
q_cd= 0.67q_peak
q_ci= 0.52q_peak
q_cc= 0.29q_peak
Strain localisation
DIC-E1
DIC-E2
DIC-E0

(a)

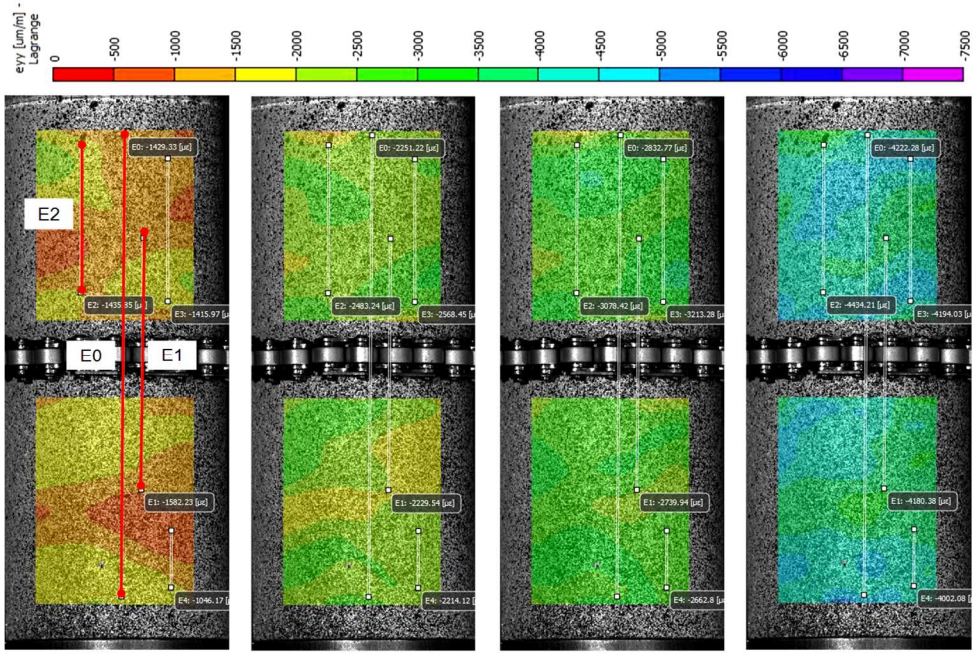

q_{cc}= 0.29q_{peak} q_{ci}= 0.52q_{peak} q_{cd}= 0.67q_{peak} q_{peak}

(b)

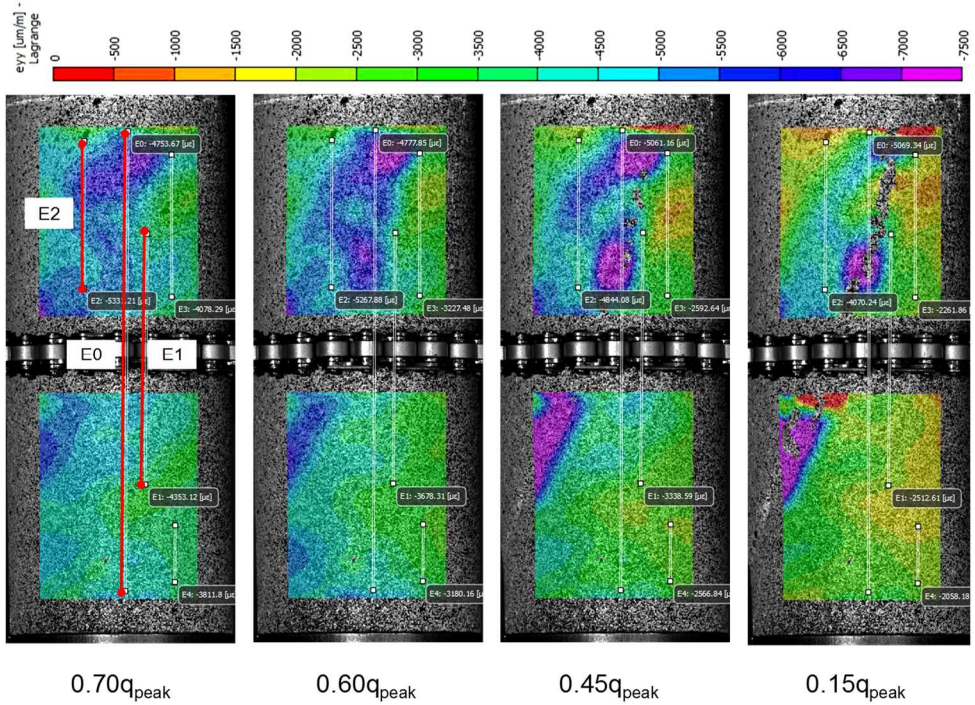

(c)

Figure 2.7 a) Stress- strain curve and b) Field of axial strains in pre-peak regime ($0.29q_{peak}$, $0.52q_{peak}$, $0.67q_{peak}$ and q_{peak}) and c) post-peak regime ($0.70q_{peak}$, $0.60q_{peak}$, $0.45q_{peak}$ and $0.15q_{peak}$) of Hawkesbury sandstone

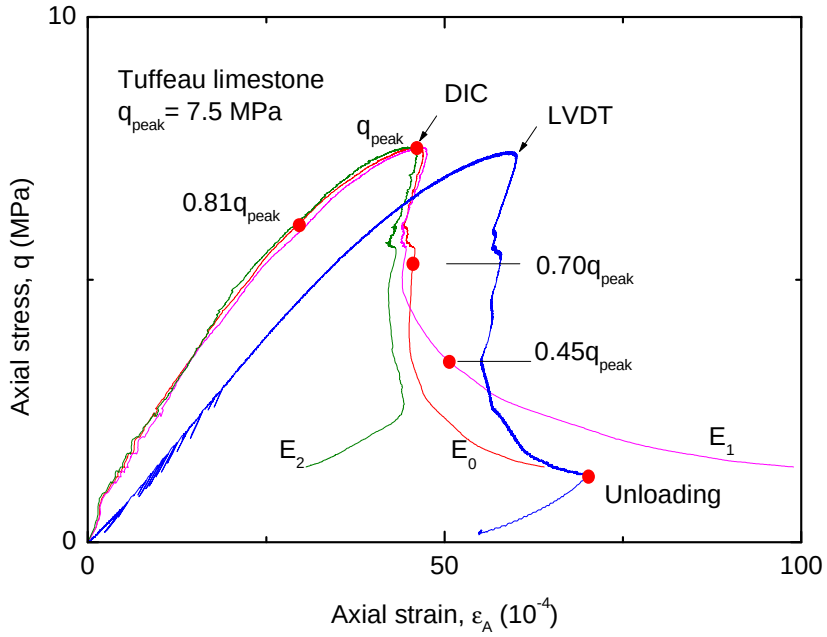
Tuffeau limestone
q_{peak}= 7.5 MPa
DIC
LVDT
q_{peak}
$0.81q_{peak}$
$0.70q_{peak}$
$0.45q_{peak}$
E_2
E_0
E_1
Unloading
Axial stress, q (MPa)
Axial strain, ε_A (10^{-4})
10
0
0
50
100

a)

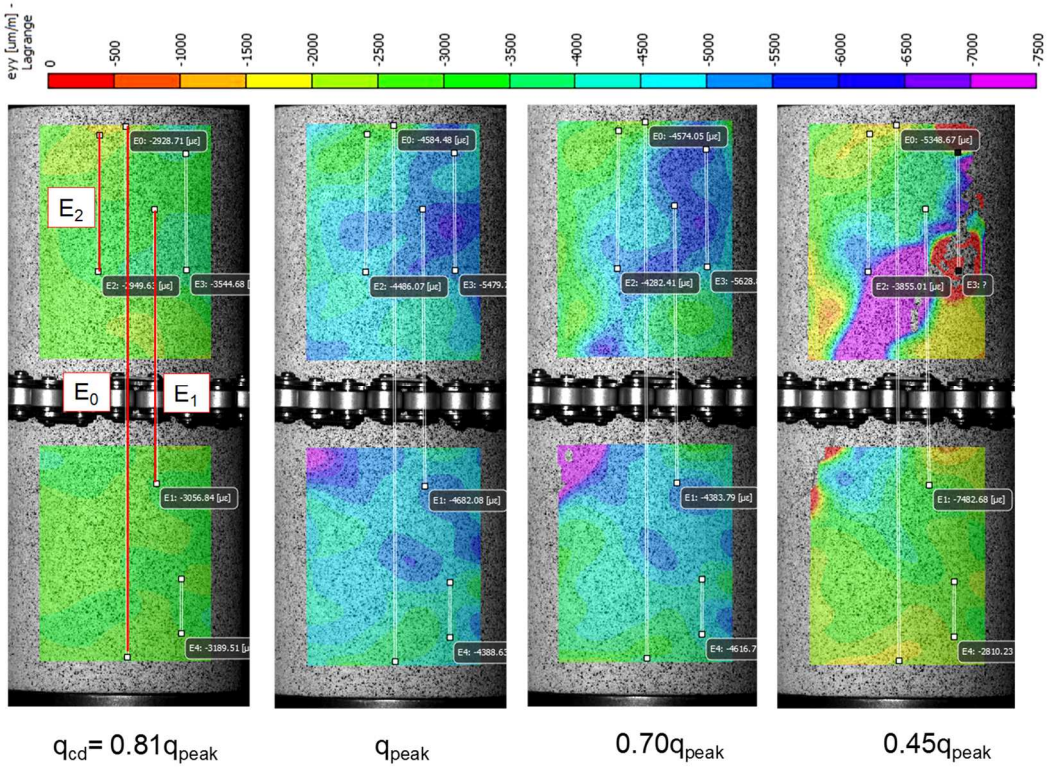

b)

Figure 2.8 a) Stress- strain curve and b) Field of axial strains developed in pre-peak regime ($0.81q_{peak}$and q_{peak}) and post-peak regime ($0.70q_{peak}$ and $0.45q_{peak}$) of Tuffeau limestone

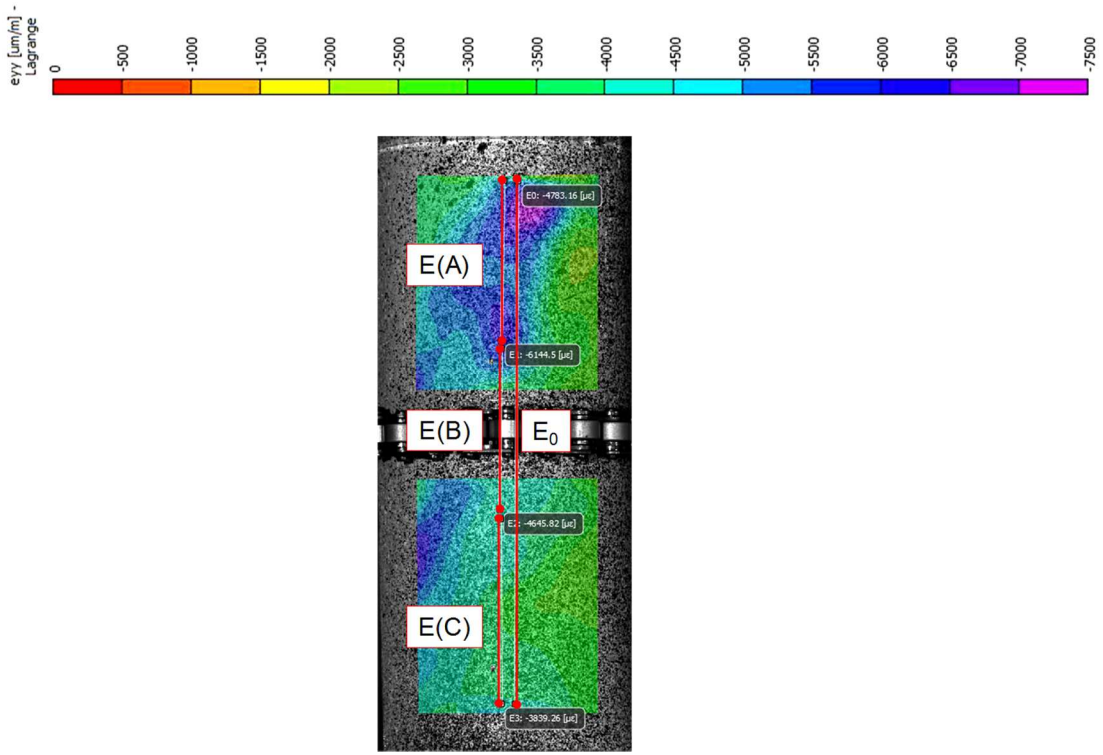
eyy [um/m] - Lagrange
0
-500
-1000
-1500
-2000
-2500
-3000
-3500
-4000
-4500
-5000
-5500
-6000
-6500
-7000
-7500
E0: -4783.16 [με]
E(A)
E1: -6144.5 [με]
E(B)
E0
E2: -4645.82 [με]
E(C)
E3: -3839.26 [με]

a)

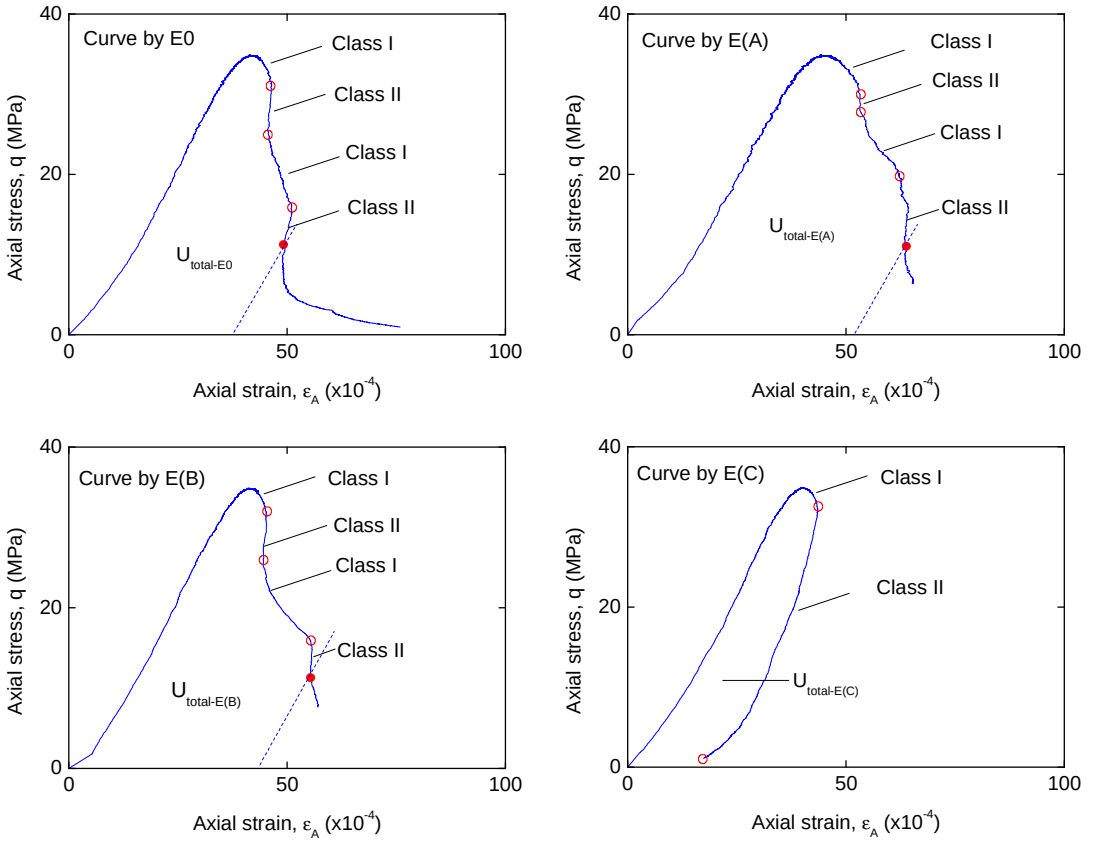
Curve by E0
Class I
Class II
Class I
Class II
U total-E0
Curve by E(A)
Class I
Class II
Class I
Class II
U total-E(A)
Curve by E(B)
Class I
Class II
Class I
Class II
U total-E(B)
Curve by E(C)
Class I
Class II
U total-E(C)
Axial stress, q (MPa)
Axial strain, ε A (x10-4)
0
20
40
0
50
100

b)

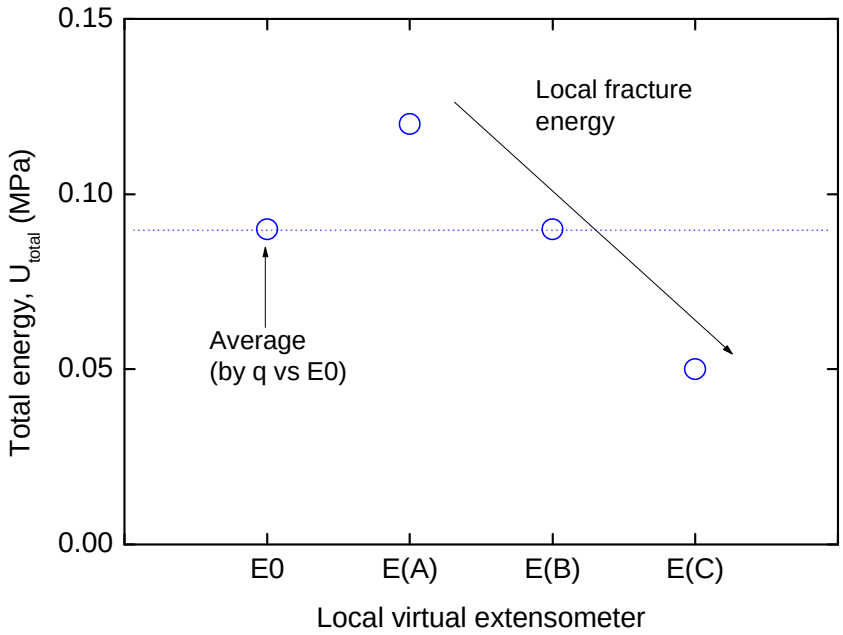

c)

Figure 2.9 a) Hawkesbury sandstone specimen and location of local virtual extensometers, b) Local stress-strain curves and c) Locally consumed energy by extensometers E(A), E(B) and E(C) and average consumed energy by E0

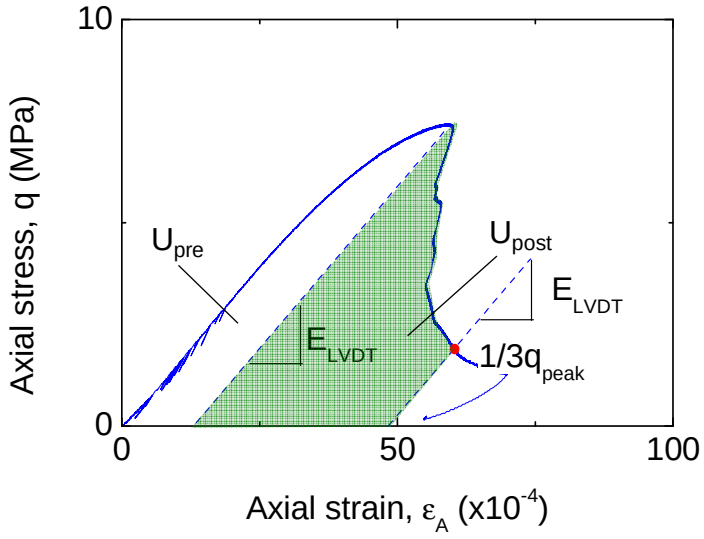
10
0
0
50
100
Axial stress, q (MPa)
Axial strain, ε_A (x10^-4)
U_pre
U_post
E_LVDT
E_LVDT
1/3q_peak

a)

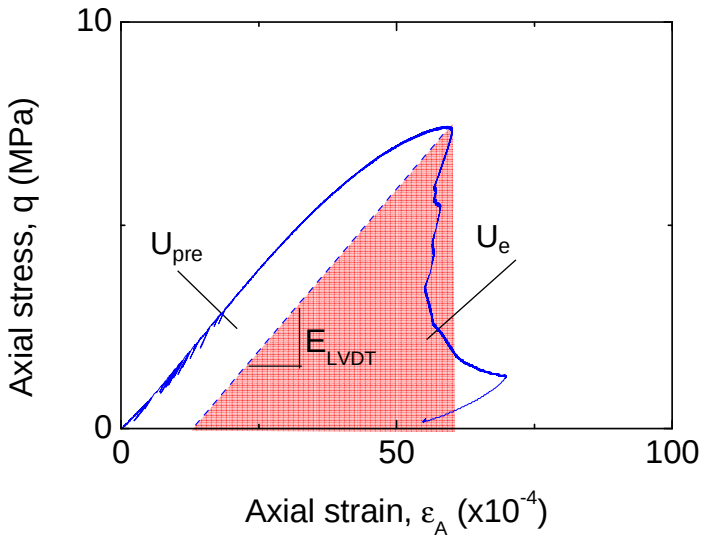
10
0
0
50
100
Axial stress, q (MPa)
Axial strain, ε_A (x10^-4)
U_pre
U_e
E_LVDT

b)

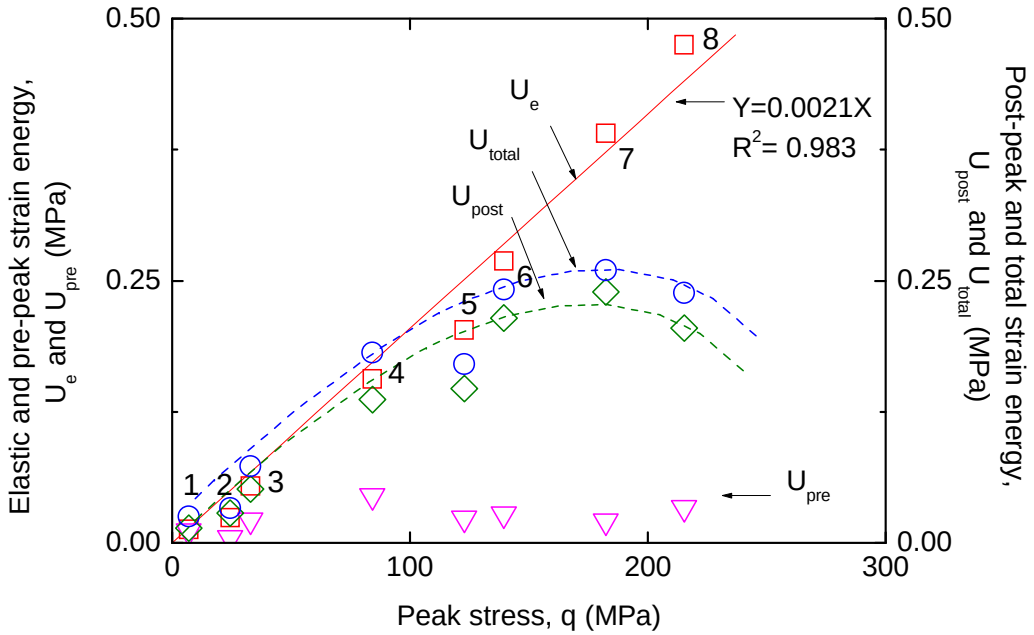

c)

Figure 2.10 a) and b) Strain energy of rock in compression and c) Strain energy quantities versus peak stress for different rocks. Numbers 1 to 8 refer to the rock type in Table 2.1

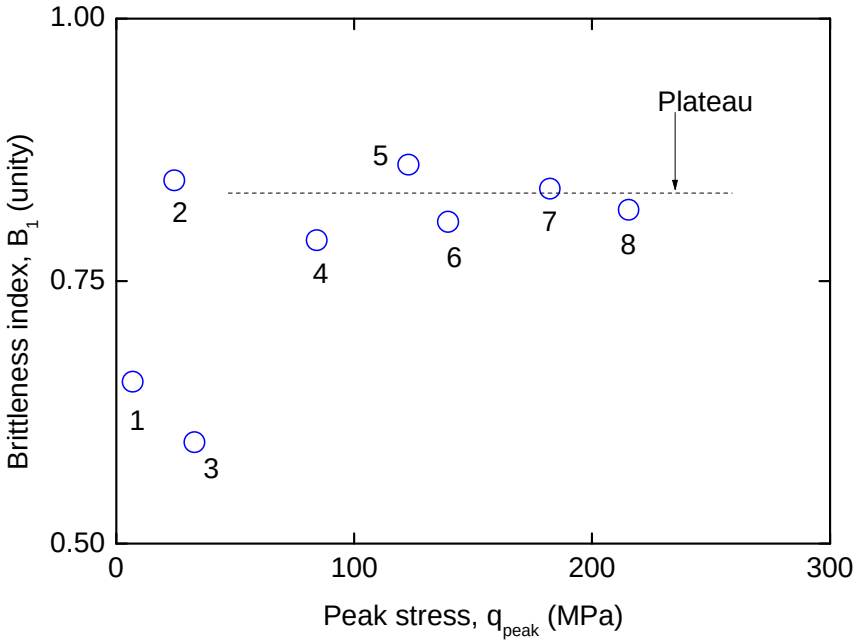
1.00
0.75
0.50
0
100
200
300
Brittleness index, B1 (unity)
Peak stress, qpeak (MPa)
Plateau
1
2
3
4
5
6
7
8

a)

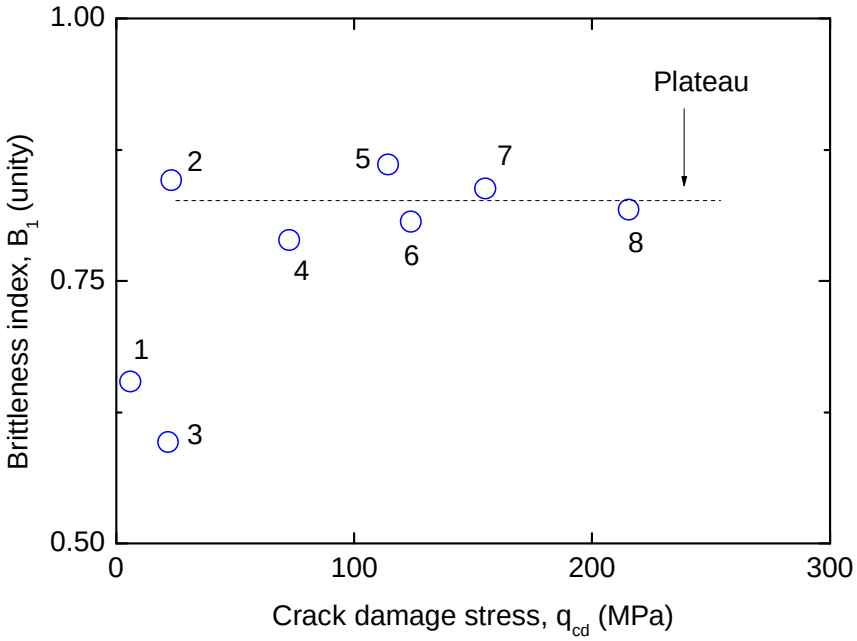
1.00
0.75
0.50
0
100
200
300
Brittleness index, B1 (unity)
Crack damage stress, qcd (MPa)
Plateau
1
2
3
4
5
6
7
8

b)

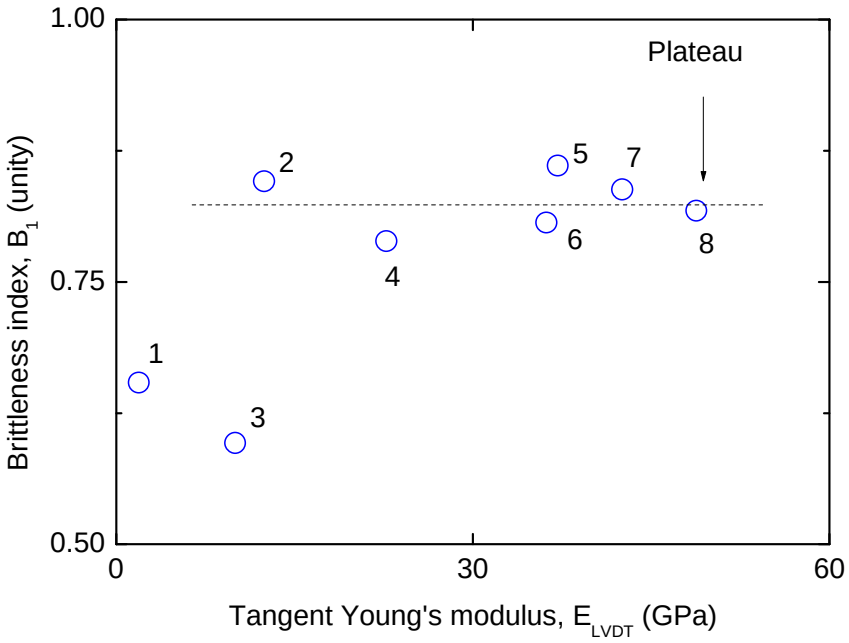

c)

Figure 2.11 Brittleness index B_1 relations with a a) peak stress, b) crack damage stress and c) tangent Young's modulus for different rock types. Numbers 1 to 8 refer to the rock type in Table 2.1

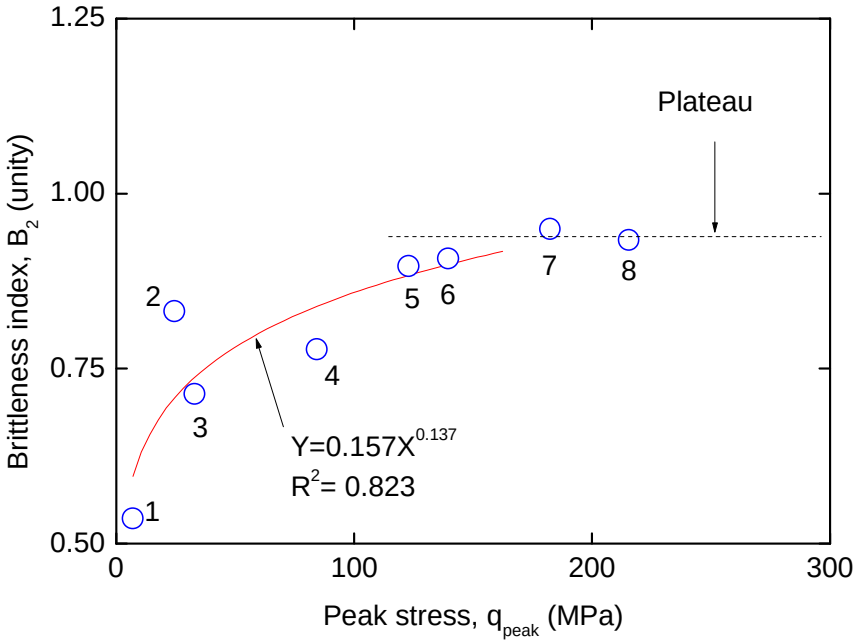
1.25
1.00
0.75
0.50
0
100
200
300
Brittleness index, B2 (unity)
Peak stress, qpeak (MPa)
Plateau
1
2
3
4
5
6
7
8
Y=0.157X0.137
R2= 0.823

a)

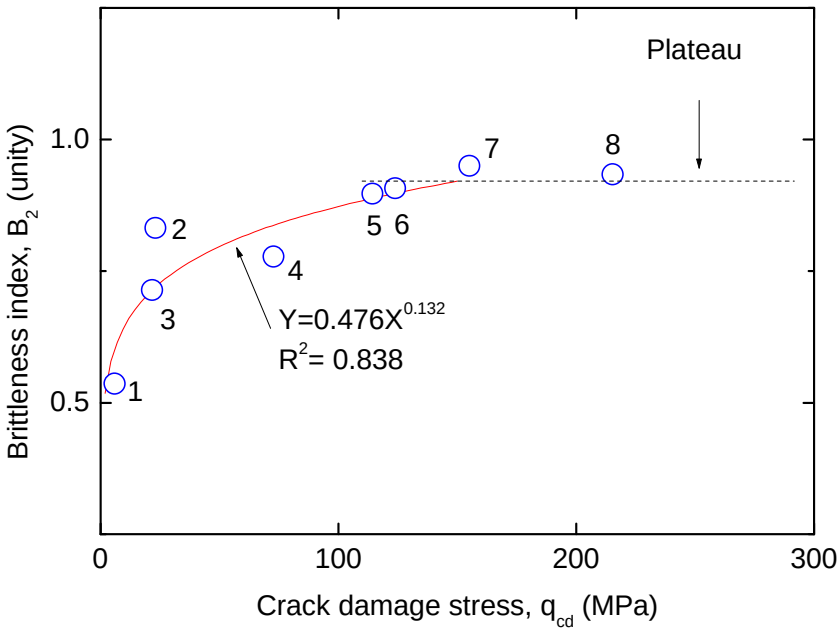
1.0
0.5
0
100
200
300
Brittleness index, B2 (unity)
Crack damage stress, qcd (MPa)
Plateau
1
2
3
4
5
6
7
8
Y=0.476X0.132
R2= 0.838

b)

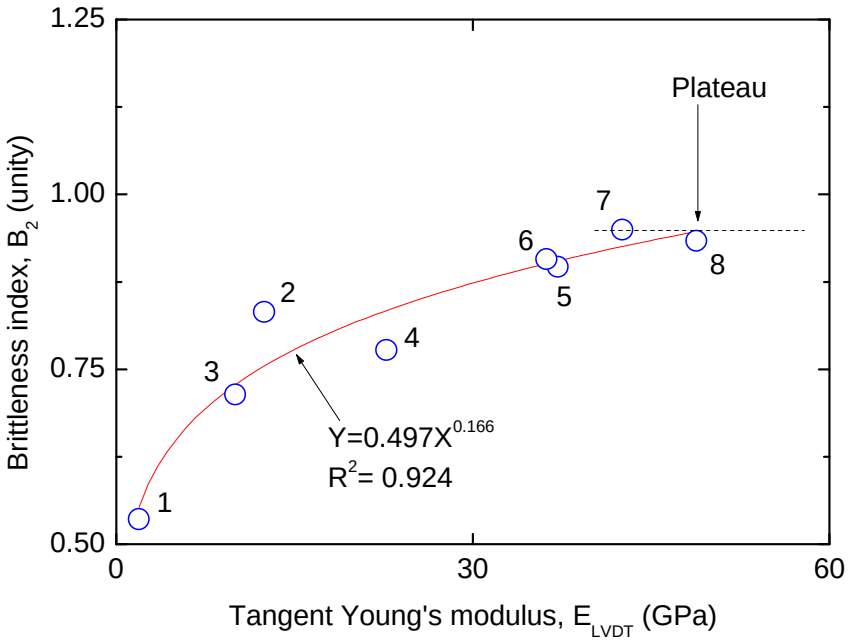

c)

Figure 2.12 Brittleness index B_2 relations with a) peak stress, b) crack damage stress and c) tangent Young's modulus for different rock types. Numbers 1 to 8 refer to the rock type in Table 2.1

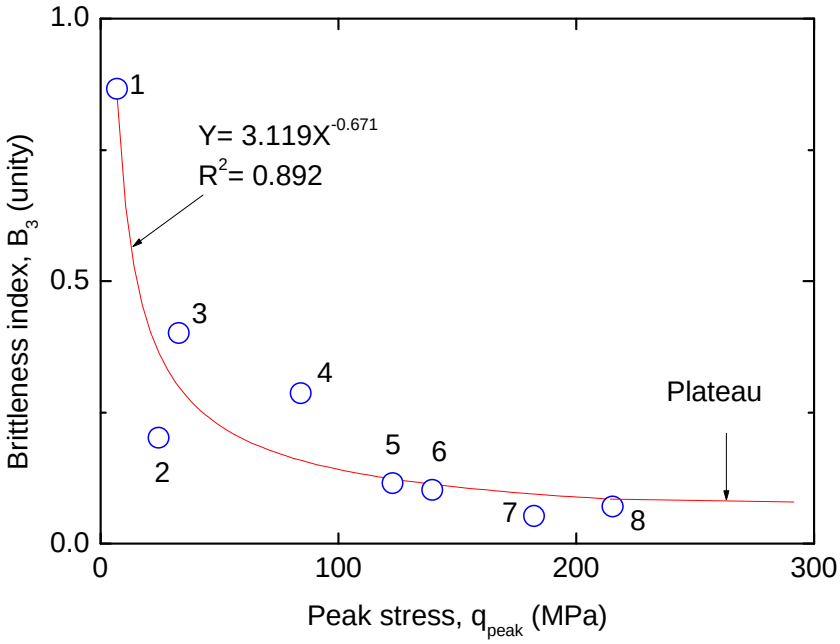
1.0
0.5
0.0
0
100
200
300
Brittleness index, B3 (unity)
Peak stress, qpeak (MPa)
Y= 3.119X-0.671
R2= 0.892
1
2
3
4
5
6
7
8
Plateau

a)

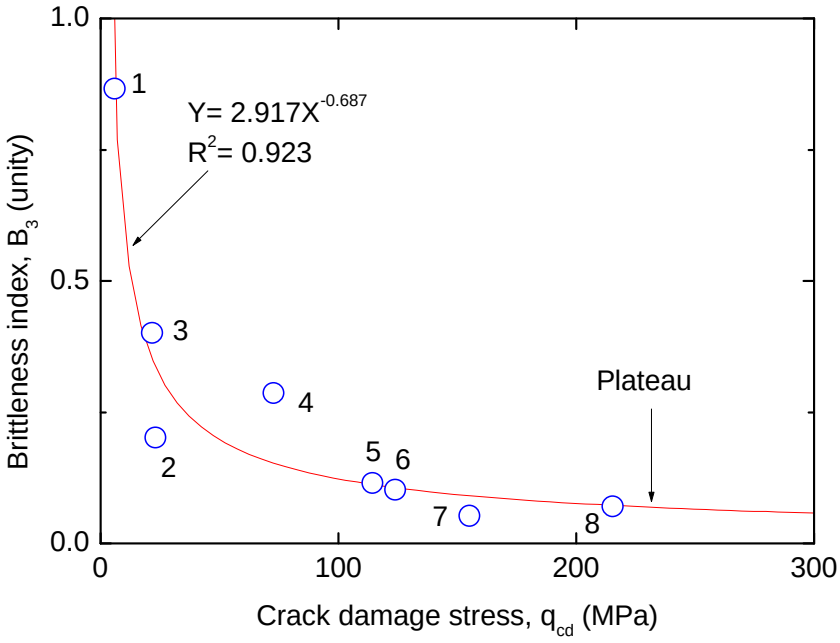
1.0
0.5
0.0
0
100
200
300
Brittleness index, B3 (unity)
Crack damage stress, qcd (MPa)
Y= 2.917X-0.687
R2= 0.923
1
2
3
4
5
6
7
8
Plateau

b)

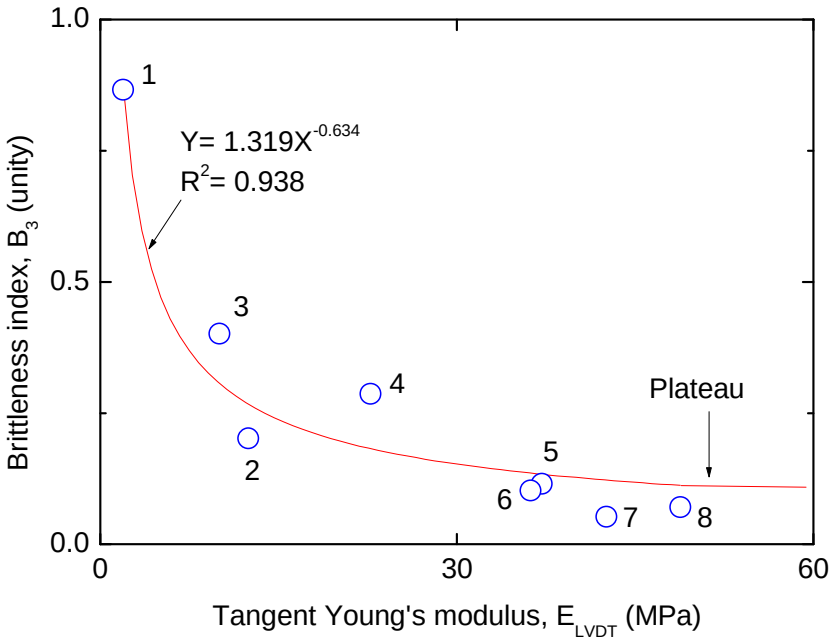

c)

Figure 2.13 Brittleness index B_3 relations with a) peak stress, b) crack damage stress and c) tangent Young's modulus for different rock types. Numbers 1 to 8 refer to the rock type in Table 2.1

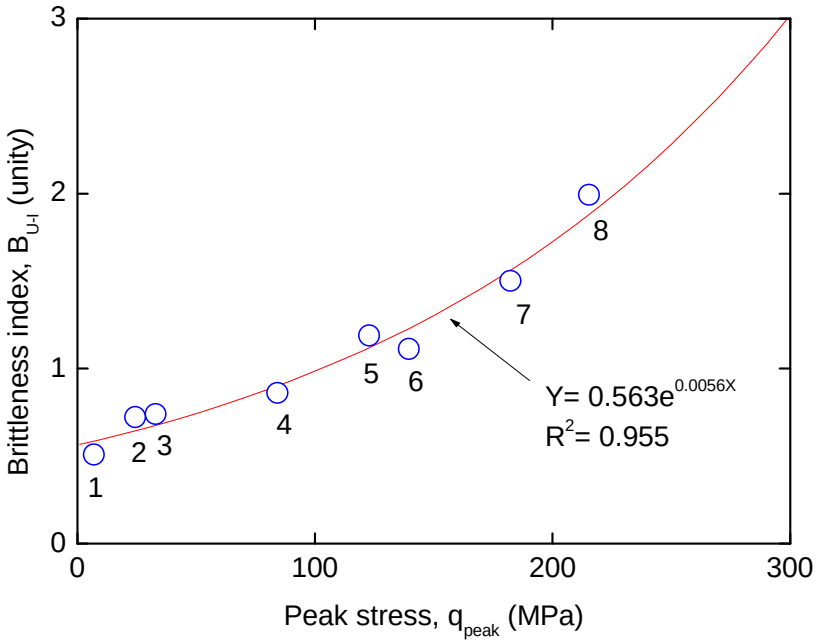
Brittleness index, B_{U-I} (unity)
Peak stress, q_{peak} (MPa)
Y= 0.563e$^{0.0056X}$
R^2= 0.955
0
1
2
3
4
5
6
7
8
0
100
200
300

a)

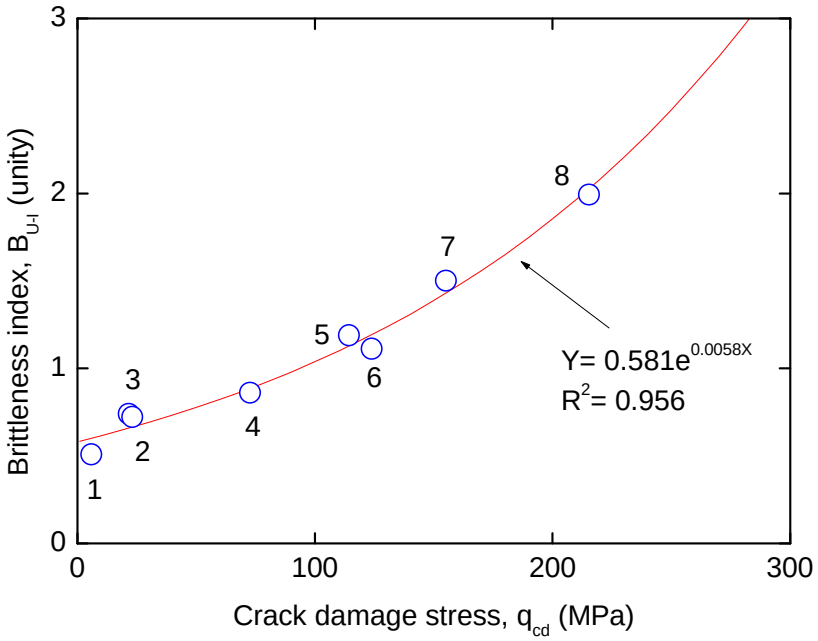
Brittleness index, B_{U-I} (unity)
Crack damage stress, q_{cd} (MPa)
Y= 0.581e$^{0.0058X}$
R^2= 0.956
0
1
2
3
4
5
6
7
8
0
100
200
300

b)

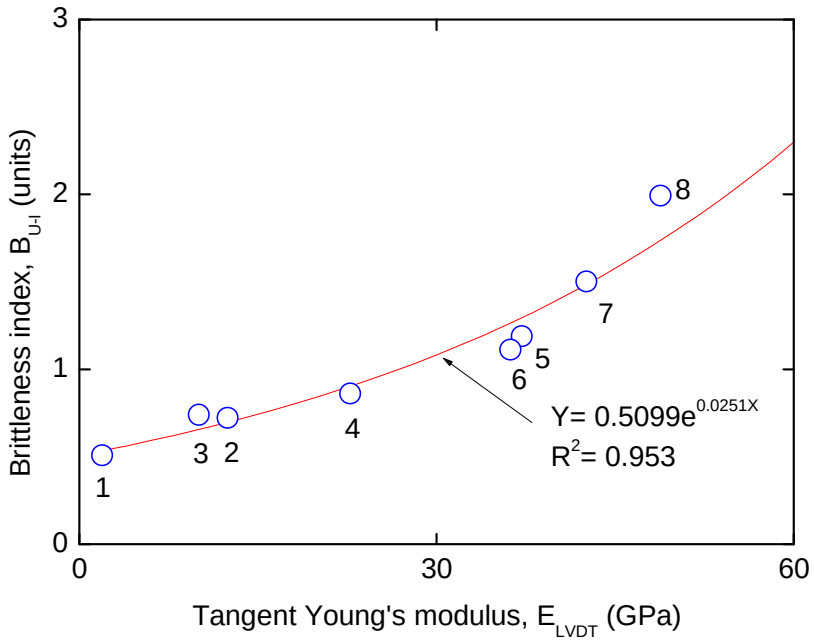

c)

Figure 2.14 Brittleness index B_{U-I} relations with a) peak stress, b) crack damage stress and c) tangent Young's modulus for different rock types. Numbers 1 to 8 refer to the rock type in Table 2.1

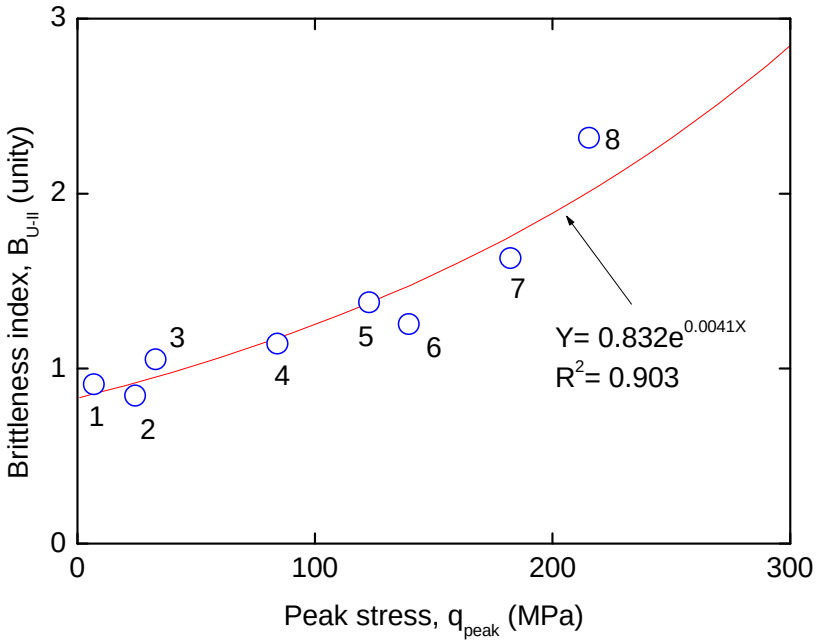
Brittleness index, B_{U-II} (unity)
Peak stress, q_{peak} (MPa)
Y= 0.832e$^{0.0041X}$
R^2= 0.903
1
2
3
4
5
6
7
8

a)

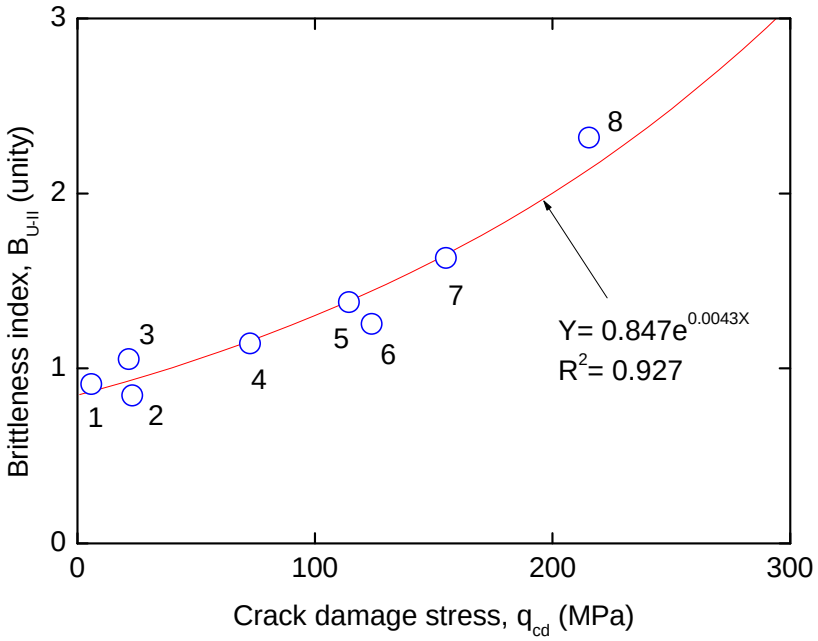
Brittleness index, B_{U-II} (unity)
Crack damage stress, q_{cd} (MPa)
Y= 0.847e$^{0.0043X}$
R^2= 0.927
1
2
3
4
5
6
7
8

b)

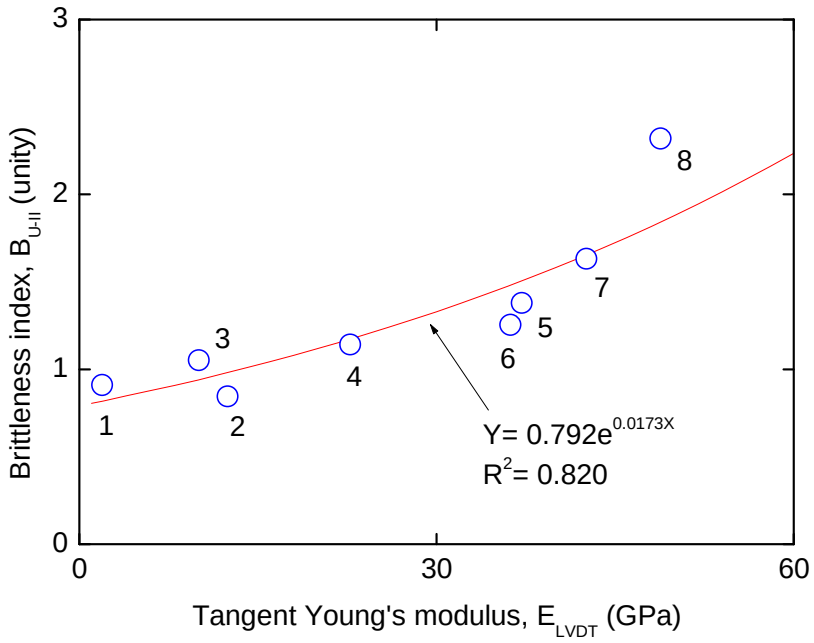

c)

Figure 2.15 Brittleness index B_{U-II} relations with a) peak stress, b) crack damage stress and c) tangent Young's modulus for different rock types. Numbers 1 to 8 refer to the rock type in Table 2.1

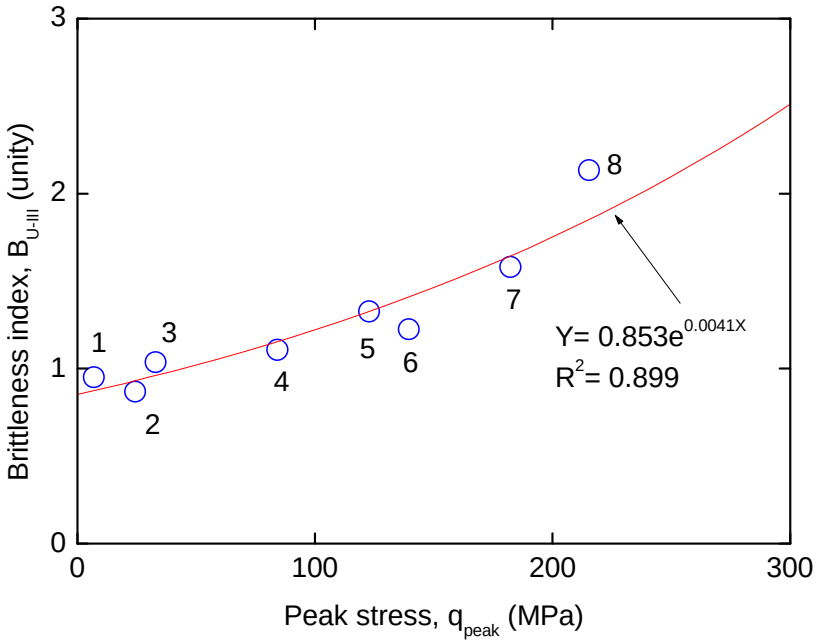
Brittleness index, B_{U-III} (unity)
Peak stress, q_{peak} (MPa)
Y= 0.853e$^{0.0041X}$
R^2= 0.899
1
2
3
4
5
6
7
8
0
1
2
3
0
100
200
300

a)

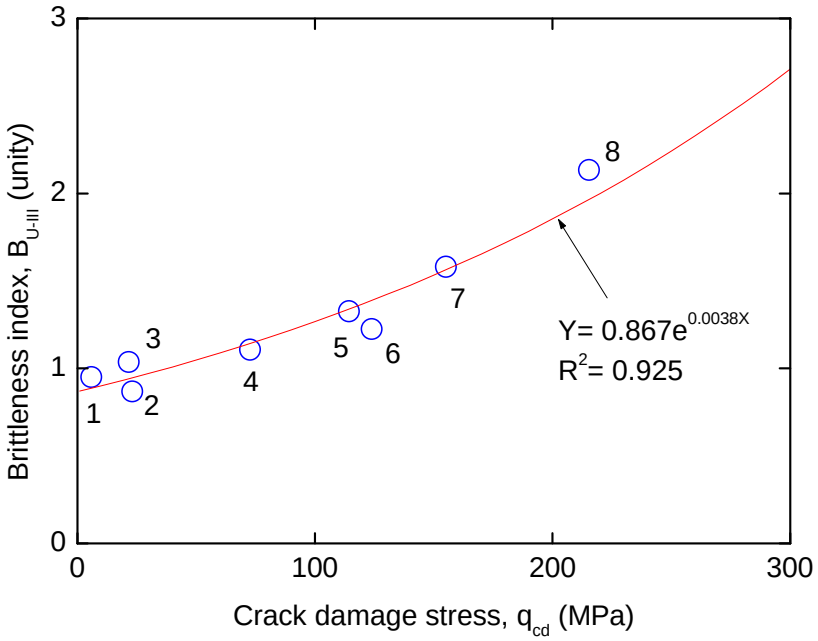
Brittleness index, B_{U-III} (unity)
Crack damage stress, q_{cd} (MPa)
Y= 0.867e$^{0.0038X}$
R^2= 0.925
1
2
3
4
5
6
7
8
0
1
2
3
0
100
200
300

b)

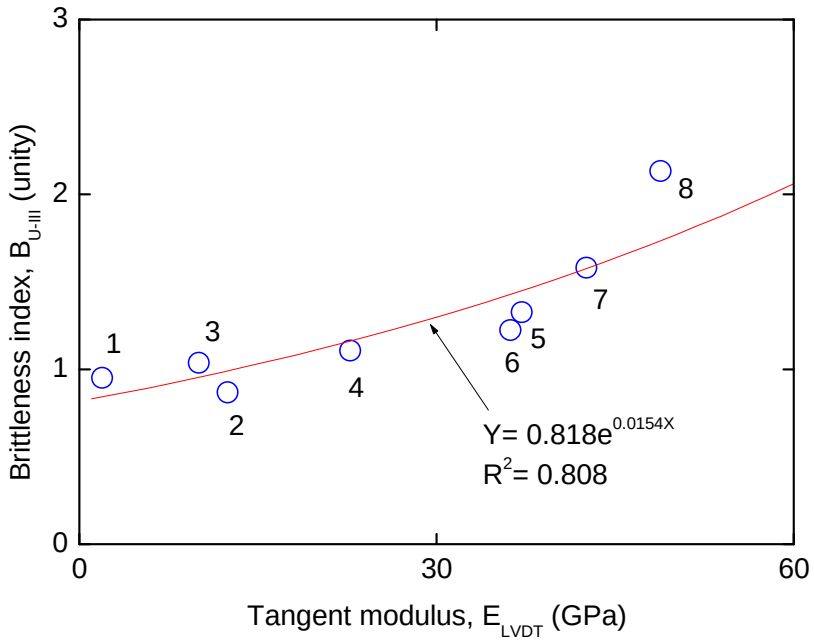

c)

Figure 2.16 Brittleness index B_{U-III} relations with a) peak stress, b) crack damage stress and c) tangent Young's modulus for different rock types. Numbers 1 to 8 refer to the rock type in Table 2.1

LIST OF TABLES

Table 2.1 Rock types investigated and their physical properties

Identification Number	Rock name	Rock type	Origin	Grain size	Dry density (g/cm^3)
1	Tuffeau	Limestone	France	Fine	1.40
2	Savonniere	Limestone	France	Fine	1.72
3	Hawksbury	Sandstone	Australia	Fine	2.26
4	Massangis	Limestone	France	Fine	2.45
5	Chassagne	Limestone	France	Fine	2.53
6	Harcourt	Granite	Australia	Medium	2.70
7	Alvand	Granite	Iran	Medium	2.65
8	Rocheron	Limestone	France	Fine	2.62

Table 2.2 Pre-peak stress-strain quantities for the rocks investigated

Rock name	Rock type	q_{peak} (MPa)	q_{cd} (MPa)	q_{peak}/q_{cd}	E_{LVDT} (GPa)
Tuffeau	Limestone	6.96	5.98	0.86	1.90
Savoniere	Limestone	24.41	23.17	0.95	12.45
Hawksebury	Sandstone	32.90	21.67	0.66	10.02
Massangis	Limestone	84.25	72.72	0.86	22.73
Chassagne	Limestone	122.84	114.40	0.93	37.15
Harcourt	Granite	139.49	123.89	0.89	36.20
Alvand	Granite	182.35	155.18	0.85	42.58
Rocheron	Limestone	215.32	215.32	1.00	48.81

Table 2.3 Pre-peak and post-peak stress-strain quantities for the rocks investigated

Rock name	Rock type	ε_{A-ir} (x10^{-4})	ε_{A-e} (x10^{-4})	U_{pre} (MPa)	U_e (MPa)	U_{peak} (MPa)	U_{post} (MPa)	U_{total} (MPa)
Tuffeau	Limestone	19.35	36.59	0.011	0.013	0.024	0.014	0.025
Savoniere	Limestone	3.57	19.61	0.005	0.024	0.029	0.028	0.033
Hawksebury	Sandstone	22.23	32.85	0.022	0.054	0.076	0.051	0.073
Massangis	Limestone	9.91	37.06	0.045	0.156	0.201	0.137	0.181
Chassagne	Limestone	5.34	33.07	0.023	0.203	0.227	0.147	0.171
Harcourt	Granite	9.25	38.53	0.027	0.269	0.296	0.214	0.242
Alvand	Granite	8.27	42.83	0.021	0.390	0.411	0.239	0.260
Rocheron	Limestone	9.83	44.13	0.034	0.475	0.509	0.205	0.238

Table 2.4 Brittleness indices for the rocks investigated

Rock name	Rock type	B_1	B_2	B_3	B_{U-I}	B_{U-II}	B_{U-III}
Tuffeau	Limestone	0.65	0.54	0.87	0.51	0.91	0.95
Savoniere	Limestone	0.85	0.83	0.20	0.72	0.85	0.87
Hawksebury	Sandstone	0.60	0.71	0.40	0.74	1.05	1.04
Massangis	Limestone	0.79	0.78	0.29	0.86	1.14	1.11
Chassagne	Limestone	0.86	0.90	0.12	1.19	1.38	1.33
Harcourt	Granite	0.81	0.91	0.10	1.11	1.25	1.23
Alvand	Granite	0.84	0.95	0.05	1.50	1.63	1.58
Rocheron	Limestone	0.82	0.93	0.07	1.99	2.32	2.13

STATEMENT OF AUTHORSHIP

Statement of Authorship

Title of Paper	Rock Cutting Characteristics on Soft-to-Hard Rocks under Different Cutter Inclinations
Publication Status	☒ Published ☐ Accepted for Publication ☐ Submitted for Publication ☐ Unpublished and Unsubmitted w ork w ritten in manuscript style
Publication Details	Munoz, H., Taheri, A., Chanda, E. (2016) Rock Cutting Characteristics on Soft-to-Hard Rocks under Different Cutter Inclinations. International Journal of Rock Mechanics and Mining Science DOI: 10.1016/j.ijrmms.2016.05.014

Principal Author

Name of Principal Author (Candidate)	Henry Munoz
Contribution to the Paper	Overall paper preparation
Overall percentage (%)	85
Certification:	This paper reports on original research I conducted during the period of my Higher Degree by Research candidature and is not subject to any obligations or contractual agreements with a third party that would constrain its inclusion in this thesis. I am the primary author of this paper.
Signature	Date 28/06/16

Co-Author Contributions

By signing the Statement of Authorship, each author certifies that:

i. the candidate's stated contribution to the publication is accurate (as detailed above);
ii. permission is granted for the candidate in include the publication in the thesis; and
iii. the sum of all co-author contributions is equal to 100% less the candidate's stated contribution.

Name of Co-Author	Abbas Taheri
Contribution to the Paper	Paper review
Signature	Date 28/06/16

Name of Co-Author	Emmanuel Chanda
Contribution to the Paper	Paper review
Signature	Date 5/7/2016

Please cut and paste additional co-author panels here as required.

ROCK CUTTING CHARACTERISTICS ON SOFT-TO-HARD ROCKS UNDER DIFFERENT CUTTER INCLINATIONS

H. Munoz[1], A. Taheri[2], E. Chanda[3]

[1]Deep Exploration Technologies Cooperative Research Centre DET CRC, Export Park, Adelaide Airport, SA 5950, Australia and School of Civil, Environmental & Mining Engineering, The University of Adelaide, SA 5005, Australia, Ph: 61 8 8313 0591, Fax: 61 8 8313 4359, Email: henry.munozprincipe@adelaide.edu.au (corresponding author)

[2]Senior Lecturer, School of Civil, Environmental & Mining Engineering, The University of Adelaide, SA 5005, Australia, Ph: 61 8 8313 0906, Fax: 61 8 8313 4359, Email: abbas.taheri@adelaide.edu.au

[3]Associate Professor, School of Civil & Environmental & Mining Engineering, The University of Adelaide, SA 5005, Australia, Ph: 61 8 8313 7410, Fax: 61 8 8303 4359, Email: emmanuel.chanda@adelaide.edu.au

KEYWORDS

Cutting performance, intrinsic specific energy, back-rake angle, compressive strength

INTRODUCTION

Rock drilling and cutting is essential in the mining industry. Rock characterisation and classification methods have been proposed to assess drilling or cutting performance (Altindag 2009; Hoseinie et al. 2008; Hoseinie et al. 2009; Kahraman 2003; Yarali and Soyer 2011). However, a generalised method to relate rock characteristics to rock cutting performance has not yet been

developed. This is due to the complexity of interactions among the variables involved in the cutting process encompassing not only rock properties, but also the nature of cutting. Cost-effective drilling is achievable by allocating the available gross energy towards the cutting action and, at the same time, reducing systematically that energy consumed in frictional processes inherent to tool-rock interactions. A set of optimum drilling parameters (i.e. the optimum weight and torque on the bit) is essential to produce the optimum drilling rate and attain higher efficiency. In this instance, extra energy may be required if the weight and torque on the bit are significantly different from their optimum values making the drilling process less efficient.

Several attempts have been made to assess drilling performance by correlating different rock properties with the drilling rate. For instance, rock texture, grain size, Unconfined Compressive Strength (UCS), Mohs hardness and rock mass structural parameters have been used to build a number of drillability indices (Altindag 2003; Altindag 2009; Hoseinie et al. 2008). However, not only rock properties, but also different sets of drilling parameters (weight and torque on the bit) and drilling techniques have an impact on the drilling performance and efficiency of the process as noticed by (Detournay and Defourny 1992; Detournay et al. 2008; Taheri et al. 2016; Teale 1965).

Through tool-rock interaction laws, it was found that Specific Energy (SE) accounts for both the energy consumed in rock cutting and the energy consumed in friction between the tool and the rock or in mechanical energy losses outside the rock (Detournay and Defourny 1992; Teale 1965). The concept of specific energy (SE) in rock drilling was introduced by Teale (Teale 1965) as the work done to excavate a unit volume of rock. In this manner, the cutting response of PDC (Polycrystalline Diamond Compact) bits derives from a combination of two major actions (Detournay and Defourny 1992): i) a pure cutting action and ii) a frictional action due to the cutter wear-flat area. The energy consumed in a pure cutting action of rock is measured by the intrinsic specific energy (ε) attainable at the cutting point (Detournay and Defourny 1992; Detournay et al. 2008; Franca 2010; Franca et al. 2015). The magnitude of the

intrinsic specific energy depends entirely on the nature of the rock (Detournay and Defourny 1992; Teale 1965), the surrounding pressure on the rock surface (Detournay and Atkinson 2000) and the drilling technique being used (Detournay et al. 2008; Franca 2010; Franca et al. 2015). Quantities of consumed energy higher than the intrinsic specific energy represent the energy consumed by frictional processes.

The intrinsic specific energy (ε) quantifies the maximum cutting efficiency associated with the optimum cutting force (Detournay and Defourny 1992; Detournay et al. 2008; Franca 2010; Franca et al. 2015) and it has become useful to estimate rock strength. In this regard, it has been found that ε approximately equals to Unconfined Compressive Strength (UCS) of rock in drilling experiments with PDC bits (Detournay et al. 2008) and roller-cone bits (Franca 2010). In addition, this finding has been supported by a significant number of cutting tests with a single PDC cutter when the back-rake angle of the cutter (θ) is 15 degrees (Richard et al. 2012), see Figure 3.1 for the definition of back-rake angle.

A literature survey indicates that there are very few studies on effect of cutting parameters on the intrinsic specific energy value. To investigate the magnitude of the intrinsic specific energy and its relation with the geometry of the cutting and peak strength of rock, cutting experiments with a single PDC were carried out on different rock types at different back-rake angles, i.e. θ of 15, 30 and 45 degrees. Additionally, the stress-strain parameters of the rocks were obtained by performing a series of uniaxial compressive tests.

ROCK CUTTING MECHANISM

Rock cutting induces two modes of failure in the rock depending on the depth of cut, d, which are plastic yielding and fracture mode of failure (Lin and Zhou 2013; Lin and Zhou 2015; Richard et al. 2012). At relatively shallow depths of cut, plastic yield mode of failure is dominant and material failure is governed by yield strength (i.e. strength-related failure mechanism). On the other hand, when the depth of cut is relatively deep, fracture mode of failure

dominates and therefore material failure is governed by its fracture properties (i.e. fracture-related failure mechanism). In these instances, UCS and fracture toughness, K, become relevant to characterise plastic yield and fracture mode of failure in cutting, respectively.

Lin and Zhou (Lin and Zhou 2013; Lin and Zhou 2015) demonstrated that rock cutting is well described by Bazant's size effect law (SEL) for quasi-brittle materials, such as concrete and rocks (Bažant 1984). SEL is expressed as a function of the nominal stress $\sigma_N = (F_s^C)_{peak}/w_c d$ and the depth of cut, d, where $(F_s^C)_{peak}$ is the peak cutting force and w_c is the cutter width, see Figure 3.1 for the geometry and nomenclature of the cutting test. In the case of rock cutting, they found that linear elastic fracture mechanics (LEFM) is relevant asymptotically to cutting data when cutting is relatively deep. In the present study it is anticipated that the cutting experiments were carried out at depths of cut smaller than 0.5 mm in compliance with plastic yield mode of failure.

EXPERIMENTAL STUDY

A series of uniaxial compressive tests and cutting tests using a single PDC (Polycrystalline Diamond Compact) cutter were carried out. Uniaxial compressive tests were conducted at The University of Adelaide and cutting tests were performed at the Australian Resource Research Centre (ARRC) CSIRO-Perth facilities. The experimental work details are summarised in Table 3.1.

ROCKS INVESTIGATED

Rock types including limestone (Tuffeau), sandstone (Mountain Gold, Hawkesbury), phyllite (Brukunga) and basalt (Mantina) were investigated. The rocks were sourced from several mines and quarries in France and Australia. Table 3.2 lists the rocks investigated and their physical and mechanical properties including grain size, uniaxial compressive strength (UCS) and Young's modulus (E) on average. The rock samples correspond to fine grain size having densities ranging from 1.5 to 2.7 g/cm^3 and uniaxial compressive strengths ranging from 9 to 249 MPa.

UNIAXIAL COMPRESSIVE TESTS

To study the stress-strain characteristics of the rocks under uniaxial compressive tests, in total 26 samples were prepared from coring rock blocks listed in Table 3.2. The diameter of cores was 42 mm and their aspect ratio (the ratio diameter to length) was maintained at 2.4. Visual inspection shows that sample diameters were more than 10 to 20 times bigger than rock grains size. Each rock was tested at least three times and consistent results were obtained from UCS tests on each rock.

Axial and lateral deformations induced by axial load on the rock samples were measured locally by either: i) a pair of axial and lateral strain gauges (FLA-30-11 and FLA-10-11 manufactured by Tokyo Sokki Kenkyujo Co.) attached directly to the surface of the rocks in axial and lateral directions, respectively, or ii) direct-contact axial and lateral extensometers (632.12F20-series manufactured by MTS Systems Co.). In addition, the axial deformation was measured externally by a pair of LVDTs (Linear variable displacement transducers). Local measurement devices are free from bedding errors (Taheri and Tani 2008) and therefore, in this study, local axial and lateral deformations measured were used.

Axial deformation feedback signal was used to control the axial loading keeping a constant axial deformation rate equal to 0.04 mm/min. For this purpose, a closed-loop servo-controlled loading machine stiff enough to allow the elastic energy not to accumulate in the testing machine was used. The testing machine has a loading capacity of 1000 kN. In all the tests, no additional friction-reducing layers in contact between the specimens and the loading platen were used. In this case, the platen was in direct contact with the specimens.

CUTTING TESTS WITH A SINGLE PDC

In total 45 PDC cutting tests were carried out on the rocks to investigate the magnitude of the intrinsic specific energy, ε. The tests were conducted following a standard practice suggested by Richard et al. (Richard et al. 2012). The cutting device used in this experiment was manufactured by Epslog SA.

This machine is equipped with a load sensor having a loading capacity of 3000 N with ±1 N of sensitivity which measures the tangential (F_s^C) and normal (F_n^C) components of the cutting force acting on the cutter (see Figure 3.1). The cutting machine is controlled by a computer program and the data is stored into a computer by a data acquisition system.

A consistent cut was applied to the lateral surface of the rock samples by means of a rectangular cutter (sharp cutter) of width w_c equal to 10 mm. In the tests, the cutter ran along a length about 10 cm under a prescribed constant velocity of 4 mm/s and at constant depth of cut, d. The depth of cut d in the tests varied from 0.1 to 0.5 mm with steps of constant increments of 0.1 mm, in general. The surface of the rocks was carefully prepared by preliminary cuts to achieve an even and smooth surface prior to setting the prescribed depth of cut and start the test. By doing so, it was assured the formation of a groove having constant cross-section area (i.e. constant $w_c d$) at constant d in each test.

Each cutting run was performed strictly over a fresh surface on the rock. Furthermore, the formation of a deep U-type groove due to successive cuts over a same spot was not allowed, so the effect of sidewall friction (cutter-groove) , that may cause an additional increase in ε values, e.g. (Richard et al. 2010), was eliminated. To investigate the influence of increasing the inclination of the back-rake angle θ of the cutter in the magnitude of the intrinsic specific energy ε, the cutting tests were performed at three different back-rake angles of 15, 30 and 45 degrees.

TEST RESULTS AND DISCUSSION

ROCK STRENGTH CHARACTERISTICS

The failure pattern of the rock samples at the end of the compressive tests consisted predominantly of a single-shear plane, although additional minor axial cracks also were noticed in the specimens. In pre-peak regime, the threshold stresses for fracture damage associated with crack closure (q_{cc}), crack initiation (q_{ci}), crack damage (q_{cd}) and peak stress (q_{peak}) were identified from the typical

stress-strain curves in accordance with Martin and Chandler (Martin and Chandler 1994). Young´s modulus (E) of the rocks were extracted from the linear-elastic portion of the stress-strain curves limited by q_{cc} and q_{ci}. The linear elastic behaviour of the rocks was considered to take place after the end of an initial loading stage where existing micro-cracks in the samples, if any, are closed. Table 3.2 summarises the average values of q_{peak} (i.e. UCS) and Young´s moduli of the rocks.

INTRINSIC SPECIFIC ENERGY FROM PDC CUTTING

Figure 3.2 depicts a sample of the cutting force histories at a prescribed depth of cut of 0.2 mm on a Mantina basalt. In this figure, cutting force versus cutter advancement for three different cutting conditions, i.e. at different back-rake angles of 15, 30 and 30 degrees, are presented. The shallow cut history shows a relatively smaller amplitude oscillation in front of the cutter.

The intrinsic specific energy, ε, then can be obtained using the following expression (Richard et al. 2012):

$$\varepsilon = F_s^C / w_c d \quad (1)$$

Where, F_s^C represents the average force on steady cutting conditions, d, is the depth of the cut and w_c, represents the cutter width (w_c of 10 mm). The cutting response of the PDC cutter on the intact rocks was characterised by a linear scaling regime between F_s^C and d or F_s^C and $w_c d$, as shown in Figure 3.3 and Figure 3.4.

Figure 3.3 shows the summary results for the case when the rocks are cut by the cutter positioned at a back-rake angle of 15 degrees. The plots between F_s^C and d show in general non-zero intercepts of the linear fitting. This behaviour may be associated to the presence of friction caused by cutter wear as explained by Zhou and Lin (Zhou and Lin 2013). Figure 3.4 shows the plots between or F_s^C and $w_c d$ for the rocks that were cut by the cutter positioned at back-rake angles of 15, 30 and 45 degrees. Again, these plots show in general non-zero intercepts of the linear fitting and it seems that the intercept of cutting

force was reduced in the case when the back-rake angle was 30 or 45 degrees. Therefore, the amount of friction decreases with an increase in rake angle.

Table 3.3 summaries the values of intrinsic specific energy which were obtained from the slope of the linear fitting in $F_s^C - w_c d$ plot showed in Figure 3.4. For the case of rocks cut at a back-rake angle of 15 degrees, the magnitude of ε varied from 9 to 220 J/cm^3 which is in good agreement with the magnitude of UCS of the rocks. This result is supporting previous findings by other researchers, e.g. (Richard et al. 2010; Richard et al. 2012) as shown in Figure 3.5 by a linear correlation.

Figure 3.6 shows that the intrinsic specific energy values increase by a factor from about 1.2 to 1.7 and 1.9 to 2.3 times, on average, when the back-rake angle of the cutter is increased to 30 and 45 degrees, respectively, in contrast to the case when rocks are cut at 15 degrees back-rake angle (see Table 3.3). In this case ε exceeds UCS values.

CONCLUSIONS

A series of cutting tests using a single PDC (Polycrystalline Diamond Compact) cutter at three different back-rake angles and uniaxial compressive tests were carried out on different rock types including limestone, sandstones, phyllite and basalt to quantify the intrinsic specific energy and strain energy. The experiment results show that, in general, the magnitude of intrinsic specific energy, i.e. the energy to cut unit volume of rock, is increased as the inclination of the cutter increases from 15 to 30 and 45 degrees, i.e. the back-rake angle, from 15 to 30 and 45 degrees, leads to a higher demand of the energy to cut the same amount of rock. The intrinsic specific energy from PDC was found to correlate well with the UCS of rock when the back-rake angle of the cutting is 15 degrees.

ACKNOWLEDGEMENT

The work has been supported by the Deep Exploration Technologies Cooperative Research Centre whose activities are funded by the Australian Government's Cooperative Research Centre Programme. This is DET CRC Document 2016/825.

REFERENCES

Altindag R (2003) Correlation of specific energy with rock brittleness concepts on rock cutting Journal of the South African Institute of Mining and Metallurgy 103:163-171

Altindag R (2009) Assessment of some brittleness indexes in rock-drilling efficiency Rock Mechanics and Rock Engineering 43:361-370 doi:10.1007/s00603-009-0057-x

Bažant Z (1984) Size Effect in Blunt Fracture: Concrete, Rock, Metal Journal of Engineering Mechanics 110:518-535 doi:doi:10.1061/(ASCE)0733-9399(1984)110:4(518)

Detournay E, Atkinson C (2000) Influence of pore pressure on the drilling response in low-permeability shear-dilatant rocks International Journal of Rock Mechanics and Mining Sciences 37:1091-1101 doi:http://dx.doi.org/10.1016/S1365-1609(00)00050-2

Detournay E, Defourny P (1992) A phenomenological model for the drilling action of drag bits International journal of rock mechanics and mining sciences & geomechanics abstracts 29:13-23 doi:- 10.1016/0148-9062(92)91041-3

Detournay E, Richard T, Shepherd M (2008) Drilling response of drag bits: Theory and experiment International Journal of Rock Mechanics and Mining Sciences 45:1347-1360 doi:10.1016/j.ijrmms.2008.01.010

Franca LFP (2010) Drilling Action of Roller-Cone Bits: Modeling and Experimental Validation Journal of Energy Resources Technology 132:043101 doi:10.1115/1.4003168

Franca LFP, Mostofi M, Richard T (2015) Interface laws for impregnated diamond tools for a given state of wear International Journal of Rock Mechanics and Mining Sciences 73:184-193 doi:http://dx.doi.org/10.1016/j.ijrmms.2014.09.010

Hoseinie SH, Aghababaei H, Pourrahimian Y (2008) Development of a new classification system for assessing of rock mass drillability index (RDi) International Journal of Rock Mechanics and Mining Sciences 45:1-10 doi:10.1016/j.ijrmms.2007.04.001

Hoseinie SH, Ataei M, Osanloo M (2009) A new classification system for evaluating rock penetrability International Journal of Rock Mechanics and Mining Sciences 46:1329-1340 doi:10.1016/j.ijrmms.2009.07.002

Kahraman s (2003) Performance analysis of drilling machines using rock modulus ratio The Journal of The South African Institute of Mining and Metallurgy 108:515-522

Lin J-S, Zhou Y (2013) Can scratch tests give fracture toughness? Engineering Fracture Mechanics 109:161-168 doi:10.1016/j.engfracmech.2013.06.002

Lin J-S, Zhou Y (2015) Rebuttal: Shallow wide groove scratch tests do not give fracture toughness Engineering Fracture Mechanics 133:211-222 doi:http://dx.doi.org/10.1016/j.engfracmech.2014.10.030

Martin C, Chandler N The progressive fracture of Lac du Bonnet granite. In: International Journal of Rock Mechanics and Mining Sciences & Geomechanics Abstracts, 1994. vol 6. Elsevier, pp 643-659

Richard T, Coudyzer C, Desmentte S (2010) Influence of groove geometry and cutter inclination in rock cutting. Paper presented at the 44th US Rock Mechanics Symposium and 5th U.S.-Canada Rock Mechanics Symposium, Salt Lake City, UT, USA,

Richard T, Dagrain F, Poyol E, Detournay E (2012) Rock strength determination from scratch tests Engineering Geology 147-148:91-100 doi:10.1016/j.enggeo.2012.07.011

Taheri A, Qao Q, Chanda E (2016) Drilling Penetration Rate Estimation using Rock Drillability Characterization Index Journal of The Institution of Engineers (India): Series D:1-12 doi:10.1007/s40033-015-0104-6

Taheri A, Tani K (2008) Use of down-hole triaxial apparatus to estimate the mechanical properties of heterogeneous mudstone International Journal of Rock Mechanics and Mining Sciences 45:1390-1402 doi:http://dx.doi.org/10.1016/j.ijrmms.2008.01.017

Teale R (1965) The concept of specific energy in rock drilling Int J Rock Mech Mining Sc 2:57-73

Yarali O, Soyer E (2011) The effect of mechanical rock properties and brittleness on drillability Scientific Research and Essays 6:1077-1078

Zhou Y, Lin J-S (2013) On the critical failure mode transition depth for rock cutting International Journal of Rock Mechanics and Mining Sciences 62:131-137 doi:http://dx.doi.org/10.1016/j.ijrmms.2013.05.004

LIST OF FIGURES

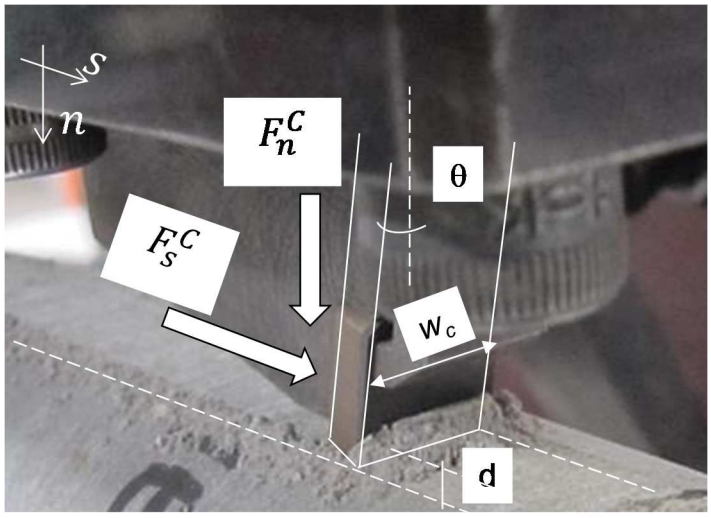

Figure 3.1 PDC cutting test at shallow depth of cut

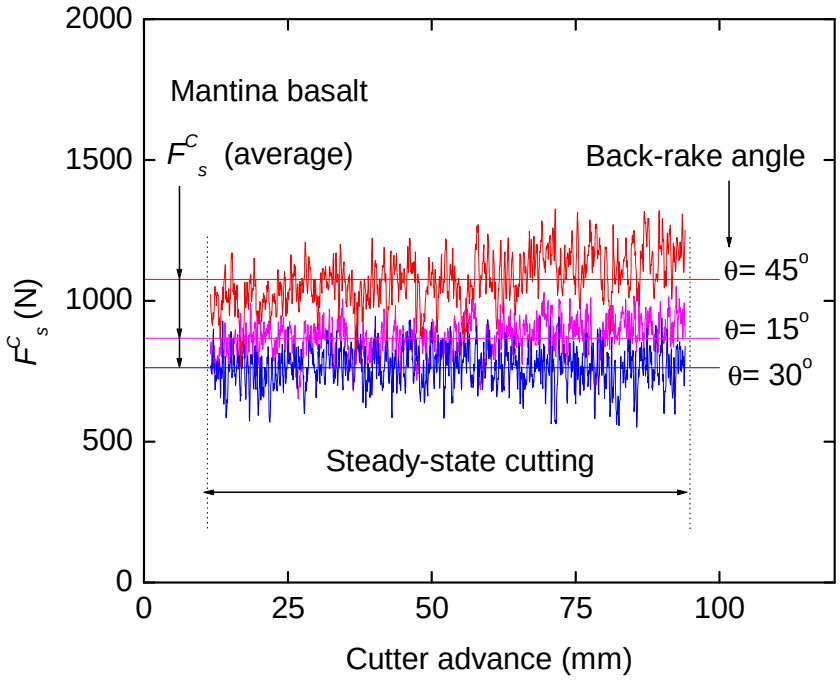

Figure 3.2 Cutting force, F_s^C, versus cutting advancement along the rock surface for Mantina basalt at a prescribed depth of cut of 0.2 mm

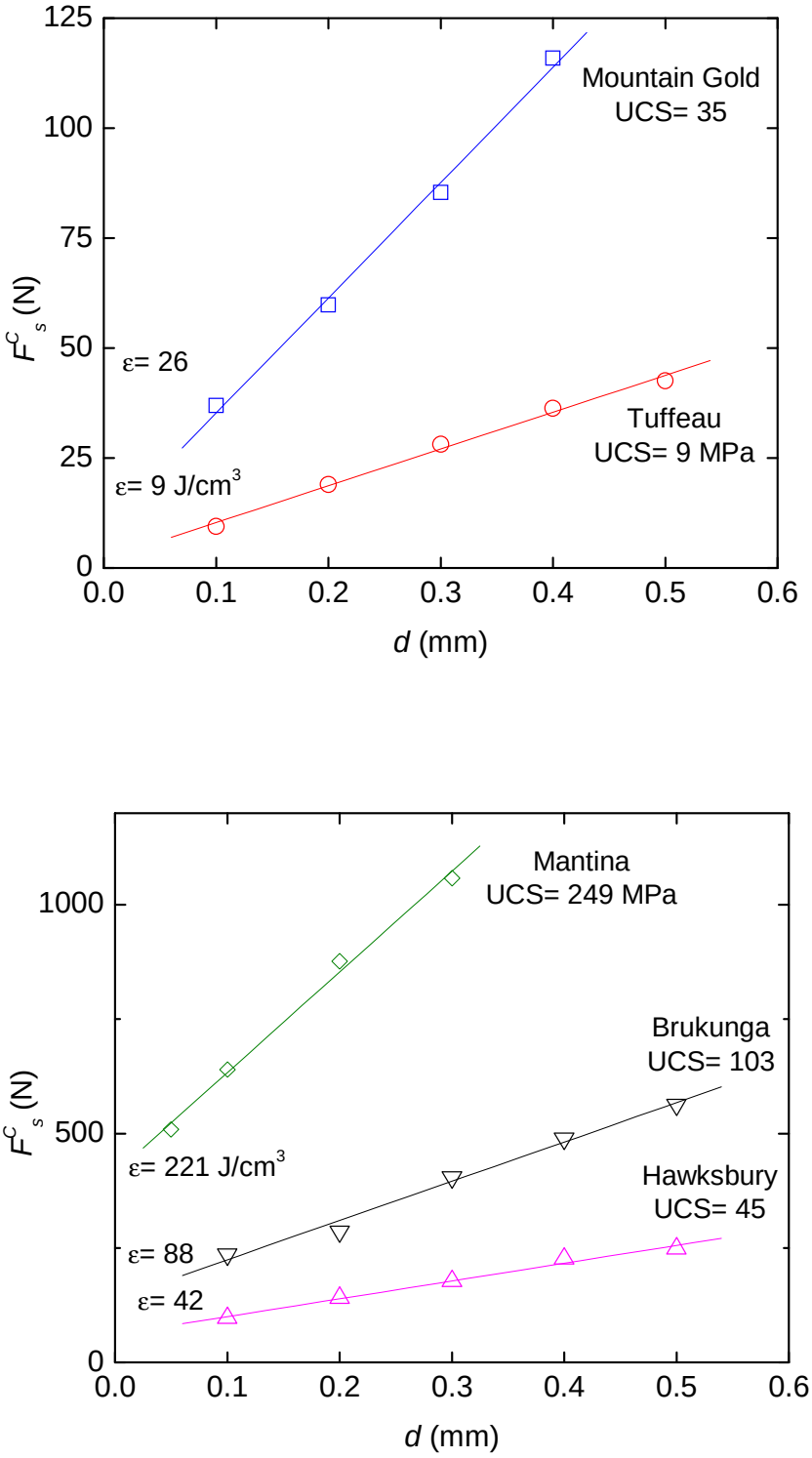

Figure 3.3 a) Cutting force, F_s^C, versus depth of cut, d, for the rocks investigated and respective intrinsic specific energy values

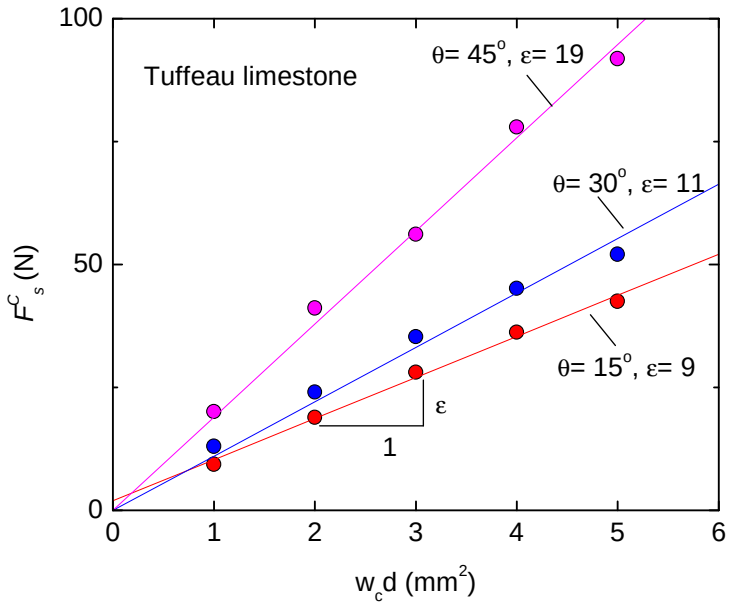
Tuffeau limestone
θ= 45°, ε= 19
θ= 30°, ε= 11
θ= 15°, ε= 9
ε
1
F_s^c (N)
$w_c d$ (mm^2)
0
50
100
0
1
2
3
4
5
6

a)

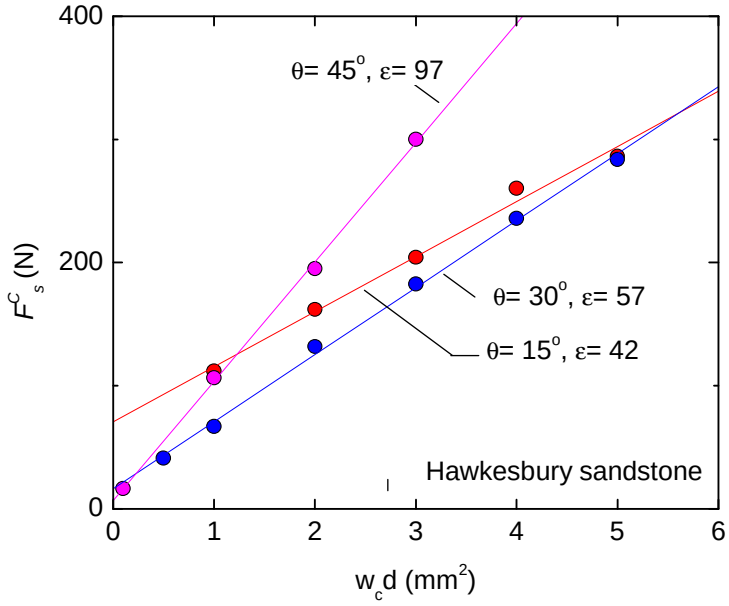
θ= 45°, ε= 97
θ= 30°, ε= 57
θ= 15°, ε= 42
Hawkesbury sandstone
F_s^c (N)
$w_c d$ (mm^2)
0
200
400
0
1
2
3
4
5
6

b)

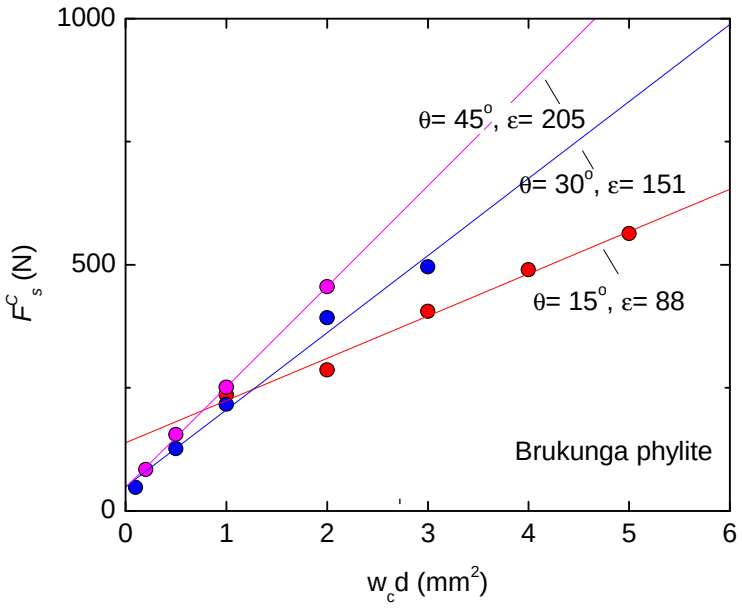

c)

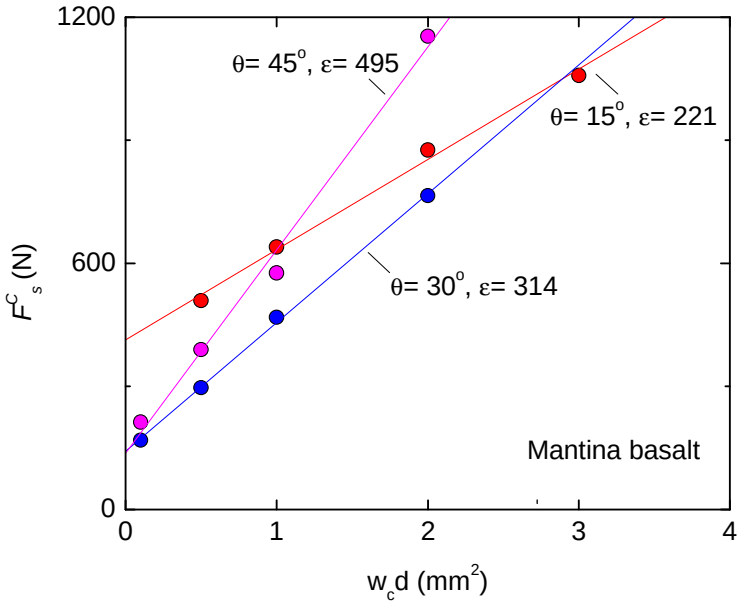

d)

Figure 3.4 Cutting force, F_s^C, versus constant cross-section area $w_c d$ for different back-rake angles for the rocks investigated

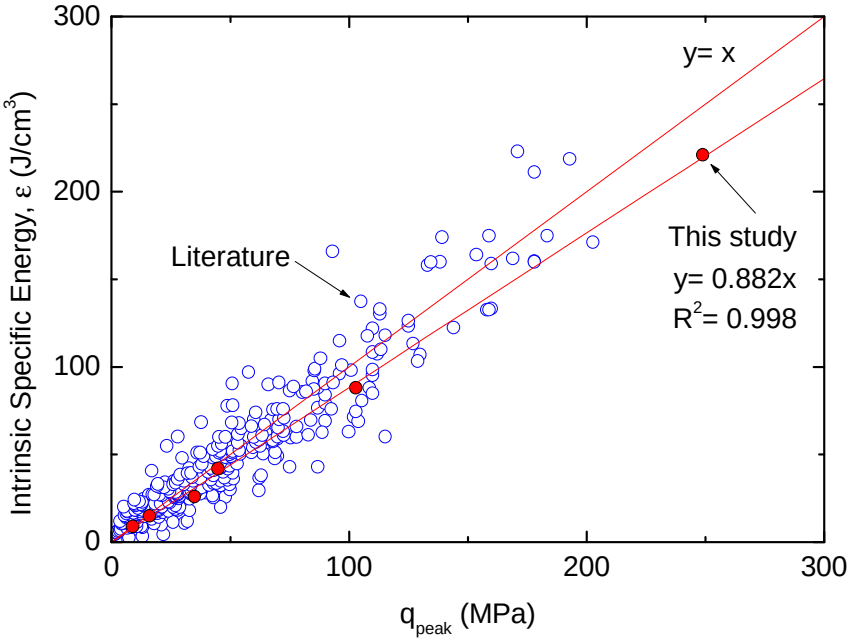

Figure 3.5 Intrinsic specific energy for a back-rake angle of 15 degrees versus unconfined compressive strength

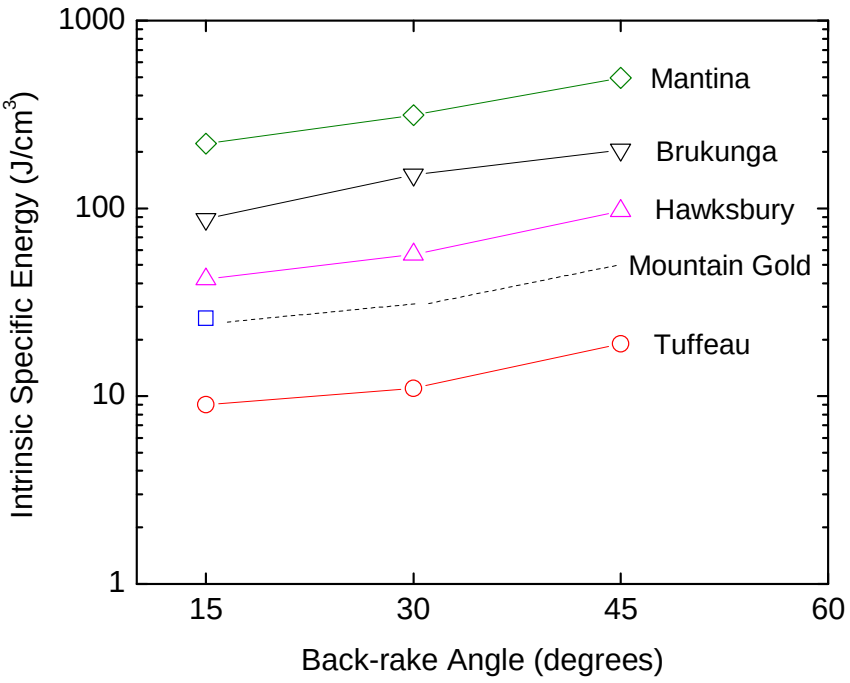

Figure 3.6 Intrinsic specific energy relation with the back-rake angle for the rocks investigated

LIST OF TABLES

Table 3.1 Experimental program

Test type	Rock name	Rock type	Rock source	Number of tests	Total tests
PDC Cutting	Tuffeau	Limestone	France	15	45
	Mountain Gold	Sandstone	Australia	15	
	Hawksbury	Sandstone	Australia	15	
	Brukunga	Phyllite	Australia	15	
	Mantina	Basalt	Australia	15	
Compressive loading	All above	All above	France, Australia	3, 4 or 5 per rock	26

Table 3.2 List of rock types investigated and their physical and mechanical properties

Rock name	Rock type	Number of UCS tests	Grain size	Dry density (g/cm^3)	Young's modulus (GPa)	UCS (MPa)
Tuffeau	Limestone	4	Fine	1.53	3.4	9
Mountain Gold	Sandstone	4	Fine	2.11	7.4	35
Hawksbury	Sandstone	5	Fine	2.26	14.4	45
Brukunga	Phyllite	5	Fine	2.81	39.1	103
Mantina	Basalt	5	Fine	2.73	52.7	249

Table 3.3 List of rock types investigated and their Intrinsic Specific Energy

Rock name	Rock type	Intrinsic specific energy (ε) (J/cm^3)		
		PDC cutter		
		θ = 15 degrees	θ= 30 degrees	θ= 45 degrees
Tuffeau	Limestone	9	11	19
Mountain Gold	Sandstone	26	-	-
Hawksbury	Sandstone	42	57	97
Brukunga	Phyllite	88	151	205
Mantina	Basalt	221	314	495

STATEMENT OF AUTHORSHIP

Statement of Authorship

Title of Paper	Rock Drilling Performance Evaluation by an Energy Dissipation Based Rock Brittleness Index
Publication Status	☒ Published ☐ Accepted for Publication ☐ Submitted for Publication ☐ Unpublished and Unsubmitted w ork w ritten in manuscript style
Publication Details	Munoz, H., Taheri, A., Chanda, E. (2016) Rock Drilling Performance Evaluation by an Energy Dissipation Based Rock Brittleness Index. Rock Mechanics and Rock Engineering DOI: 10.1007/s00603-016-0986-0

Principal Author

Name of Principal Author (Candidate)	Henry Munoz
Contribution to the Paper	Overall paper preparation
Overall percentage (%)	85
Certification:	This paper reports on original research I conducted during the period of my Higher Degree by Research candidature and is not subject to any obligations or contractual agreements with a third party that would constrain its inclusion in this thesis. I am the primary author of this paper.
Signature	Date 28/06/16

Co-Author Contributions

By signing the Statement of Authorship, each author certifies that:

i. the candidate's stated contribution to the publication is accurate (as detailed above);

ii. permission is granted for the candidate in include the publication in the thesis; and

iii. the sum of all co-author contributions is equal to 100% less the candidate's stated contribution.

Name of Co-Author	Abbas Taheri
Contribution to the Paper	Paper review
Signature	Date 28/06/16

Name of Co-Author	Emmanuel Chanda
Contribution to the Paper	Paper review
Signature	Date 5/7/2016

Please cut and paste additional co-author panels here as required.

ROCK DRILLING PERFORMANCE EVALUATION BY AN ENERGY DISSIPATION BASED ROCK BRITTLENESS INDEX

H. Munoz[1], A. Taheri[2], E. K. Chanda[3]

[1]Deep Exploration Technologies Cooperative Research Centre DET CRC, Export Park, Adelaide Airport, SA 5950, Australia, and School of Civil, Environmental & Mining Engineering, The University of Adelaide, SA 5005, Australia, Ph: 61 8 8313 0591, Fax: 61 8 8313 4359, Email: henry.munozprincipe@adelaide.edu.au (corresponding author)

[2]Senior Lecturer, School of Civil, Environmental & Mining Engineering, The University of Adelaide, SA 5005, Australia, Ph: 61 8 8313 0906, Fax: 61 8 8313 4359, Email: abbas.taheri@adelaide.edu.au

[3]Associate Professor, School of Civil & Environmental & Mining Engineering, The University of Adelaide, SA 5005, Australia, Ph: 61 8 8313 7410, Fax: 61 8 8303 4359, Email: emmanuel.chanda@adelaide.edu.au

ABSTRACT

In order to reliably estimate drilling performance both tool-rock interaction laws along with a proper rock brittleness index are required to be implemented. In this study the performance of a single PDC (Polycrystalline Diamond Compact) cutter cutting and different drilling methods including PDC rotary drilling, roller-cone rotary drilling and percussive drilling were investigated. To investigate drilling performance by rock strength properties, laboratory PDC cutting tests were performed on different rocks to obtain cutting parameters. In addition, results of laboratory and field drilling on different rocks found elsewhere in literature were used. Laboratory and field cutting and drilling

test results were coupled with values of a new rock brittleness index proposed herein and developed based on energy dissipation withdrawn from the complete stress-strain curve in uniaxial compression. To quantify cutting and drilling performance, the intrinsic specific energy in rotary-cutting action, i.e. the energy consumed in pure cutting action, and drilling penetration rate values in percussive action were used. The results show that the new energy-based brittleness index successfully describes the performance of different cutting and drilling methods and therefore is relevant to assess drilling performance for engineering applications.

KEYWORDS

Brittleness index, uniaxial compression, energy dissipation, cutting performance, drilling performance

INTRODUCTION

Rock drilling is an essential task in mining engineering and deep exploration industry. In this sense, drilling performance is one of the most important parameters to take into account when evaluating project feasibility and economy. Equipment type and specifications is strongly dependent on predicting the performance of the cutting tool in the field. In this sense, several attempts have been made to assess drilling performance by correlating different rock mechanical and physical properties with the drilling penetration rate. For instance, unconfined compressive strength (UCS) has been determined as the dominant rock property in penetration rate prediction for rotary drills (Kahraman 1999) and among rock properties, uniaxial compressive strength, Brazilian tensile strength, point load strength and Schmidt hammer value have been determined as the dominant rock properties affecting the penetration rate of percussive drills (Kahraman et al. 2003). In this same manner, force-indentation curves of indentation tests have been deemed relevant develop a drillability index for the prediction of penetration rates of rotary blast-hole drills and rock formations mechanical and physical properties (Kahraman et al. 2000). Furthermore, rock texture, grain size, density, P-wave velocity, unconfined

compressive strength, Mohs hardness and rock mass structural parameters have been used to build a number of drillability indices (Altindag 2003; Altindag 2009; Hoseinie et al. 2008; Taheri et al. 2016).

A generalised method to relate drilling performance with rock strength characteristics has not been developed yet. This is due to the complexity of interactions among the variables involved in the drilling process encompassing not only rock properties, but also the nature of drilling. Therefore, not only rock properties, but also different sets of drilling forces acting on rock as well as drilling method all have impacts on the drilling performance (Detournay and Defourny 1992; Detournay et al. 2008; Franca 2010; Franca 2011; Franca et al. 2015; Hustrulid and Fairhurst 1971b; Teale 1965). In this view, by coupling relevant drilling parameters with relevant rock properties, a reliable drilling performance prediction method can be developed.

On one hand, to predict rock drilling performance and optimisation of drilling operation, tool-rock interaction laws, i.e. the relations between forces acting on the tool in contact with rock, are essential (Detournay and Defourny 1992; Detournay et al. 2008; Franca 2010; Franca 2011; Franca et al. 2015; Hustrulid and Fairhurst 1971a; Hustrulid and Fairhurst 1972a; Hustrulid and Fairhurst 1971b; Hustrulid and Fairhurst 1972b). For instance, through tool-rock interaction laws, it was found that during rotary drilling, the Specific Energy (SE), the work done to excavate a unit volume of rock (Teale 1965), accounts for both energy consumed in rock cutting and energy consumed in friction between the tool and the rock (Detournay and Defourny 1992; Teale 1965). In this instance, the energy consumed in pure cutting action of rock is measured by the intrinsic specific energy (ε) attainable at the cutting point (Detournay and Defourny 1992; Detournay et al. 2008; Franca 2010; Franca et al. 2015). The intrinsic specific energy quantifies the maximum cutting efficiency associated with the optimum cutting force and its magnitude depends on the nature of the rock (Detournay and Defourny 1992; Teale 1965), the surrounding pressure on the rock (Detournay and Atkinson 2000) and the drilling technique being used (Detournay et al. 2008; Franca 2010; Franca et al. 2015). In the case of

percussive drilling, tool-rock interactions are focused mostly in the prediction of the penetration rate and the optimum thrust. Experimental results with wedge-shaped cutter percussive bits show that tool-rock interaction can be simulated by linear relationships in an idealised force–penetration curve for percussive action and percussive penetration rate (Franca 2011; Hustrulid and Fairhurst 1971a; Hustrulid and Fairhurst 1972a; Hustrulid and Fairhurst 1971b; Hustrulid and Fairhurst 1972b).

On the other hand, rock brittleness is a concept yet to be investigated as there is not a unique criterion able to describe rock brittleness quantitatively nor consensus about the most suitable and reliable brittleness index to apply to different rock engineering works encountered in the field. For instance, previously a number of different criteria to assess rock brittleness have been developed upon pre-peak stress-strain characteristics in uniaxial compression experiments including ratios between elastic to plastic strain (Hucka and Das 1974) as well as strain-energy relations (Hucka and Das 1974; Kidybiński 1981). However, those criteria are insufficient in order to describe unambiguously a scale of brittleness to ductility of rock (Munoz et al. 2016; Tarasov and Potvin 2013; Tarasov and Randolph 2011). In the same manner, some brittleness indices which are defined upon rock compressive strength, UCS, and tensile strength, TS, (Altindag 2002; Hucka and Das 1974; Kahraman 2002), cannot describe a scale of brittleness to ductility of rock (Tarasov and Potvin 2013). This is mainly because, rock failure behaviour cannot be described by a ratio between compressive and tensile strength and, generally, compressive and tensile strength can be obtained from each other. In addition, those brittleness indices cannot correlate well with the rock compressive strength. Figure 4.1 shows uniaxial compressive-to-tensile-strength brittleness indices defined as B_1 (Altindag 2002), B_2 (Hucka and Das 1974) and B_3 (Altindag 2002), see expressions below, plotted against the respective rock uniaxial compressive strength values. In this figure, data found in the literature elsewhere (Howarth 1987; Paone et al. 1969; Schmidt 1972; Selim and Bruce 1970) is plotted.

$$B_1 = \frac{UCS}{TS} \quad (1)$$

$$B_2 = \frac{UCS-TS}{UCS+TS} \quad (2)$$

$$B_3 = \frac{UCSxTS}{2} \text{ [MPaxMPa]} \quad (3)$$

As it may be seen in Figure 4.1, in general, brittleness indices, B_1 and B_2 are not able to describe a scale of brittleness with rock compressive strength increasing, i.e. a soft rock may have the same brittleness B_1 and B_2 as a hard rock. Thus, if B_1 and B_2 are used to assess drilling performance of either rotary or percussive drilling, it can be expected to obtained no sound relationships between B_1 and B_2 and drilling parameters for instance the drilling penetration rate, as demonstrated in previous studies (Altindag 2009; Altindag 2010). Although B_3 shows a better correlation with the drilling penetration rate (Altindag 2009; Altindag 2010), the foundation of brittleness B_3 gives conflicting results to describe rock brittle to ductile scale (Tarasov and Potvin 2013).

The discussion presented above, demonstrated that in order to predict drilling performance successfully, firstly tool-rock interaction laws should be implemented to quantify drilling. In this respect, it was found that there are very few studies that consider tool-rock interaction to characterise drilling performance. Secondly, a proper brittleness index is required to describe rock failure characteristics in drilling. As a result, the present study aims at evaluating drilling performance by taking into account both the drilling response from tool-rock interaction laws and by defining a new energy-based rock brittleness index that considers rock failure behaviour which is able to describe an ambiguous brittleness scale from ductile to brittle.

In this study, the performance of two major mechanical drilling methods, namely rotary drilling and percussive drilling, are investigated against rock brittleness capacity by the new energy-based brittleness index. The intrinsic specific energy and rate of penetration, as two main drilling performance

parameters, were coupled with rock brittleness. To validate this proposal, cutting experiments with a single PDC cutter were carried out on different rock types. In addition, independent rotary drilling as well as percussive drilling results from laboratory and field tests from the literature were used.

NEW ENERGY-BASED BRITTLENESS INDEX

A recently developed brittleness index by Munoz et al. (Munoz et al. 2016) upon fracture strain-energy quantities withdrawn from the area under complete stress-strain curve of rocks in uniaxial compressive tests is proposed herein to study drilling performance by rock brittleness capacity. This brittleness index takes into account post-peak instability in uniaxial compression as post-peak instability of rock during compression can be treated as a manifestation of rock brittleness (Tarasov and Randolph 2011). That is, an increase in the post-peak energy indicates an increase of stability (i.e. a decrease in brittleness). In the same manner, a dramatic decrease of post-peak energy indicates less stability of the failure process (i.e. an increase in brittleness). Pre-peak and post-peak energy relations are the basis of the proposed brittleness index. Pre-peak energy is considered to dissipate due to micro cracking during the loading process up to the peak (Daniel C. Jansen and Edwin 1995; Jansen and Shah 1997). On the other hand, energy dissipated in post-peak regime represents that energy dissipated during coalescence of micro fractures initiated before peak stress and energy dissipated in the localised zone (i.e. the damaged zone), which encompasses deformations associated with the formation and coalescence of distributed longitudinal cracks and deformations at the localised zone (Bažant 1989; Jansen and Shah 1997; Markeset and Hillerborg 1995). In this framework, the total fracture energy (U_{total}) comprises of pre-peak energy (U_{pre}) and post-peak energy (U_{pre}) and it is expressed by the following expression:

$$U_{total} = U_{pre} + U_{post} \tag{4}$$

Pre-peak energy per unit volume of rock is estimated to be the area under the stress-strain curve enclosed by loading the specimen up to the peak stress

and then unloading it completely. The unloading path was assumed to be linear having a slope equal to E_{LVDT} (i.e. the tangent Young's modulus measured by external LVDTs) as shown in Figure 4.2a. On the other hand, post-peak energy was calculated taking into account the area under the post-peak stress-inelastic strain. That is, the area under the unloaded pre-peak stress-strain curve (assuming that unloading curve's Young's modulus, E_{un}, is equal to loading curve's Young's modulus, E_{LVDT}) and under the post-peak stress-inelastic strain as shown in Figure 4.2a. Herein, the post-peak fracture energy was defined until a post-peak stress level equal to about one third of the peak stress, i.e. $0.33q_{peak}$, a stress level where the stress-strain curve is terminated by drawing a linear unloading following a slope equal to E_{LVDT} (Daniel C. Jansen and Edwin 1995; Jansen and Shah 1997). In addition, an elastic energy (U_e) at the peak stress was calculated by the following equation (see Figure 4.2b for the notation of U_e).

$$U_e = \frac{UCS^2}{2E_{LVDT}} \tag{5}$$

Different rock types, sourced from different quarries in France, Australia and Iran, including five limestones, a sandstone and two granites, which are presented in Table 4.1 (UCS is ranging between 7 to 215 MPa), were tested in order to obtain the energies quantities involved during compression in a series of uniaxial compressive tests under quasi-static monotonic loading conditions. The compressive tests complied with the application of a prescribed constant lateral strain-rate of $2\text{x}10^{-6}$/s as a feedback signal to control the axial load which was found to be a suitable loading rate to measure the complete stress-strain response for the rocks presented in Table 4.1 as shown in Figure 4.2c. Figure 4.2d shows the relationship of energies quantities U_{total} and U_e with the respective UCS of the studied rocks. This figure shows that U_e clearly increases in a linear fashion with an increase in UCS. The total energy U_{total}, however, increases first and then decreased as UCS increases. This trend complies with low energy enclosed in the stress-strain curve of rocks with higher strength that behave following class I-II or class II behaviour as shown in Figure 4.2c. To

quantify failure characteristics of different rocks, the following energy-based brittleness index is proposed;

$$B_{U-I} = \frac{U_e}{U_{total}} \quad (6)$$

As can be seen in Figure 4.3, unlike a number of brittleness indices including B_1, B_2 and B_3 proposed in previous studies (Altindag 2009; Altindag 2010), the proposed brittleness index B_{U-I} is able to describe properly a monotonic and unambiguous scale of brittleness and brittleness relations with increasing rock strength (i.e. UCS). Furthermore, brittleness index B_{U-I} describes a monotonic and unambiguous scale of brittleness with increasing pre-peak strength parameters such as crack damage strength and tangent Young's modulus of rock. This outcome becomes relevant in order to better understand material brittleness associated with the progressive fracture process characterised by the typical threshold damage stresses and the elasticity parameters. The brittleness index B_{U-I} scale indicates that a higher brittleness index means that rock is more brittle which corresponds to higher strength rocks. From Figure 4.3 a non-linear relationship having a coefficient of correlation, R^2, of 0.955 between the brittleness index B_{U-I} and UCS can be established by the following expression:

$$B_{U-I} = 0.563e^{0.0056UCS} \quad (7)$$

The expression above is used to calculate brittleness index of different rocks investigated in this study from their UCS values.

PDC CUTTING PERFORMANCE

CUTTING EXPERIMENTS CONDUCTED IN THE PRESENT STUDY

Rock cutting induces either plastic yielding or fracture mode of failure in the rock depending on the depth of cut, d, (Lin and Zhou 2013; Lin and Zhou 2015; Richard et al. 2012). This is, at relatively shallow depths of cut, plastic yield mode of failure is dominant and material failure is governed by yield strength (i.e. strength-related failure mechanism). On the other hand, when the

depth of cut is relatively deep, fracture mode of failure dominates and therefore material failure is governed by its fracture properties (i.e. fracture-related failure mechanism). In these instances, unconfined compressive strength, UCS, and fracture toughness, K, become relevant to characterise plastic yield and fracture mode of failure in cutting, respectively. Lin and Zhou (Lin and Zhou 2013; Lin and Zhou 2015) demonstrated that rock cutting is well described by Bazant's size effect law (SEL) for quasi-brittle materials, such as concrete and rocks (Bažant 1984). SEL is expressed as a function of the nominal stress $\sigma_N = (F_s^C)_{peak}/w_c d$ and the depth of cut, d , where $(F_s^C)_{peak}$ is the peak cutting force and w_c is the cutter width, see Figure 4.4 for the geometry and nomenclature of the cutting test.

In this view, a series of cutting experiments using a single PDC (Polycrystalline Diamond Compact) cutter under steady cutting conditions were carried out at depths of cut smaller than 0.5 mm in compliance with plastic yield mode of failure. In doing so, as shown in Table 2.2, different rock types (UCS is ranging from 9 to 249 MPa) including a limestone (i.e. Tuffeau), three sandstones (i.e. Castlegate, Mountain Gold and Hawkesbury), a phyllite (i.e. Brukunga) and a basalt (i.e. Mantina), which were sourced from several mines and quarries in France and Australia, were used.

The cutting tests were performed at the Australian Resource Research Centre (ARRC), CSIRO-Perth facilities. The cutting tests were conducted following a standard practice suggested in a previous research (Richard et al. 2012). The cutting device used in the experiment (manufactured by Epslog SA) is equipped with a load sensor which measures the tangential (F_s^C) and normal (F_n^C) components of the cutting force acting on the cutter (see Figure 4.4). The cutting machine is controlled by a computer program and the data is stored into a computer by a data acquisition system.

A consistent cut was applied to the surface of the rock samples by means of a rectangular cutter (i.e. a sharp cutter) of width w_c equal to 10 mm. In the tests, the cutter ran along a length of 10 cm under a prescribed constant velocity

of 4 mm/s and at a constant depth of cut, d. The rocks were cut at a back-rake angle θ of 15 degrees in all the tests. The depth of cut, d, in the tests varied from 0.1 to 0.5 mm with steps of constant increments of 0.1 mm, in general. The surface of the rocks was carefully prepared by preliminary cuts to achieve an even and smooth surface prior to setting the prescribed depth of cut and start the cutting test. By doing so, it was assured the formation of a groove having constant cross-section area (i.e. a constant $w_c d$) at constant d in each test. Each cutting run was performed strictly over a fresh surface on the rock. Furthermore, the formation of a deep U-type groove due to successive cuts over a same spot was not allowed, so the effect of sidewall friction (cutter-groove), that may cause an additional increase in the intrinsic specific energy spent in cutting the rock (ε) was eliminated (Richard et al. 2010).

INTRINSIC SPECIFIC ENERGY FROM PDC CUTTING

The intrinsic specific energy, ε, from PDC cutting can be obtained using the following expression (Richard et al. 2012):

$$\varepsilon = F_s^C / w_c d \tag{8}$$

Where, F_s^C represents the average force on steady cutting conditions, d, is the depth of the cut and w_c, represents the cutter width (w_c of 10 mm).

The cutting response of the PDC cutter on the intact rocks presented in Table 4.2 was characterised by a linear scaling regime between F_s^C and d, as shown in Figure 4.5a. The plot between F_s^C and d shows non-zero intercepts in all the tests. This behaviour may be associated to the presence of friction caused by cutter wear (Zhou and Lin 2013). Table 4.2 summaries the values of intrinsic specific energy (ε) which were obtained from the slope of the linear fitting in the $F_s^C - w_c d$ plot. The values of ε varied from 9 to 220 J/cm^3 for the rocks in Table 4.2 and they are in good agreement with the magnitude of the UCS of their respective rocks. This result is supporting previous findings by other researchers (Richard et al. 2010; Richard et al. 2012) where the intrinsic specific energy increases with an increase in compressive strength. Rock failure governed by

plastic yield mode (i.e. strength-related failure mechanism) is demonstrated in Figure 4.5b through Bazant's size effect law (SEL) where cutting data at relatively shallow depths of cut, in this case smaller than 0.5 mm, falls into plastic yielding region.

INTRINSIC SPECIFIC ENERGY AND BRITTLENESS INDEX

Figure 4.6 shows the relationship between the intrinsic specific energy (ε) from the cutting tests and the brittleness index B_{U-I}. The values of B_{U-I} were calculated for the rocks from their respective UCS values as summarised in Table 4.2 (see the values of UCS and B_{U-I} in Table 4.2). From this figure, a strong correlation between the intrinsic specific energy and the proposed energy-based brittleness index was found. That is, a correlation coefficient R^2 of 0.999 was yielded by a logarithmic fitting in the form of $\varepsilon = 158LN(B_{I-U}) + 90$.

In Figure 4.6, the intrinsic specific energy, which increases with an increase in compressive strength, obviously shows an increasing trend in a non-linear fashion with increasing B_{U-I} as high strength rocks show a higher brittleness capacity by higher B_{U-I} values.

ROTARY DRILLING PERFORMANCE

DRILLING EXPERIMENTS FROM LITERATURE

Independent drilling data found elsewhere in the literature was used to study the relationship between the intrinsic specific energy in drilling with the proposed brittleness index B_{U-I}. In doing so, small-diameter PDC rotary drilling tests at atmospheric pressure (Stavropoulou 2006) on three marble rocks (i.e. Gioia, Cervaiole and Dionysios) were re-examined to calculate the values of intrinsic specific energy and brittleness index, B_{U-I}. Table 4.3 lists these rocks and their respective strength parameters. In this case, the small-diameter drilling experiments were conducted using a PDC bit with a diameter of 5 mm with a clearance angle 10 degrees. The back-rake angle θ in the tests was equal to 30 degrees.

In addition, rotary drilling experiments at atmospheric pressure with roller-cone bits (Franca 2010) on two limestones (i.e. Tuffeau and Savonniere) and two sandstones (i.e. Castlegate and Mountain Gold) were re-examined to withdraw the values of intrinsic specific energy from the drilling performance and brittleness index B_{U-I} from rock compressive strength, respectively. Table 4.4 lists these rocks and their respective strength parameters. In this table, the tensile strength (TS) values for Tuffeau, Savonniere, Castlegate and Mountain Gold were obtained after conducting a series of Brazil tests (Suggested methods for determining tensile strength of rock materials 1978) as part of the present study. The drilling experiments in this case were conducted with an in-house designed drilling rig having a bit assembly consisting of a roller-cone bit (i.e. an insert bit IADC 531 of 2 1/2 and non-insert bit IADC 321 of 2 15/16), a shaft, and a sophisticated anvil.

Finally, additional rotary drilling experiments of roller-cone bits conducted on a sandstone (i.e. Kimachi), an andesite (i.e. Shinkomatsu), and a granite (i.e. Sori (A)) reported by Karasawa et al. (Karasawa et al. 2002a; Karasawa et al. 2002b) presented in Table 4.4 were also re-examined. In this case, all the drilling tests were performed at atmospheric pressure using milled-tooth bits (i.e. IADC 221S of 98.4 mm) and insert-tooth bits (i.e. IADC 537X of 101.6 mm). Franca (Franca 2010) reports the details and analysis of the experimental data obtained by Karasawa et al. (Karasawa et al. 2002a; Karasawa et al. 2002b) on the drilling response to obtain the respective intrinsic specific energy.

INTRINSIC SPECIFIC ENERGY FROM ROTARY DRILLING

The cutting response of PDC (Polycrystalline Diamond Compact) bits, used in a rotary drilling, derives from a combination of two major actions (Detournay and Defourny 1992): i) a pure cutting action and ii) a frictional action due to the cutter wear-flat area. The energy consumed in a pure cutting action of rock is measured by the intrinsic specific energy (ε) attainable at the cutting point (Detournay and Defourny 1992; Detournay et al. 2008; Franca 2010; Franca et al. 2015). In this instance, drilling efficiency is increased when the energy

consumed by the frictional forces are minimised at the optimum weight and torque on the bit to produce the optimum depth of cut. Quantities of consumed energy higher than the intrinsic specific energy represent the energy consumed by frictional processes.

The drilling response of PDC drag bits is characterised by a linear relation between weight, torque on the bit and depth of cut per revolution (Detournay and Defourny 1992; Detournay et al. 2008). Then, the PDC bit response in terms of the Specific Energy is given by the following expression:

$$SE = \frac{t}{d} = \varepsilon(1 - \mu tan(\theta + \psi)) + \mu\frac{w}{d} \quad (9)$$

Where SE is the specific energy, t and w are the normalised weight and torque on the bit, respectively, d is the depth of cut per revolution, μ is the coefficient of friction in the wear flat area of a blunt cutter of the bit, and ε is the intrinsic specific energy. Following this approach, the values of intrinsic specific energy for the marble rocks undergoing the small-diameter rotary drilling action in Table 4.3 were calculated. From Table 4.3, it can be seen that the values of intrinsic specific energy ε varied from 88 to 125 MPa and are in reasonable agreement with the respective values of UCS of the rocks. This result is supporting previous findings by others (Detournay and Defourny 1992; Detournay et al. 2008) showing that the magnitude of intrinsic specific energy is very similar to the UCS.

The drilling action of roller-cone bits can be considered as a combination of two distinct processes: indentation and cutting actions (Franca 2010). In the case of rotary drilling with roller-cone bits, bit-rock interaction laws are based on the approach initially developed for PDC drag bits as explained above. In this framework, energy dissipation at the bit-rock interaction can be considered as a combination of three independent processes: pure cutting action, pure indentation action, and frictional contact along the wear flat rock interface (Franca 2010), then the drilling response in this cases is given in terms of the Specific Energy presented as follows:

$$SE = \frac{t}{d} = \varepsilon(1 - \mu\zeta) + \mu\frac{w}{d} \quad (10)$$

Where ζ is a number that characterises the ratio of the cutting-indentation strength to the intrinsic specific energy. Following this approach, Table 4.4 summarises the intrinsic specific energy values for the limestone and sandstone rocks undergoing roller-cone drilling action obtained by Franca (Franca 2010). In addition, this table includes the intrinsic specific energy values obtained from the experimental data reported by Karasawa et al. (Karasawa et al. 2002a; Karasawa et al. 2002b) on Kimachi sandstone, Shinkomatsu andesite, and Sori (A) granite analysed and reported by Franca (Franca 2010). These results are also included in Table 4.4. From Table 4.4, it can be seen that the values of intrinsic specific energy ε for these different rock types varied from 14 to 168 MPa and they have values very similar in magnitude to the UCS of their respective rocks.

INTRINSIC SPECIFIC ENERGY AND BRITTLENESS INDEX

Analysis on the correlations of the intrinsic specific energy and other brittleness indices previously proposed to study the drilling performance including B_1 , B_2 and B_3, extracted from the data set (i.e. from UCS and TS) presented in Table 4.3 and Table 4.4, indicates that there is not any notable correlations between the intrinsic specific energy from the drilling experiments with brittleness indices B_1, B_2 and B_3 as shown in Figure 4.7 Intrinsic specific energy and its relation with the brittleness index a) B_1, b) B_2 and c) B_3 from rotary drilling tests. In this view, it is examined in this section whether the new brittleness index B_{U-I} can be reasonably correlated with the drilling parameters obtained from rotary drilling.

Figure 4.8 Intrinsic specific energy from rotary drilling tests and its relation with the brittleness index B_{U-I} shows the relationship between the intrinsic specific energy from Table 4.3 and Table 4.4 and their respective brittleness index B_{U-I}. Here, B_{U-I} values were calculated from the UCS quantities of the respective rocks and they are presented in Table 4.3 and Table 4.4. Figure 4.8 shows that there exists a sound correlation between the intrinsic

specific energy from roller-cone rotary drilling and PDC small-diameter rotary drilling and the proposed energy-based brittleness index B_{U-I}. A logarithmic fitting in the form of $\varepsilon = 169LN(B_{I-U}) + 101$, with a coefficient of correlation R^2 of 0.982 were obtained which supports this statement. It is noteworthy that PDC single cutter cutting tests results also lie in a logarithmic fitting curve close to that obtained for the drilling tests results as shown in Figure 4.8.

Furthermore, similar to the results with PDC single cutter tests presented earlier, in Figure 4.8, the intrinsic specific energy, which increases with increasing compressive strength, obviously increases in a non-linear fashion with B_{U-I} as high strength rocks show a higher brittleness capacity by higher B_{U-I} values.

PERCUSSIVE DRILLING PERFORMANCE

DRILLING EXPERIMENTS FROM LITERATURE

In the case of percussive drilling, tool-rock interactions are mostly focused on the prediction of the penetration rate and selection of the optimum thrust (Franca 2011; Hustrulid and Fairhurst 1971a; Hustrulid and Fairhurst 1972a; Hustrulid and Fairhurst 1971b; Hustrulid and Fairhurst 1972b). To examine the application of the proposed brittleness index B_{U-I} in assessing the percussive drilling performance, independent data set from percussive drilling tests carried out in field conditions on a wide variety of rocks with a wide range of uniaxial compressive strength values ranging from 69 to 418 MPa, reported by Schmidt (Schmidt 1972), was used. Here, percussive drilling performance is given in terms of the rate of penetration. Table 4.5 shows the strength parameters of the rocks and their respective rate of penetration (PR) obtained under bit diameter of 66.68 mm (H-thread carbide bit), operating pressure of 690 kPa, piston weight of 2 kg and air-type flushing.

PENETRATION RATE AND BRITTLENESS INDEX

In this section, first brittleness indicesB_1 , B_2 and B_3, proposed in previous studies, and their relations with the penetration rate PR were examined.

These brittleness indices were extracted from the data set presented in Table 4.5 by Schmidt (Schmidt 1972). Results of similar analysis can be found in the literature elsewhere (Altindag 2009). The results of this analysis are presented in Figure 4.9. It can be seen in this figure that, B_1 and B_2 show no correlation with the penetration rate. In addition, B_3 does not show a correlation as good as B_{U-I} does with the penetration rate as it is demonstrated later in Figure 4.10.

Table 4.5 reports the values of the brittleness index B_{U-I} calculated from the respective values of UCS of the rocks. Figure 4.10a shows the plot penetration rate PR versus the brittleness index B_{U-I}. This figure shows that there is a reasonable correlation between the penetration rate PR and the proposed energy-based brittleness index B_{U-I}. This correlation is stronger than others presented in Figure 4.9. An exponential fitting in the form of $PR = 39.49\ B_{U-I}^{-0.59}$ which yielded a coefficient of correlation R^2 of 0.753. In Figure 4.10a, in general, the penetration capacity given by the penetration rate of the rocks decreases non-linearly with an increase in brittleness index B_{U-I} (i.e. with an increase in compressive strength of the rocks). This is mainly because penetration rate in stronger rocks drops and stronger rocks have higher B_{U-I} values.

In order to improve the correlation between penetration rate PR and B_{U-I} data, the penetration rate values were normalised with respect to the uniaxial compressive strength, i.e. by dividing the penetration rate by the respective UCS of rocks producing the normalised penetration rate PRN = PR/UCS. This normalisation has also been proposed and used in previous studies on the application of brittleness index to predict drilling performance (Altindag 2009; Altindag 2010).

The results of normalisation, in Figure 4.10b, show that the normalised penetration rate values PRN decreases non-linearly as the brittleness B_{U-I} increases and a correlation coefficient R^2 of 0.914 was yielded with an exponential fitting of $PRN = 0.35\ B_{U-I}^{-1.44}$. Brittleness indices B_1 , B_2 and B_3 and their relations with the penetration rate normalised PRN were also examined

(results are not shown here). In this respect, B_1 and B_2 were not able to produce any correlation and B_3 did not show a correlation as good as B_{U-I} did with the normalised penetration rate data.

CONCLUSIONS

In this study drilling performance is evaluated by rock brittleness capacity. In this respect, to reliably estimate drilling performance both tool-rock interaction laws along with a proper brittleness index should be implemented. Therefore, tool-rock interaction laws together with a new brittleness index able to picture both an ambiguous brittleness scale from ductile to brittle and brittleness scale with rock strength were implemented. This new brittleness index B_{U-I}, which is based on the relation of the energy dissipation quantities withdrawn from the complete stress-strain curve in uniaxial compression, was deemed to be relevant to this purpose.

The performance of PDC (Polycrystalline Diamond Compact) single-cutter cutting tests and different drilling methods including PDC rotary drilling, roller-cone rotary drilling and percussive drilling were investigated against rock brittleness capacity. PDC single-cutter cutting experiments were carried out on different rock types. In addition, independent rotary as well as percussive drilling results from laboratory and field tests, found in the literature, were used. To quantify cutting and drilling performance, the intrinsic specific energy, which is the energy consumed in pure cutting action, and drilling penetration rate values were implemented. The results show that the new energy-based brittleness index B_{U-I} successfully describes the performance of the studied cutting and drilling methods.

In addition, the performance of several brittleness indices which are proposed based on relations between compressive and tensile strength, i.e. B_1 , B_2 and B_3, were investigated and compared with the proposed brittleness index B_{U-I}. These brittleness indices, however, are not able to quantify rock failure behaviour and cannot correlate well with rock strength. As a result, no

correlation was found between brittleness B_1 and B_2 with either cutting or drilling performance parameters. Brittleness index B_3, showed some correlation with drilling performance parameters, however, in all drilling cases, B_3 showed weaker correlations with drilling performance parameters as compared to the correlations obtained by B_{U-I}. The brittleness index B_{U-I} proposed in the present study offered the strongest correlation with the drilling performance, either case cutting, rotary or percussive drilling. Therefore, the new energy-based brittleness index is deemed to be relevant to assess drilling performance by rock brittleness capacity.

ACKNOWLEDGEMENT

The work has been supported by the Deep Exploration Technologies Cooperative Research Centre whose activities are funded by the Australian Government's Cooperative Research Centre Programme. This is DET CRC Document 2016/169. Special thanks to Dr L Franca from (formerly) the Australian Resource Research Centre (ARRC), CSIRO Perth, for facilitating the cutting experiments, the fruitful discussions and providing some rock samples.

REFERENCES

Altindag R (2002) The evaluation of rock brittleness concept on rotary blast hole drills Journal-South African Institute of Mining and Metallurgy 102:61-66

Altindag R (2003) Correlation of specific energy with rock brittleness concepts on rock cutting Journal of the South African Institute of Mining and Metallurgy 103:163-171

Altindag R (2009) Assessment of some brittleness indexes in rock-drilling efficiency Rock Mechanics and Rock Engineering 43:361-370 doi:10.1007/s00603-009-0057-x

Altindag R (2010) Reply to the Discussion by Yagiz on “Assessment of Some Brittleness Indexes in Rock-Drilling Efficiency” by Altindag, Rock Mechanics and Rock Engineering, DOI: 10.1007/s00603-009-0057-x Rock mechanics and rock engineering 43:375-376

Bažant Z (1984) Size Effect in Blunt Fracture: Concrete, Rock, Metal Journal of Engineering Mechanics 110:518-535 doi:doi:10.1061/(ASCE)0733-9399(1984)110:4(518)

Bažant Z (1989) Identification of strain softening constitutive relation from uniaxial tests by series coupling model for localisation Cement and Concrete Research 19:973-997

Detournay E, Atkinson C (2000) Influence of pore pressure on the drilling response in low-permeability shear-dilatant rocks International Journal of Rock Mechanics and Mining Sciences 37:1091-1101 doi:http://dx.doi.org/10.1016/S1365-1609(00)00050-2

Detournay E, Defourny P (1992) A phenomenological model for the drilling action of drag bits International journal of rock mechanics and mining sciences & geomechanics abstracts 29:13-23 doi:- 10.1016/0148-9062(92)91041-3

Detournay E, Richard T, Shepherd M (2008) Drilling response of drag bits: Theory and experiment International Journal of Rock Mechanics and Mining Sciences 45:1347-1360 doi:10.1016/j.ijrmms.2008.01.010

Franca LFP (2010) Drilling Action of Roller-Cone Bits: Modeling and Experimental Validation Journal of Energy Resources Technology 132:043101 doi:10.1115/1.4003168

Franca LFP (2011) A bit–rock interaction model for rotary–percussive drilling International Journal of Rock Mechanics and Mining Sciences 48:827-835 doi:10.1016/j.ijrmms.2011.05.007

Franca LFP, Mostofi M, Richard T (2015) Interface laws for impregnated diamond tools for a given state of wear International Journal of Rock Mechanics and Mining Sciences 73:184-193 doi:http://dx.doi.org/10.1016/j.ijrmms.2014.09.010

Hoseinie SH, Aghababaei H, Pourrahimian Y (2008) Development of a new classification system for assessing of rock mass drillability index (RDi) International Journal of Rock Mechanics and Mining Sciences 45:1-10 doi:10.1016/j.ijrmms.2007.04.001

Howarth D The effect of pre-existing microcavities on mechanical rock performance in sedimentary and crystalline rocks. In: International Journal of Rock Mechanics and Mining Sciences & Geomechanics Abstracts, 1987. vol 4. Elsevier, pp 223-233

Hucka V, Das B (1974) Brittleness determination of rocks by different methods International Journal of Rock Mechanics and Mining Sciences & Geomechanics Abstracts 11:389-392 doi:http://dx.doi.org/10.1016/0148-9062(74)91109-7

Hustrulid W, Fairhurst C A theoretical and experimental study of the percussive drilling of rock Part II—force-penetration and specific energy determinations. In: International Journal of Rock Mechanics and Mining Sciences & Geomechanics Abstracts, 1971a. vol 4. Elsevier, pp 335-356

Hustrulid W, Fairhurst C A theoretical and experimental study of the percussive drilling of rock part III—experimental verification of the mathematical theory. In: International Journal of Rock Mechanics and Mining Sciences & Geomechanics Abstracts, 1972a. vol 3. Elsevier, pp 417-418

Hustrulid WA, Fairhurst C (1971b) A theoretical and experimental study of the percussive drilling of rock part I—theory of percussive drilling International Journal of Rock Mechanics and Mining Sciences & Geomechanics Abstracts 8:311-333 doi:http://dx.doi.org/10.1016/0148-9062(71)90045-3

Hustrulid WA, Fairhurst C (1972b) A theoretical and experimental study of the percussive drilling of rock Part IV—application of the model to actual percussion drilling International Journal of Rock Mechanics and Mining Sciences & Geomechanics Abstracts 9:431-442 doi:http://dx.doi.org/10.1016/0148-9062(72)90007-1

ISRM (1978) Suggested methods for determining tensile strength of rock materials International Journal of Rock Mechanics and Mining Sciences & Geomechanics Abstracts 15:99-103 doi:http://dx.doi.org/10.1016/0148-9062(78)90003-7

Jansen DC, Shah S (1997) Effect of Length on Compressive Strain Softening of Concrete Journal of Engineering Mechanics 123:25-35 doi:doi:10.1061/(ASCE)0733-9399(1997)123:1(25)

Jansen DC, Shah SP, Rossow EC (1995) Stress-Strain Results of Concrete from Circumferential Strain Feedback Control Testing Materials Journal 92 doi:10.14359/9774

Kahraman S (1999) Rotary and percussive drilling prediction using regression analysis International Journal of Rock Mechanics and Mining Sciences 36:981-989 doi:http://dx.doi.org/10.1016/S0148-9062(99)00050-9

Kahraman S (2002) Correlation of TBM and drilling machine performances with rock brittleness Engineering Geology 65:269-283 doi:10.1016/S0013-7952(01)00137-5

Kahraman S, Balcı C, Yazıcı S, Bilgin N (2000) Prediction of the penetration rate of rotary blast hole drills using a new drillability index International Journal of Rock Mechanics and Mining Sciences 37:729-743 doi:http://dx.doi.org/10.1016/S1365-1609(00)00007-1

Kahraman S, Bilgin N, Feridunoglu C (2003) Dominant rock properties affecting the penetration rate of percussive drills International Journal of Rock Mechanics and Mining Sciences 40:711-723 doi:http://dx.doi.org/10.1016/S1365-1609(03)00063-7

Karasawa H, Ohno T, Kosugi M, Rowley JC (2002a) Methods to Estimate the Rock Strength and Tooth Wear While Drilling With Roller-Bits—Part 1: Milled-Tooth Bits Journal of Energy Resources Technology 124:125 doi:10.1115/1.1482405

Karasawa H, Ohno T, Kosugi M, Rowley JC (2002b) Methods to Estimate the Rock Strength and Tooth Wear While Drilling With Roller-Bits—Part 2: Insert Bits Journal of Energy Resources Technology 124:133 doi:10.1115/1.1482406

Kidybiński A (1981) Bursting liability indices of coal International Journal of Rock Mechanics and Mining Sciences & Geomechanics Abstracts 18:295-304 doi:http://dx.doi.org/10.1016/0148-9062(81)91194-3

Lin J-S, Zhou Y (2013) Can scratch tests give fracture toughness? Engineering Fracture Mechanics 109:161-168 doi:10.1016/j.engfracmech.2013.06.002

Lin J-S, Zhou Y (2015) Rebuttal: Shallow wide groove scratch tests do not give fracture toughness Engineering Fracture Mechanics 133:211-222 doi:http://dx.doi.org/10.1016/j.engfracmech.2014.10.030

Markeset G, Hillerborg A (1995) Softening of concrete in compression — Localization and size effects Cement and Concrete Research 25:702-708 doi:http://dx.doi.org/10.1016/0008-8846(95)00059-L

Munoz H, Taheri A, Chanda E (2016) Fracture energy-based brittleness index development and brittleness quantification by pre-peak strength parameters in rock uniaxial compression. Rock Mechanics and Rock Engineering doi:10.1007/s00603-016-1071-4

Paone J, Madson D, Bruce WE (1969) Drillability studies: laboratory percussive drilling. Bureau of Mines, Twin Cities, MN (USA). Twin Cities Mining Research Center,

Richard T, Coudyzer C, Desmentte S (2010) Influence of groove geometry and cutter inclination in rock cutting. Paper presented at the 44th US Rock Mechanics Symposium and 5th U.S.-Canada Rock Mechanics Symposium, Salt Lake City, UT, USA,

Richard T, Dagrain F, Poyol E, Detournay E (2012) Rock strength determination from scratch tests Engineering Geology 147-148:91-100 doi:10.1016/j.enggeo.2012.07.011

Schmidt RL (1972) Drillability studies: percussive drilling in the field REPORT OF INVESTIGATIONS 7684, 31 P, 1972 11 FIG, 10 TAB, 11 REF

Selim AA, Bruce WE (1970) Prediction of penetration rate for percussive drilling REPORT OF INVESTIGATIONS 7396, JUNE, 1970 21 P, 13 TAB, 10 REF, APPEND

Stavropoulou M (2006) Modeling of small-diameter rotary drilling tests on marbles International Journal of Rock Mechanics and Mining Sciences 43:1034-1051 doi:10.1016/j.ijrmms.2006.03.008

Taheri A, Qao Q, Chanda E (2016) Drilling Penetration Rate Estimation using Rock Drillability Characterization Index Journal of The Institution of Engineers (India): Series D:1-12 doi:10.1007/s40033-015-0104-6

Tarasov B, Potvin Y (2013) Universal criteria for rock brittleness estimation under triaxial compression International Journal of Rock Mechanics and Mining Sciences 59:57-69 doi:http://dx.doi.org/10.1016/j.ijrmms.2012.12.011

Tarasov BG, Randolph MF (2011) Superbrittleness of rocks and earthquake activity International Journal of Rock Mechanics and Mining Sciences 48:888-898 doi:http://dx.doi.org/10.1016/j.ijrmms.2011.06.013

Teale R (1965) The concept of specific energy in rock drilling Int J Rock Mech Mining Sc 2:57-73

Zhou Y, Lin J-S (2013) On the critical failure mode transition depth for rock cutting International Journal of Rock Mechanics and Mining Sciences 62:131-137 doi:http://dx.doi.org/10.1016/j.ijrmms.2013.05.004

LIST OF FIGURES

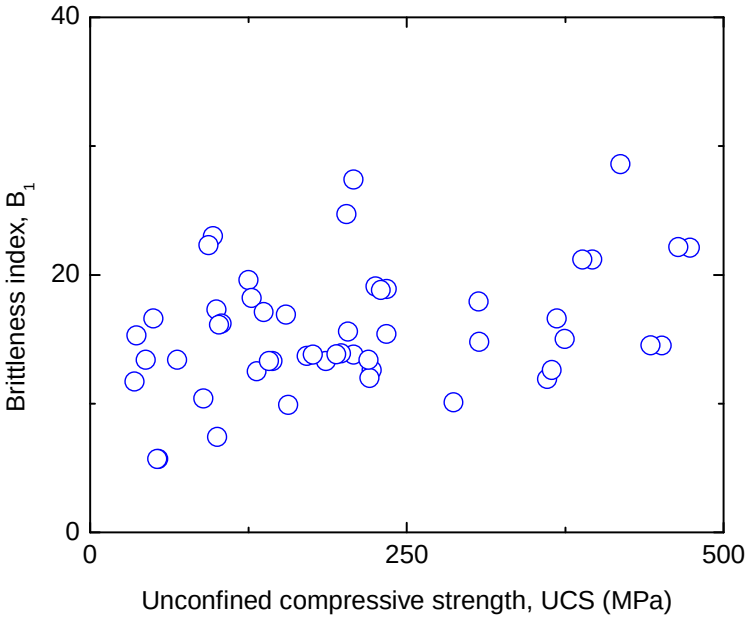

a)

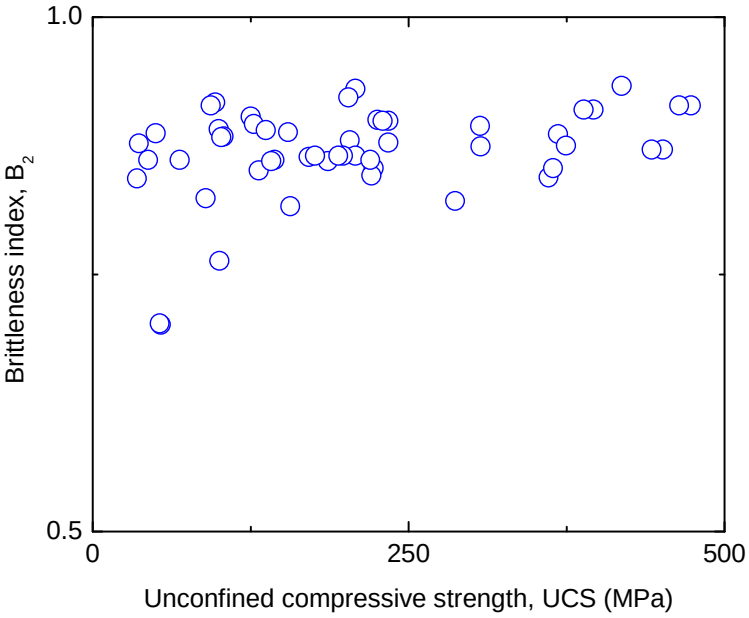

b)

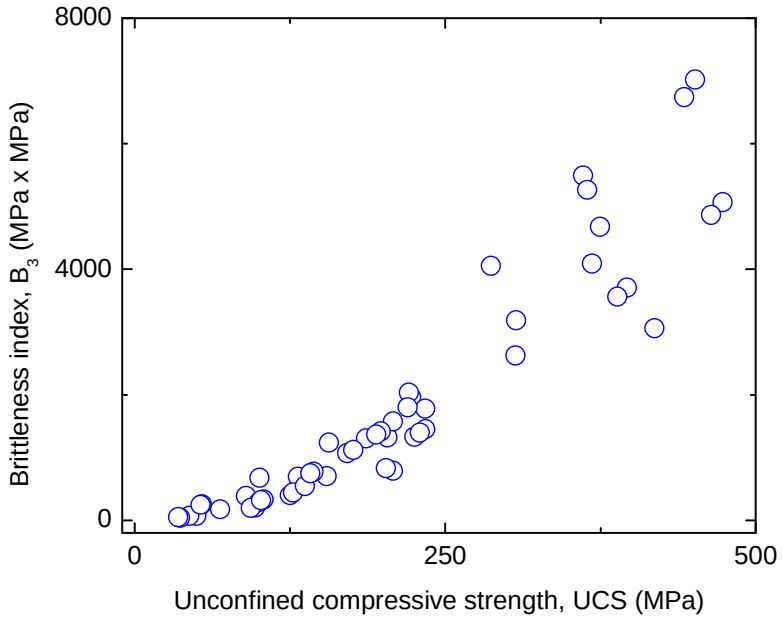

c)

Figure 4.1 Relations between compressive-to-tensile brittleness indices a) B_1, b) B_2 and c) B_3 with unconfined compressive strength. Data from literature (Howarth 1987; Paone et al. 1969; Schmidt 1972; Selim and Bruce 1970)

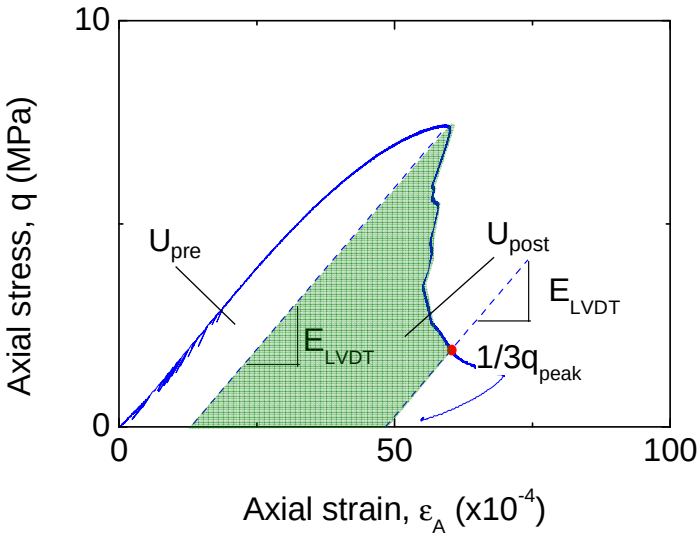
10
0
0
50
100
Axial stress, q (MPa)
Axial strain, ε_A (x10^-4)
U_pre
U_post
E_LVDT
E_LVDT
1/3q_peak

a)

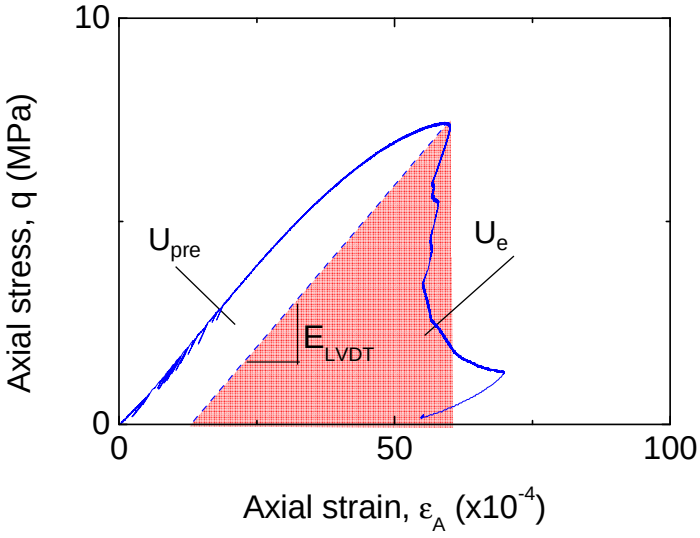
10
0
0
50
100
Axial stress, q (MPa)
Axial strain, ε_A (x10^-4)
U_pre
U_e
E_LVDT

b)

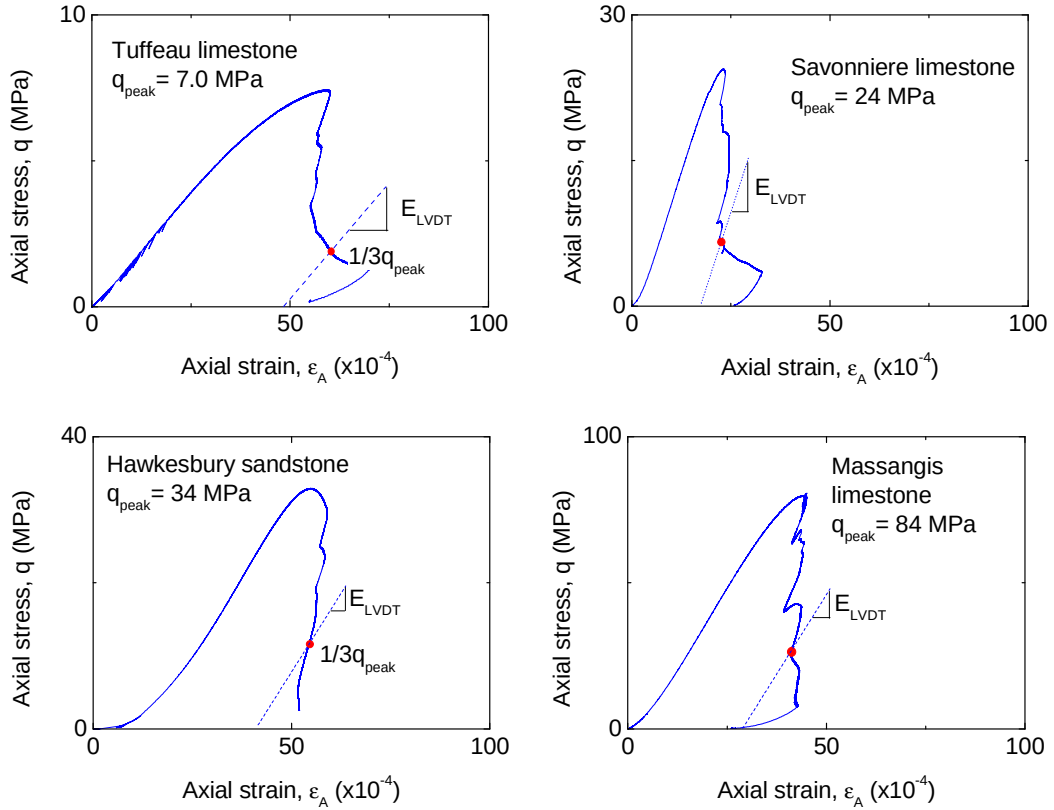
Tuffeau limestone
q_{peak}= 7.0 MPa
E_{LVDT}
1/3q_{peak}
Savonniere limestone
q_{peak}= 24 MPa
E_{LVDT}
Hawkesbury sandstone
q_{peak}= 34 MPa
E_{LVDT}
1/3q_{peak}
Massangis limestone
q_{peak}= 84 MPa
E_{LVDT}
Axial stress, q (MPa)
Axial strain, ε_A (x10^{-4})
0
50
100
10
30
40

c)

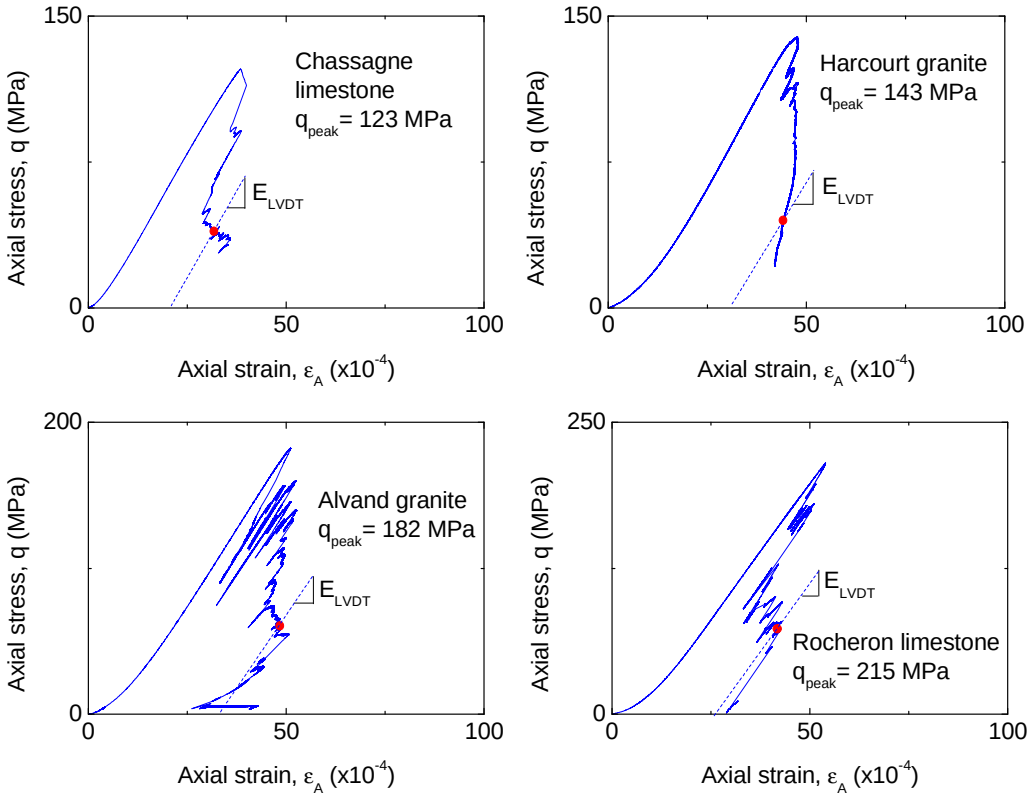
Chassagne limestone
q_{peak}= 123 MPa
E_{LVDT}
Harcourt granite
q_{peak}= 143 MPa
E_{LVDT}
Alvand granite
q_{peak}= 182 MPa
E_{LVDT}
Rocheron limestone
q_{peak}= 215 MPa
E_{LVDT}
Axial stress, q (MPa)
Axial strain, ε_A (x10^{-4})
0
50
100
150
200
250

c) (Continued)

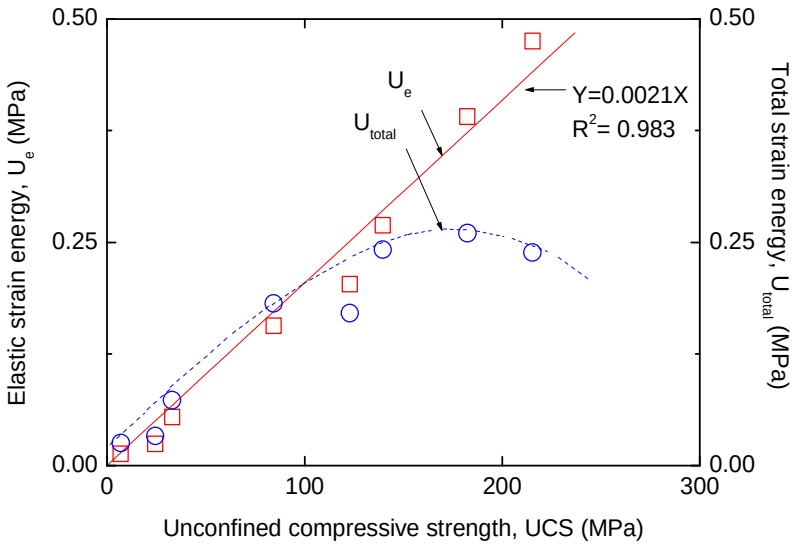

d)

Figure 4.2 a) and b) Strain energy of rock in compression, c) typical complete stress-strain curves for different rocks under lateral strain-rate control and d) strain energy quantities with compressive strength for different rock types

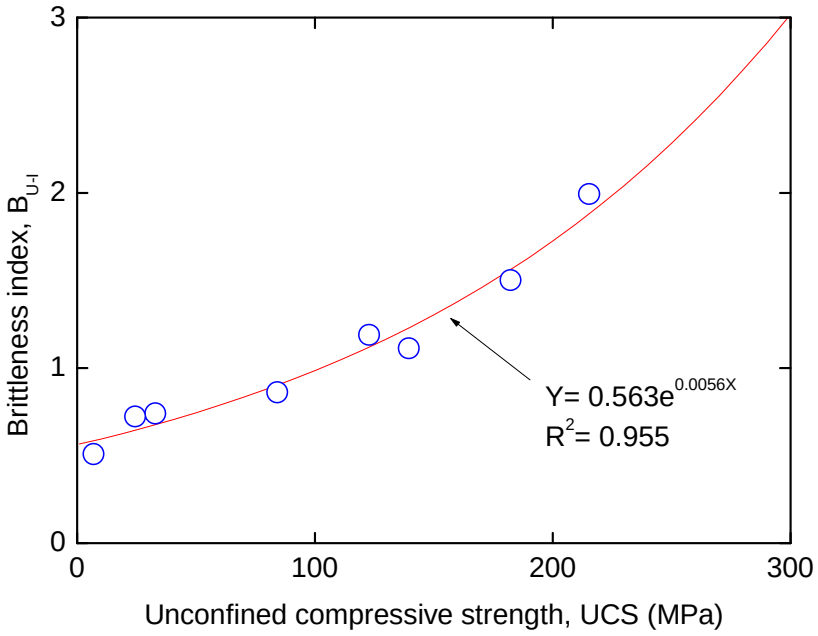

Figure 4.3 Brittleness index B_{U-I} relations with unconfined compressive strength for different rock types

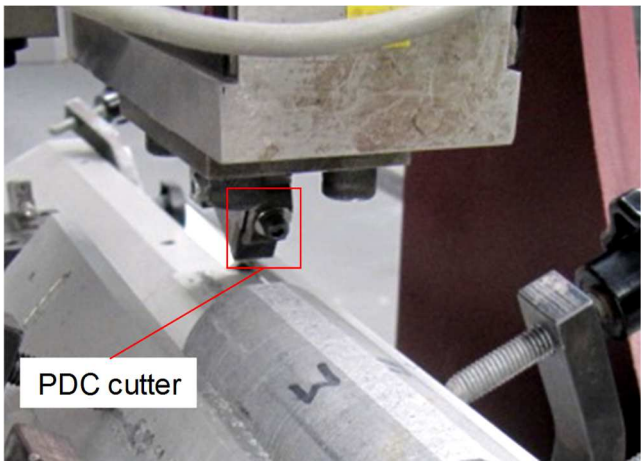

a)

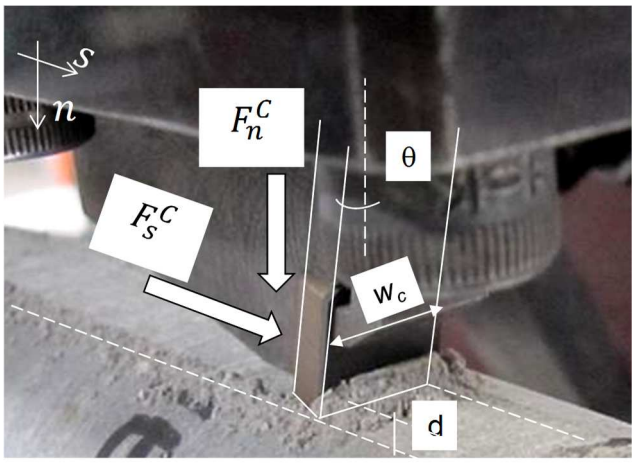

b)

Figure 4.4 a) PDC cutting test at shallow depth of cut and b) geometry of cutting and forces acting on the PDC cutter

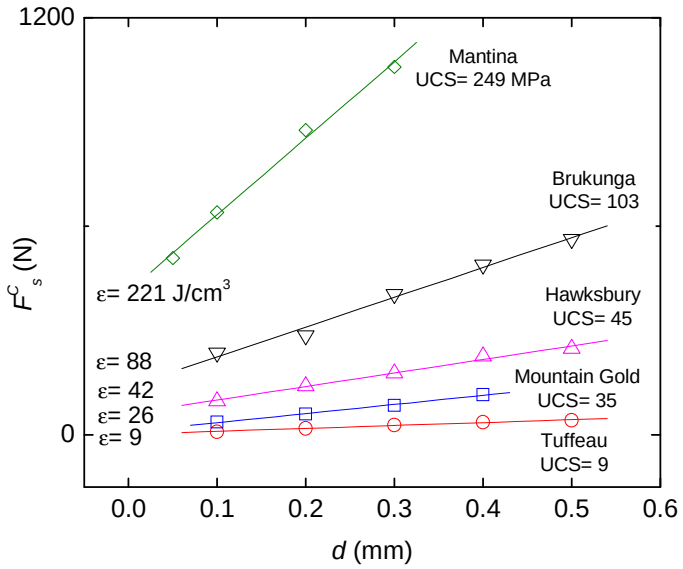

a)

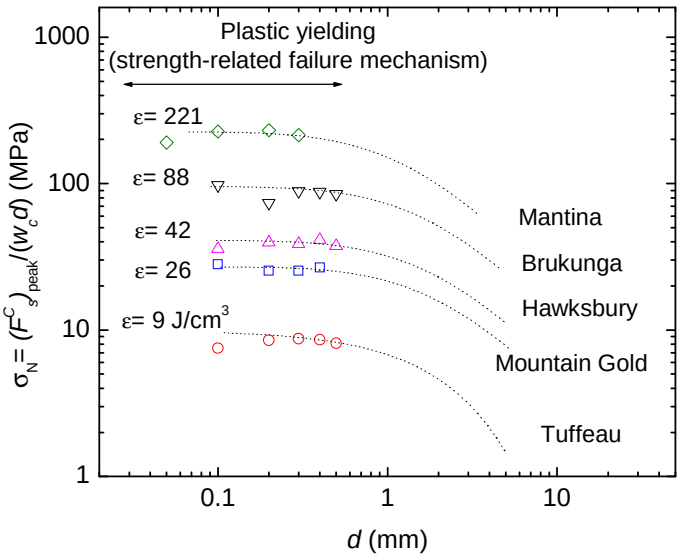

b)

Figure 4.5 a) Cutting force, F_s^C, versus depth of cut, d, b) SEL for the rock investigated and intrinsic specific energy

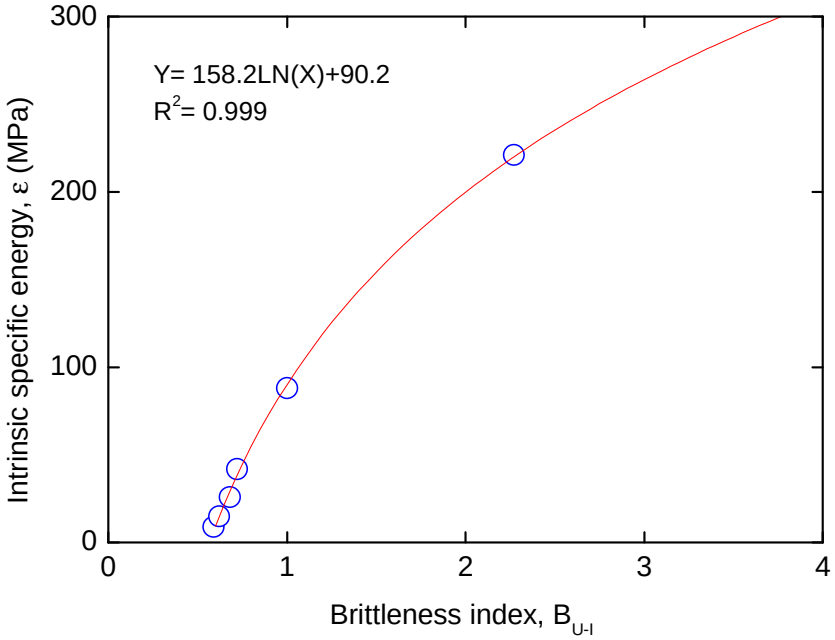

Figure 4.6 Intrinsic specific energy from PDC cutting tests and its relation with the brittleness index B_{U-I}

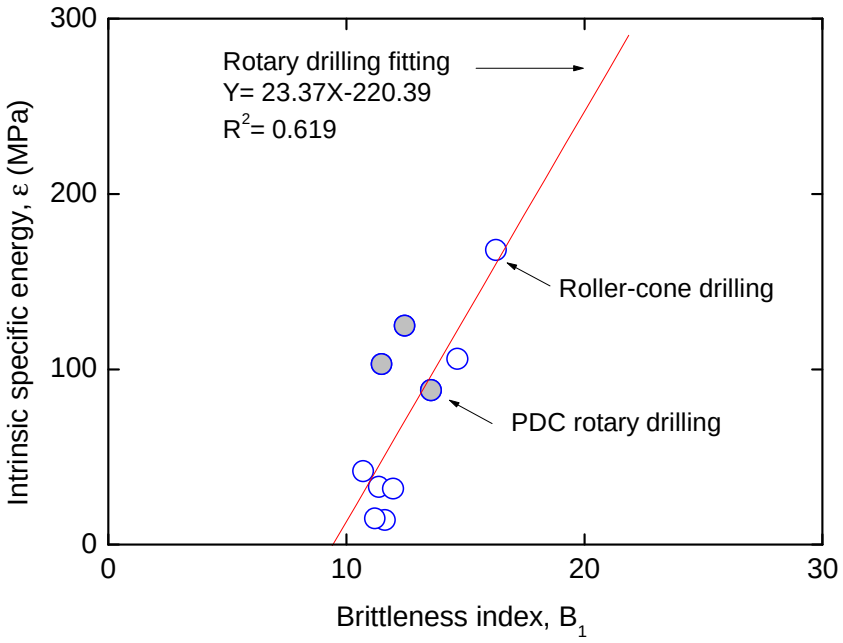
Rotary drilling fitting
Y= 23.37X-220.39
R2= 0.619
Roller-cone drilling
PDC rotary drilling
Intrinsic specific energy, ε (MPa)
Brittleness index, B1
300
200
100
0
0
10
20
30

a)

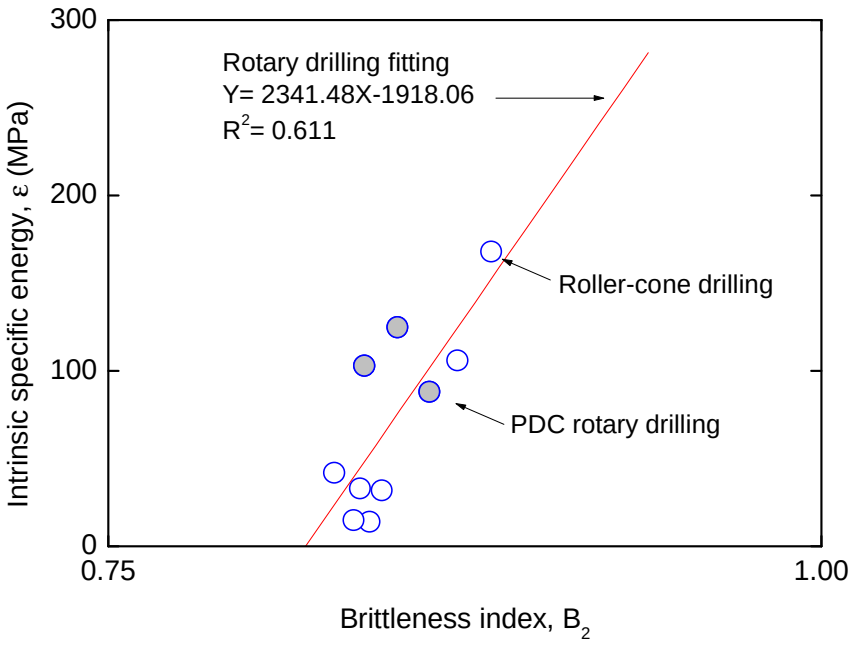
Rotary drilling fitting
Y= 2341.48X-1918.06
R2= 0.611
Roller-cone drilling
PDC rotary drilling
Intrinsic specific energy, ε (MPa)
Brittleness index, B2
300
200
100
0
0.75
1.00

b)

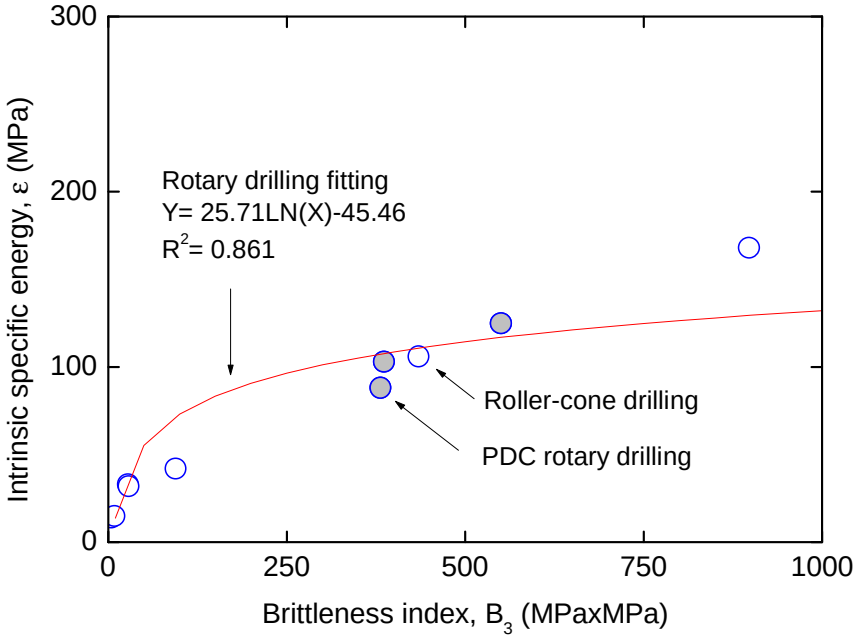

c)

Figure 4.7 Intrinsic specific energy and its relation with the brittleness index a) B_1, b) B_2 and c) B_3 from rotary drilling tests

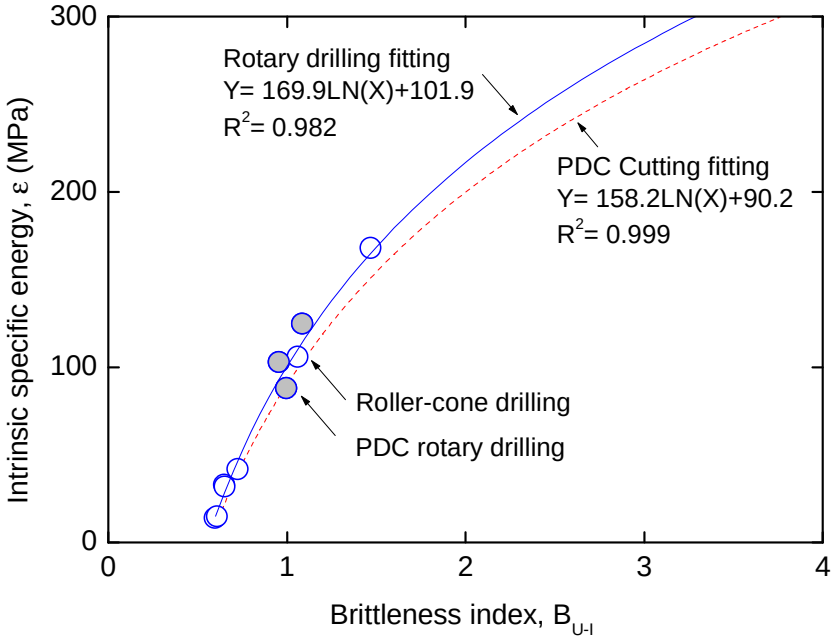

Figure 4.8 Intrinsic specific energy from rotary drilling tests and its relation with the brittleness index B_{U-I}

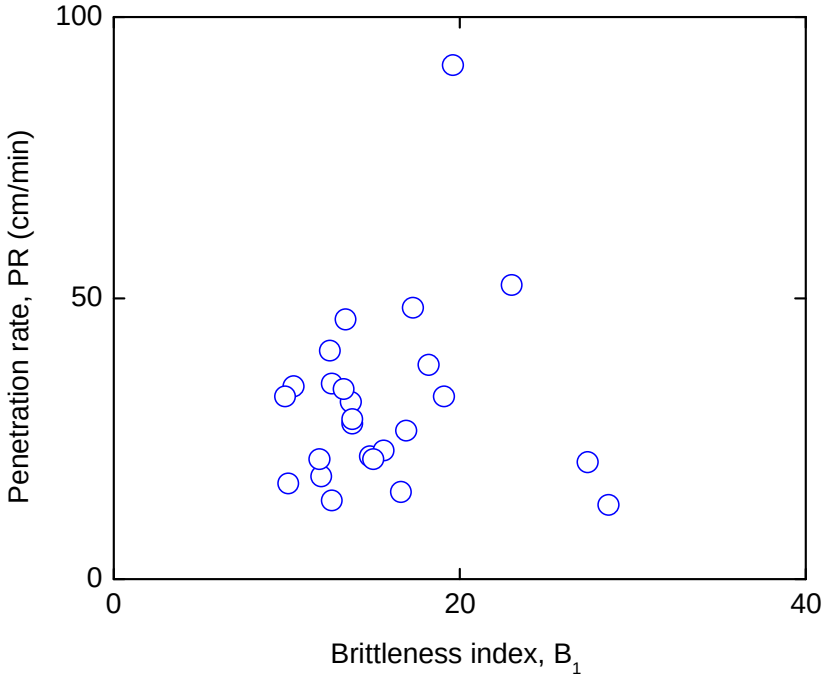
100
50
0
0
20
40
Penetration rate, PR (cm/min)
Brittleness index, B1

a)

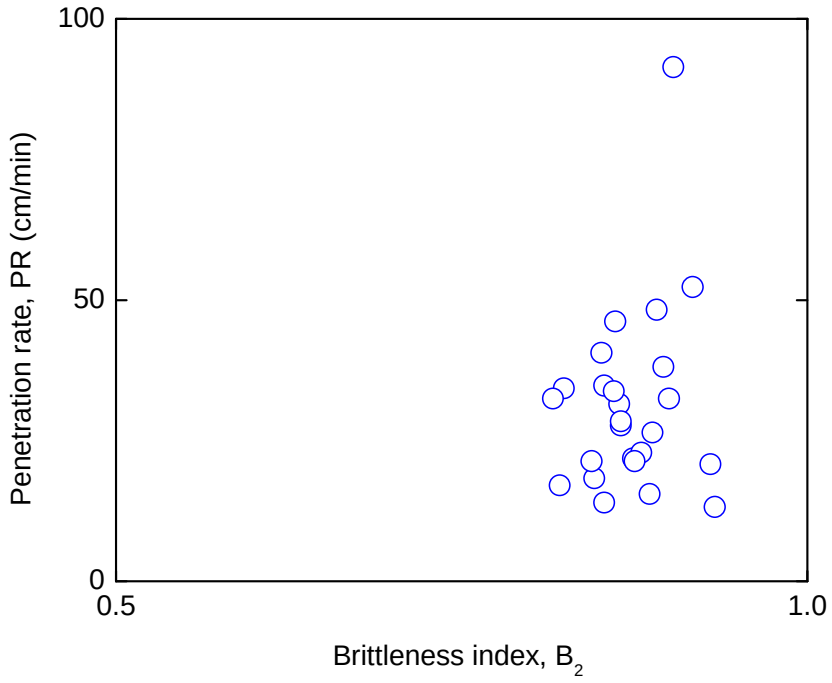
100
50
0
0.5
1.0
Penetration rate, PR (cm/min)
Brittleness index, B2

b)

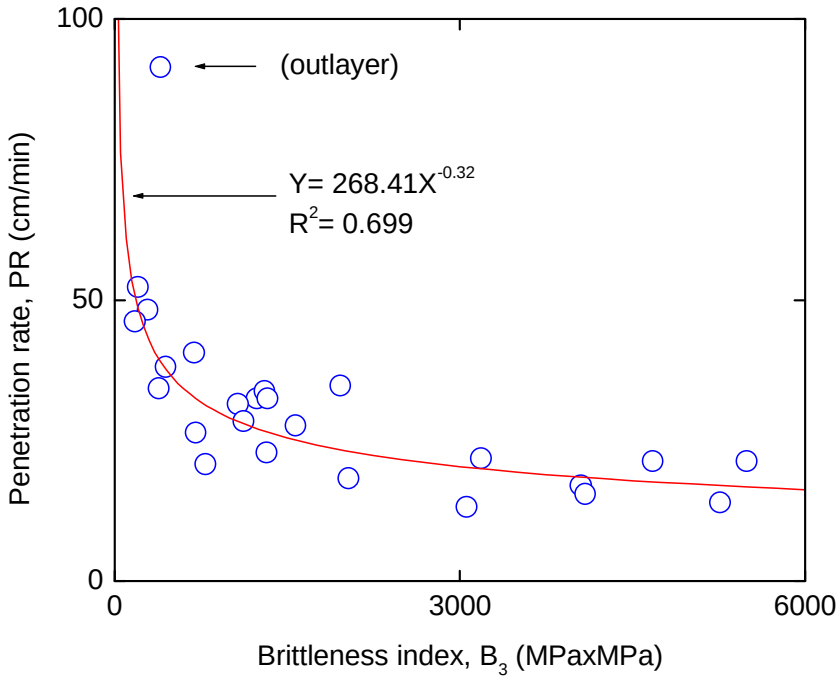

c)

Figure 4.9 Penetration rate and its relation with the brittleness index a) B_1, b) B_2 and c) B_3 from percussive drilling tests

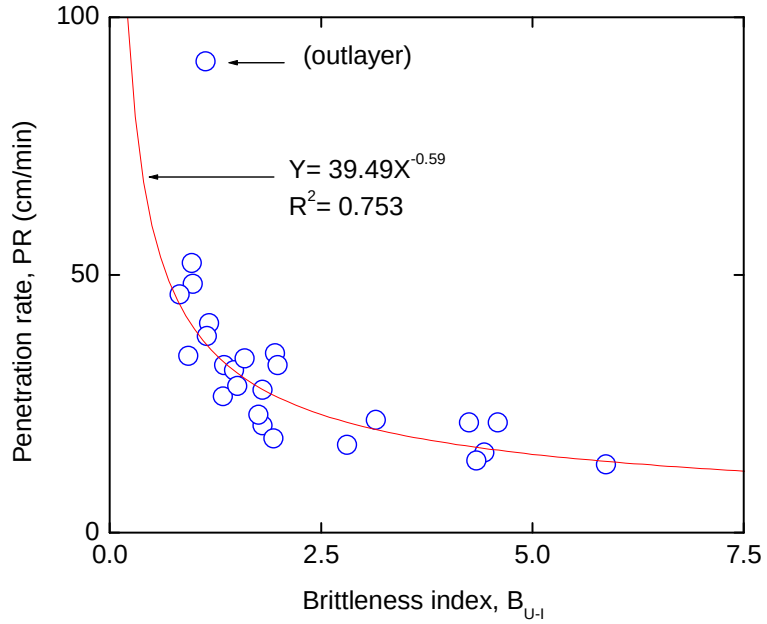

a)

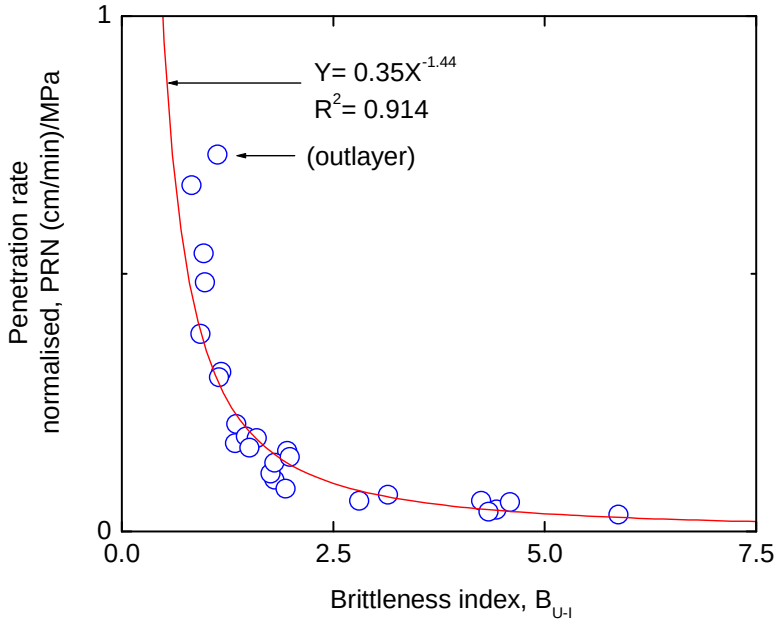

b)

Figure 4.10 a) Penetration rate and b) penetration rate normalised from percussive drilling tests and their relation with the brittleness index B_{U-I}

LIST OF TABLES

Table 4.1 Rocks investigated to develop a energy-based brittleness index B_{U-I}

Rock name	Rock type	UCS (MPa)
Tuffeau	Limestone	7
Savoniere	Limestone	24
Hawksebury	Sandstone	33
Massangis	Limestone	84
Chassagne	Limestone	123
Harcourt	Granite	139
Alvand	Granite	182
Rocheron	Limestone	215

Table 4.2 Rocks tested for PDC cutting performance

Rock name	Rock type	UCS (MPa)	ε (MPa)	B_{U-I}
Tuffeau	Limestone	9	9	0.59
Castlegate	Sandstone	16	15	0.62
Mountain Gold	Sandstone	35	26	0.68
Hawksbury	Sandstone	45	42	0.72
Brukunga	Phyllite	103	88	1.00
Mantina	Basalt	249	221	2.27

Table 4.3 Rocks for PDC drilling performance and brittleness index

Rock name[1]	Rock type[1]	UCS (MPa) [1]	TS (MPa) [1]	ε (MPa) [2]	B_{U-I} [2]
Gioia	Marble	101.7	7.5	88	1.00
Cervaiole	Marble	117.1	9.4	125	1.08
Dionysios	Marble	94.2	8.2	103	0.95

[1] Data from literature (Stavropoulou 2006)

[2] Calculated by the authors

Table 4.4 Rocks for roller-cone drilling performance and brittleness index

Rock name[1] [2]	Rock type[1] [2]	UCS (MPa)	TS (MPa)	ε (MPa) [1]	B_{U-I}[3]
Tuffeau	Limestone	10[1]	0.86[3]	14	0.60
Savonniere	Limestone	25[1]	2.20[3]	33	0.65
Castlegate	Sandstone	14[1]	1.25[3]	15	0.61
Mountain Gold	Sandstone	26[1]	2.17[3]	32	0.65
Kimachi	Sandstone	45[2]	4.2[2]	42	0.72
Shinkomatsu	Andesite	113[2]	7.7[2]	106	1.06
Sori (A)	Granite	171[2]	10.5[2]	168	1.47

[1] Data from literature (Franca 2010)

[2] Data from literature (Karasawa et al. 2002a; Karasawa et al. 2002b)

[3] Calculated by the authors.

Table 4.5 Rocks for percussive drilling performance and brittleness index

Rock type[(1)]	UCS (MPa) [(1)]	TS (MPa) [(1)]	PR (cm/min) [(1)]	PRN [(2)] (cm/min)/MPa	B_{U-I}[(2)]
Iron	418.6	14.6	13.21	0.03	5.87
Schist	208.1	7.5	20.83	0.10	1.8
Pegmatite	89.6	8.6	34.29	0.38	0.93
Quartzite	222.5	17.6	34.8	0.15	1.95
Argillite	220.7	18.4	18.29	0.083	1.93
Dolomite	97.0	4.2	52.32	0.53	0.96
Mankato	125.1	6.4	91.44	0.73	1.13

(Continues below)

Rock type[1]	UCS (MPa) [1]	TS (MPa) [1]	PR (cm/min) [1]	PRN [2] (cm/min)/MPa	B_{U-I}[2]
Quartzite	156.4	15.8	32.51	0.20	1.35
Quartzite	307.2	20.7	21.84	0.07	3.14
Granite	154.6	9.1	26.42	0.17	1.33
Granite	203.5	13.0	22.86	0.11	1.75
Granite	171.1	12.5	31.5	0.18	1.46
Basalt	286.8	28.2	17.02	0.05	2.80
Limestone	99.8	5.7	48.26	0.48	0.98
Taconite	360.9	30.4	21.34	0.05	4.25
Taconite	368.3	22.2	15.49	0.04	4.42
Taconite	364.5	28.8	13.97	0.03	4.33

Rock type[1]	UCS (MPa) [1]	TS (MPa) [1]	PR (cm/min) [1]	PRN [2] (cm/min)/MPa	B_{U-I} [2]
Diabase	374.7	24.9	21.34	0.05	4.58
Gabbro	208.0	15.1	27.69	0.13	1.80
Trap	68.8	5.1	46.23	0.67	0.82
Anorthosite	131.4	10.5	40.64	0.30	1.17
Basalt	186.3	13.9	33.78	0.18	1.59
Marble	127.5	7.0	38.1	0.29	1.15
Gabbro	176.1	12.7	28.45	0.16	1.50
Iron	225.3	11.8	32.51	0.14	1.98

[1] Data from literature (Schmidt 1972).

[2] Calculated by the authors